CO-CRYSTALLISATION OF α,ω-DICARBOXYLIC ACIDS WITH NICOTINAMIDE AND ISONICOTINAMIDE

by

RAJA SEKHAR VOGURI

under the supervision of Dr. Maryjane Tremayne

A thesis submitted to

The University of Birmingham

for the degree of

MASTER OF RESEARCH

School of Chemistry

The University of Birmingham

September 2010

ABSTRACT

Pharmaceutical co-crystallisation is an alternative and potentially reliable method to manipulate physical properties of API's via supramolecular synthesis. A number of binary co-crystals were synthesised using different solvents, different stoichiometric ratios (ratio of starting materials) and different methods of synthesis (solvent-mediated crystallisation, solvent-drop grinding and neat grinding), with a view to investigate solvent and stoichiometric effects on the materials formed. Selected α,ω-alkanedicarboxylic acids (HOOC-$(CH_2)_n$-COOH) were crystallised with nicotinamide for n = 0, 1, 2, 4, 5, 6, 7 and isonicotinamide for n = 5, 6, 7 yielding 12 new solid materials. The melting point of the starting materials and new products are determined and analysed, and the new crystalline materials characterised using NMR, FTIR, powder X-ray diffraction data (PXRD) and single X-ray diffraction data (SXRD). For azelaic acid : nicotinamide (1:1), structure solution was carried out using powder X-ray diffraction data and the direct space methods are applied through differential evolution (DE) approach. The crystal structure of adipic acid : nicotinamide (1:2) was solved using single crystal X-ray diffraction. The crystal structures of both, display strong O-H···N*(pyridine)*, O-H···O=C and N-H···O=C intermolecular bonds.

Other new materials formed were oxalic acid:nicotinamide (1:1 and 1:2), malonic acid : nicotinamide (1:1 and 1:2), succinic acid : nicotinamide (1:1), pimelic acid : nicotinamide (1:1), suberic acid : nicotinamide (1:1), azelaic acid : nicotinamide (1:1), pimelic acid : isonicotinamide (1:1), suberic acid : isonicotinamide (1:1 and 1:2) and azelaic acid : isonicotinamide (1:1), but these were not fully characterised by X-diffraction.

ACKNOWLEDGEMENTS

I am grateful to Dr. Maryjane Tremayne for her supervision and freedom given to my thoughts throughout my project and who made this thesis possible. It is pleasure to thank Dr. Louise Male who trained me in solving crystal structures and supported with patience. I owe my deepest gratitude to Adam Cowell for his guidance and assistance in numerous ways. I offer my regards to the rest of the research group, colleagues and friends for their support.

I am very thankful to my parents for funding and moral support.

CONTENTS

1. Introduction 1

1.1 Supra molecular crystalline materials and crystal engineering 1

1.2 Characterisation of organic materials from X-ray diffraction methods (PXRD and SXRD) 3

1.3 Aims of project 5

2. Materials under Investigation 7

2.1 Synthon flexibility 10

2.2 Methods and materials 19

2.2.1 Solvent mediated crystallization 19

2.2.2 Solvent drop grinding or liquid assisted grinding (SDG) 22

2.2.3 Salts and co-crystals 23

2.2.4 Co-crystal solvates 24

2.2.5 Co-crystal hydrates 26

3. Experimental 28

3.1 Solution mediated crystallisation 28

3.2 Solvent drop grinding 28

3.3 Powder X-ray diffraction data 28

3.4 Single crystal X-ray diffraction data 29

3.5 ^{1}H NMR 29

3.6 Infra-red spectra 29

4. Methodology 30

4.1 Indexing 30

4.2 Le bail pattern decomposition 30

4.3 Differential Evolution (DE) structure solution 31

4.4 Rietveld Refinement 34

4.5 Single crystal X-ray diffraction 34

5. Results 36

5.1 Oxalic acid and nicotinamide 37

5.2 Malonic acid and nicotinamide 43

5.3 Succinic acid and nicotinamide 48

5.4 Adipic acid and nicotinamide 51

5.4.1 Determination of crystal structure from single crystal X-ray diffraction data 54

5.4.2 Determination of crystal structure from powder X-ray diffraction data 58

5.5 Pimelic acid and nicotinamide 62

5.6 Pimelic acid and isonicotinamide 65

5.7 Suberic acid and nicotinamide 68

5.8 Suberic acid and isonicotinamide 71

5.9 Azelaic acid and nicotinamide 74

5.9.1 Determination and refinement of unit cell parameters from X-ray powder diffraction data 76

5.9.2 Determination of structure solution using Differential Evolution (DE) 78

5.9.3 Crystal structure determination using Rietveld refinement 80

5.10 Azelaic acid and isonicotinamide 89

5.11 Melting point alternations 93

6. Conclusion 96

7. Appendices 99

8. Bibliography 121

LIST OF ILLUSTRATIONS

LIST OF FIGURES

2.1 Molecular structures of (a) Nicotinamide and (b) Isonicotinamide.

2.2(a) Molecular structure of oxalic acid

2.2(b) Molecular structure of malonic acid

2.2(c) Molecular structure of Succinic acid

2.2(d) Molecular structure of adipic acid

2.2(e) Molecular structure of pimelic acid

2.2(f) Molecular structure of suberic acid

2.2(g) Molecular structure of azelaic acid

2.1.1 Schematic diagram showing potential supra-molecular synthons in co-crystals formed by isonicotinamide and di-carboxylic acids.

2.1.2 Molecules capable of forming a variety of hydrogen bonded synthons: (a) isonicotinamide, (b) 2-amino-3-nitropyridine, (c) 4-chlorobenzamide and (d) maleic hydrazide.

2.1.3 Carboxylic acid : isonicotinamide (1:1) co-crystal showing different intermolecular interactions between the molecules.

2.1.4 Venlafaxine saccharinate showing intermolecular bonds having supramolecular synthons consisting of $N^{(+)}$-H···N and O-H···O=C interactions.

2.1.5 A view of the crystal structure of oxalic acid and isonicotinamide (1:2) form I showing intermolecular interactions.

2.1.6 A view of the crystal structure of oxalic acid and isonicotinamide (1:2) form II showing intermolecular interactions.

2.1.7 A view of the crystal structure of malonic acid and isonicotinamide (1:2) showing intermolecular interactions.

2.1.8 A view of the crystal structure of succinic acid and isonicotinamide (1:2) showing intermolecular interactions.

2.1.9 A view of the crystal structure of glutaric acid:isonicotinamide (1:2) showing intermolecular interactions.

2.1.10 A view of the crystal structure of glutaric acid:isonicotinamide (1:1) showing intermolecular interactions.

2.1.11 A view of the crystal structure of adipic acid:isonicotinamide (1:1) co-crystal showing intermolecular interactions.

2.1.12 A view of the crystal structure of adipic acid and isonicotinamide (1:2) co-crystal showing intermolecular interactions.

2.1.13 Folded S-conformer of the adipic acid in adipic acid:isonicotinamide (1:2) co-crystal. The intramolecular C-H···O hydrogen bonds is shown with bold dash lines.

2.2.1.1 (a) A schematic ternary phase diagram for a highly soluble co-crystal system in solution at constant temperature. (b) A schematic phase diagram for slightly soluble components and co-crystal

2.2.3.1 Formation of a supramolecular adduct and as ionised adduct of benzoic acid : dichloropyridine in (a) co-crystal and (b) salt forms.

2.2.3.2 Example showing both proton transfer and supra-molecular synthons in 3-(4-pyridinium)-pyrazolepentamethylbenzoate pentamethyl benzoate:pentamethylbenzoic acid.

2.2.3.1 Formation of supramolecular adduct and ionised adduct in benzoic acid : dichloro pyridine in (a) co-crystal and (b) salt forms.

2.2.3.2 Example showing both proton transfer and supra-molecular synthesis in 3-(4-pyridinium)-pyrazolepentamethylbenzoate pentamethyl benzoate: pentamethylbenzoic acid adduct.

2.2.5.1 Theophylline : citric acid monohydrate co-crystal showing supramolecular adducts.

4.1 An example of an evolutionary progress plot for DE calculations.

4.2 An example of a 2D hypersurface clearly showing the global minimum which represents the best structure solution[1]. A local minimum is also shown.

5.1.1 X-ray powder diffraction patterns for nicotinamide and oxalic acid and products of crystallisation using methanol.

5.1.2 ^{1}H NMR for the product of oxalic acid and nicotinamide adduct (from 1:1 starting ratio) using DMSO as solvent. ^{1}H NMR 300MHz (DMSO-d_6): δ = 13.18(s, 2H), 9.04(dd, 1H), 8.69(dd, 1H), 8.22(dt, 1H), 8.18(s, 1H), 7.62(s, 1H), 7.51(ddd, 1H).

5.1.3 ^{1}H NMR for the product of oxalic acid and nicotinamide adduct (from 1:2 starting ratio) using DMSO as solvent. ^{1}H NMR 300MHz (DMSO-d_6): δ = 11.95(s, 2H), 9.05(dd, 2H), 8.70(dd, 2H), 8.19(dt, 2H), 8.17(s, 2H), 7.63(s, 2H), 7.52(ddd, 2H).

5.1.4 FTIR spectra for the product of oxalic acid and nicotinamide crystallisation (1:1).

5.1.5 The Le bail profile fitting for the product of oxalic acid and nicotinamide crystallisation (1:1).

5.2.1 X-ray powder diffraction patterns for nicotinamide and malonic acid and products of crystallisation using methanol.

5.2.2 ^{1}H NMR of malonic acid and nicotinamide (1:1) crystallisation using DMSO as solvent. ^{1}H NMR 300MHz (DMSO-d_6): δ= 12.51(s, 2H),

9.03(dd, 1H), 8.70(dd, 1H), 8.20(dt, 1H), 8.17(s, 1H), 7.61(s, 1H), 7.51(ddd, 1H), 3.26(s, 2H).

5.2.3 ^{1}H NMR of malonic acid and nicotinamide (1:2) crystallisation using DMSO as solvent. ^{1}H NMR 300MHz (DMSO-d_6): δ= 12.67(s, 2H), 9.03(dd, 2H), 8.68(dd, 2H), 8.21(dt, 2H), 8.19(s, 2H), 7.61(s, 2H), 7.48(ddd, 2H), 3.25(s, 2H).

5.2.4 FTIR spectra of malonic acid and nicotinamide and products of crystallisation (1:1).

5.2.5 FTIR spectra of malonic acid and nicotinamide and products of crystallisation (1:2).

5.2.6 The Le bail profile fitting for nicotinamide and malonic acid crystallisation (1:1).

5.3.1 Powder X-ray diffraction patterns of succinic acid and nicotinamide and products of crystallisation using methanol.

5.3.2 ^{1}H NMR of succinic acid and nicotinamide (1:1) crystallisation using DMSO as solvent. ^{1}H NMR 300MHz (DMSO-d_6): δ= 12.15(s, 2H) 9.02(dd, 1H), 8.68(dd, 1H), 8.19(dt, 1H), 8.16(s, 1H), 7.59(s, 1H), 7.48(ddd, 1H), 2.42(s, 4H).

5.3.3 FTIR spectra of succinic acid and nicotinamide and products of crystallisation (1:1).

5.4.1 X-ray powder diffraction patterns of nicotinamide and adipic acid and products of crystallisation using methanol.

5.4.2 ^{1}H NMR of nicotinamide and adipic acid crystallisation using DMSO as solvent. ^{1}H NMR 300MHz (DMSO-d_6): δ = 12.032(s, 2H), 9.02(dd, 2H), 8.68(dd, 2H), 8.19(dt, 2H), 7.62(s, 2H), 7.50(ddd, 2H), 2.50(m, 4H), 2.30(m, 4H).

5.4.3 FTIR spectra of adipic acid and nicotinamide and products of crystallisation (1:2).

5.4.1.1 ORTEP diagram of the adipic acid:nicotinamide (1:2) co-crystal showing the strong hydrogen bond interaction between the two former molecules. Thermal ellipsoids are drawn at the 50% probability level.

5.4.1.2 (I) A view of the crystal structure of adipic acid:nicotinamide (1:2) down [010] showing the intermolecular interactions between the molecules within a sheet.

5.4.1.2 (II) A view of the crystal structure showing a projection down [100] illustrating the padding of sheets in adipic acid : nicotinamide (1:2) and zigzag sheets.

5.4.2.1 The Le bail profile fit for the adipic acid : nicotinamide (1:2) co-crystal.

5.4.2.2 Molecular structures of nicotinamide and one half of adipic acid molecules showing the torsion angles used in the direct-space structure solution calculation.

5.4.2.3 Evolutionary progress plot for DE calculations for the product of adipic acid and nicotinamide crystallisation (1:2).

5.4.2.4 A view of the crystal structure of adipic acid:nicotinamide (1:2) showing the different amide conformation obtained from the structure solution from PXRD.

5.5.1 X-ray powder diffraction pattern for pimelic acid and nicotinamide acid and product of crystallisation using methanol.

5.5.2 H^1 NMR of pimelic acid and nicotinamide crystallisation (1:1) using DMSO as solvent. ^{1}H NMR 300MHz (DMSO-d_6): δ = 12.60(s, 2H), 9.03 (dd, 1H), 8.68(dd, 1H), 8.19(dt, 1H), 7.61(s, 1H), 7.49(ddd, 1H), 2.18(m, 4H), 1.48(m, 4H), 1.25(m, 2H).

5.5.3 FTIR spectra of pimelic acid and nicotinamide and the product of crystallisation.

5.6.1 X-ray powder diffraction pattern for pimelic acid and isonicotinamide and products of crystallisation using methanol.

5.6.2 ^{1}H NMR of pimelic acid and isonicotinamide (1:1) crystallisation using DMSO as solvent. ^{1}H NMR 300MHz (DMSO-d_6): δ = 12.52 (s, 2H), 8.69(dd, 2H), 8.26(s, 1H), 7.75(dd, 2H), 7.73(s, 1H), 2.38(m, 4H), 1.43(m, 4H), 1.26(m, 2H).

5.6.3 FTIR spectra of pimelic acid and isonicotinamide and the product of crystallisation.

5.7.1 X-ray powder diffraction pattern for suberic acid and nicotinamide and products of crystallisation using methanol.

5.7.2 ^{1}H NMR of suberic acid and nicotinamide (1:1) adduct (from 1:1 starting ratio) using DMSO as solvent. ^{1}H NMR 300MHz (DMSO-d_6): δ = 11.97(s, 2H), 9.02(dd, 1H), 8.68(dd, 1H), 8.19(dt, 1H), 8.16(s, 1H), 7.60(s, 1H), 7.47(ddd, 1H), 2.18(m, 4H), 1.47(m, 4H), 1.25(m, 4H).

5.7.3 ^{1}H NMR of suberic acid and nicotinamide (1:2) adduct (from 1:2 starting ratio) using DMSO as solvent. ^{1}H NMR 300MHz (DMSO-d_6): δ= 11.99(s, 2H), 9.04(dd, 1H), 8.69(dd, 1H), 8.20(dt, 1H), 7.62(s, 1H), 7.49(ddd,1H), 2.18(m,4H), 1.47(m,4H), 1.25(m,4H).

5.7.4 FTIR spectra of suberic acid and nicotinamide and product of crystallisation (1:1).

5.8.1 X-ray powder diffraction patterns of suberic acid and isonicotinamide and products of crystallisation using methanol.

5.8.2 ^{1}H NMR of suberic acid and isonicotinamide adduct (from 1:1 starting ratio) using DMSO as solvent. ^{1}H NMR 300MHz (DMSO-d_6): δ = 12.01(s, 2H), 8.70(dd, 2H), 8.25(s, 1H), 7.77(dd, 2H), 7.73(s, 1H), 2.17(m, 4H), 1.47(m, 4H), 1.24(m, 4H).

5.8.3 FTIR spectra of suberic acid and isonicotinamide and product of crystallisation (1:1).

5.9.1 X-ray powder diffraction pattern for nicotinamide and azelaic acid and products of crystallisation using methanol.

5.9.2 ^{1}H NMR for product of nicotinamide and azelaic acid crystallisation using DMSO as solvent. ^{1}H NMR 300MHz (DMSO-d_6): δ = 11.97(s, 2H), 9.03(dd, 1H), 8.68(dd, 1H), 8.19(dt, 1H), 7.60(s, 1H), 7.49(ddd, 1H), 2.18(m, 4H), 1.47(m, 4H), 1.23(s, 6H).

5.9.3 FTIR spectra of azelaic acid and nicotinamide and product of crystallisation (1:1).

5.9.1.1 The Le Bail profile fitting for product of azelaic acid and nicotinamide (1:1) adduct. The greeen solid line is calculated intensities and points superimposed on it are observed intensities. The difference between the calculated and observed intesities is shown by pink line. Reflections are also shown.

5.9.2.1 Evolutionary progress plot for DE calculations for product of nicotinamide and azelaic acid crystallisation for N_p=35, K=0.99, F=0.2

5.9.2.2 Evolutionary progress plot for DE calculations for the product of nicotinamide and azelaic acid crystallisation for N_p=35, K=0.99, F=0.3

5.9.2.3 Evolutionary progress plot for DE calculations for product of nicotinamide and azelaic acid crystallisation for N_p=35, K=0.99, F=0.4

5.9.2.4 Evolutionary progress plot for DE calculations for product of nicotinamide and azelaic acid crystallisation for N_p=35, K=0.99, F=0.5

5.9.3.1 Rietveld refinement of azelaic acid : nicotinamide (1:1) adduct. The greeen solid line is calculated intensities and points superimposed on it are observed intensities. The difference between the calculated and observed intesities is shown by pink line below. Reflections positions are also shown.

5.9.3.2 Molecular modules of nicotinamide molecule showing possible conformations of amide functional group with respect to pyridine ring and vice versa.

5.9.3.3 Project on the [001] plane for the structural solution of azelaic acid : nicotinamide (1:1) adduct.

5.9.3.4 Project on the [001] plane for the structure solution of azelaic acid:nicotinamide (1:1) adduct.

5.9.3.5 Project on the [001] plane for the structure solution of azelaic acid : nicotinamide (1:1) adduct with swapped atoms.

5.9.3.6 Projection on the [001] plane for the crystal structure of azelaic acid:nicotinamide (1:1) adduct showing $R_2^2(8)$ and $R_4^4(28)$ rings in the unit cell.

5.9.3.7 ORTEP diagram of the azelaic acid : nicotinamide (1:1) adduct showing labelling of atoms and the interaction between the two former molecules. Thermal ellipsoids are drawn at the 50% probability level.

5.9.3.8 Stereoview of azelaic acid : nicotinamide (1:1) adduct, showing $R_4^4(8)$ and C(14) spiral molecular ladder along (1/2, 1, Z).

5.10.1 X-ray powder diffraction pattern for isonicotinamide and azelaic acid and product of crystallisation.

5.10.2 ^{1}H NMR of azelaic acid and isonicotinamide and product of crystallisation using DMSO as solvent. ^{1}H NMR 300MHz (DMSO-d_6): δ = 11.98(s, 2H), 8.70(dd, 2H), 8.25(s, 1H), 7.76(dd, 2H), 7.73(s, 1H) 2.18(m, 4H), 1.47(m, 4H), 1.23(m, 6H).

5.10.3 FTIR spectra for azelaic acid and isonicotinamide and product of crystallisation (1:1).

5.10.4 The Le Bail profile fitting for the product of isonicotinamide and azelaic acid crystallisation (1:1).

LIST OF TABLES

5.1.1 Indexed and refined cell parameters obtained for the product of oxalic acid and nicotinamide.

5.2.1 Indexed cell parameters of malonic acid and nicotinamide.

5.4.1 Summary of crystal data for adipic acid and nicotinamide co-crystal obtained form SXRD.

5.4.2 Intermolecular hydrogen bond lengths [Å] and angles [°] in the adipic acid and nicotinamide (1:2) co-crystal.

5.4.2.1 Cell parameters and space group from powder diffraction and single crystal data.

5.9.1.1 Indexed and refined cell parameters obtained for the product of azelaic acid and nicotinamide.

5.10.1 Indexed and refined cell parameters obtained for the product of azelaic acid and nicotinamide.

5.11.1 Table of new materials includes stoichiometries, status and corresponding starting materials.

LIST OF CHARTS

1.2.4.1 The percentage of published crystal structures which contain co-crystallized organic solvent molecules.

1.2.4.2 The percentage of solvates in which there are two or more different types of solvent molecules.

2.2.5.1 The percentage (in %) of the published co-crystal hydrates.

5.11.1 Chart showing melting points of starting materials corresponding products of crystallisation.

LIST OF ABBREBATIONS

API	Active pharmaceutical ingredient
GRAS	Generally Recognised As Safe
SDG	Solvent Drop Grinding
PXRD	Powder X-ray Diffraction Data
SXRD	Single crystal X-ray Diffraction Data
GSAS	General Structure Analysis System
DE	Differential Evolution
NMR	Nuclear Magnetic Resonance
FTIR	Fourier Transform Infrared spectroscopy
CSD	Cambridge Structure Database

LIST OF VARIABLES

F(s)	Fourier coefficient
$\rho(r)$	Electron density function
v	Volume of fundamental parallelepiped
F (DE)	Recombination
K	Mutation
Child	Child structure
Parent	Parent structure
$Random_1$, $Random_2$, $Random_3$	Random structures

1. INTRODUCTION

1.1 Supramolecular crystalline materials and crystal engineering

Over the past few decades, the 'crystal engineering' concept has stimulated interests in scientists belonging to many disciplines in materials chemistry and solid state chemistry[2]. The concept of crystal engineering was first introduced by Pepinsky in 1955[3, 4]. The engineering of organic crystalline structures designed on the basic principles of supramolecular chemistry and the application of its concepts to the synthesis of crystalline materials[4]. The term crystal engineering can be defined as "*the understanding of intermolecular interactions in the context of crystal packing and in the utilization of such understanding in the design of new solids with desired physical and chemical properties*"[5].

Crystal engineering has a wide range of applications in many fields, most recently through the development of pharmaceutical co-crystals[6]. Pharmaceutical co-crystallization is a method that has the potential to alter the physicochemical properties of an API (active pharmaceutical ingredient) without affecting its pharmacological properties[7]. Co-crystallization is a method of combining two or more "former" molecules using intermolecular interactions between the molecules without making or breaking covalent bonds[8]. This is often referred to as supramolecular synthesis. Co-crystals are most commonly thought of as structurally homogenous crystalline materials that contain two or more neutral building blocks that are present in definite stoichiometric amounts. By definition, these are materials that are prepared from reactants that are solids under ambient conditions (i.e. not hydrates or other solvates)[9]. However, the absolute definition of co-crystals is significantly still under debate in scientific journals and at conferences[5]. The construction of molecular co-crystals began as a predominantly academic interest for crystal engineers to investigate intermolecular interactions and intermolecular networks in families of molecular materials. The study of crystal behaviour enabled a wider range of materials to be systematically investigated as an alternative for covalent synthesis[10]. The results from this early work resulted in greater understanding of intermolecular interactions and self assembly contributing to key developments such as Etter's rules[11].

Solid state synthesis of pharmaceutical materials offers great potential in the context of green chemistry[12]. These methods give a high yield with out using any solvent or little solvent with maximum prevention from the formation of by-products[13]. The application of these ideas has more recently been seen in solid state drug design. Many drug molecules are not able to show their maximum potential due to their poor physical properties[9]. This novel approach has been used to address poor physiochemical properties via supra-molecular modification. Properties such as bioavailability, solubility and physical stability can be tremendously improved through co-crystallization and the process of co-crystallization is not restricted by the requirement of an ionisable centre on the API molecule[8]. The stability and reproducibility of these crystalline forms is also more preferable than common amorphous solids. The development of these new co-crystalline forms is expected to provide fertile ground for the creation of new patents and intellectual property[14].

A proper understanding of the solid state properties of crystal and amorphous forms is important in the development of pharmaceutical co-crystals[7]. Crystallization of two or more organic compounds with appropriate (donor and acceptor) functional groups using a solvent can result in the formation of co-crystals, ionic salts, solvates, hydrates or polymorphs. There is considerable interest in the pharmaceutical industry to identify all possible solid state forms of an API as their properties often vary from one form to another subsequently showing effect on physical properties and medicinal activity[15].

The phenomenon of polymorphism was recognised by Mitscherlich in 1822. The Aarone's definition of polymorphism says 'a solid crystalline phase of a given compound in the solid state' and this definition is appropriate in the context of pharmaceutical materials manifest themselves in to multiple modes of self assembly[15, 16]. A good co-crystallizing agent would form heteromeric intermolecular interactions with good flexibility towards different unit cell formations within the co-crystal[17]. Synthon flexibility and polymorphic behaviour are the essential qualities for a co-crystallizing agent. The ability of forming fruitful and multiple (different) intermolecular interactions between the molecules can be considered as synthon flexibility. The ability of H-bonding between molecules depends on donor and acceptor functional groups in the molecules[17].

1.2 Characterisation of organic materials from X-ray diffraction methods (PXRD and SXRD)

Crystal structure determination of organic materials from Powder X-ray diffraction (PXRD) data is feasible due to the recent advancements of 20th century in *ab initio* crystal structure determination studies, software data analysis and direct space methods. The Single X-ray diffraction (SXRD) technique is a powerful tool for determination of crystal structures and the structural information obtained from SXRD would be more accurate when compared to information obtains from PXRD[18]. But because of limitations towards microcrystalline materials and quality of crystalline materials, crystal structure determination from PXRD is a considered as potential method for structural characterisation despite of materials size and quality[13].

PXRD is most commonly used in the qualitative identification of materials for its property of having a unique characteristic finger print for each material. The aim of the crystal structure determination from either SXRD or PXRD is to establish the distribution of electron density in the unit cell and this requires the extraction of information in the form of diffraction intensities from the experimental data. The data obtained from PXRD and SXRD contains same structure information but in SXRD, the diffraction intensities are distributed in three dimensional space and in latter, the three dimensional data is compressed to one dimensional. As a result the information on individual diffraction intensities is obscured and hence the compressed one dimensional data would lose phase information[19].

The electron density within a unit cell is the reverse Fourier transform (FT^{-1}) of the diffraction pattern. The diffraction pattern from a crystal would be obtained from the below expression (see equation 1.2.6.1). The inverse of the above expression gives latter expression (see equation 1.2.6.2) for the electron density within the unit cell. The structure factors can be obtained from the diffraction peak intensities, but data for $\alpha(S)$ cannot be obtained. This is known as the Phase Problem. The direct crystal structure determination would be possible if both amplitude and phase information can be obtained from the powder X-ray diffraction data[20].

$$F(s) = \left| F(S) \right| \exp[2\pi i\alpha(s)] = \int \rho(r)\exp(2\pi is.r)dr \longrightarrow \quad (1.2.6.1)$$

$$\rho(r) = 1/v \sum \left| F(S) \right| \exp[\alpha(S)-2\Pi is.r] \longrightarrow (1.2.6.2)$$

Where F(s) = Fourier coefficient

$\rho(r)$ = electron density function

v = volume of fundamental parallelepiped

The crystal structure determination from PXRD mainly involves three steps. The first step is indexing X-ray diffraction patterns to obtain lattice parameters, crystal system and space group. The success rate of the whole method mainly depends on the first step. The second step is the application of direct space methods to obtain approximate structure solution for the crystal structure[13]. Differential search algorithms have been applied for the structural solutions throughout the current project. This optimisation technique is implemented based on the Darwinian principles of natural evolution which involves the processes of mating, mutation and natural selection. The last step involves refinement of structure solution using Rietveld refinement to obtain accurate crystal structure. The refinement of structure involves subjecting the molecular structural model to various bond lengths and bond angle restraints[18].

1.3 AIMS OF PROJECT

The aim of the current project is to synthesize binary co-crystals using solvent mediated crystallisation and solvent drop grinding methods using different solvents (methanol and ethanol) and stoichiometric ratios. The former molecules chosen for study have complementary functional groups (donor and acceptor) that can form potential supra-molecular bonds in the crystallisation process. Pyridine ring and amide functional groups on nicotinamide and isonicotinamide can form hydrogen bonds with carboxylic acid functional groups on di-carboxylic acids producing co-crystals or potentially salts. The crystal structures of any new materials will be solved using powder X-ray diffraction and Single crystal X-ray diffraction methods by the application of direct space and direct methods respectively. In PXRD, crystal structures are solved using differential evolution and Rietveld refinement techniques. This project also aims to investigate the potential effects of the variation of methods of synthesis, solvents and stoichiometric ratios on the cocrystallization behaviour and crystal structure of the resulting materials.

SPECIFIC AIMS:

- The synthesis of cocrystalline molecular materials of nicotinamide and isonicotinamide with a series of selected α,ω–alkanedicarboxylic acids:
    - Oxalic acid
    - Malonic acid
    - Succinic acid
    - Adipic acid
    - Pimelic acid
    - Suberic acid
    - Azelaic acid
- Attempted synthesis of these materials by solvent mediated crystallization from ethanol and methanol under ambient conditions and from solvent drop grinding.
- Co-crystallization of from different starting stoichiometric ratios.

- Characterization using powder X-ray diffraction data to conform the formation of new material.
- Characterization of new materials using NMR (to identify stoichiometries) and IR techniques (co-crystal formation).
- Analysis of melting points of new materials with respect to the starting materials.
- Crystal structure determination using single X-ray diffraction and powder X-ray diffraction methods.
- Discussion and analysis of new structures relative to each other and other previously published structures.

2. MATERIALS UNDER INVESTIGATION

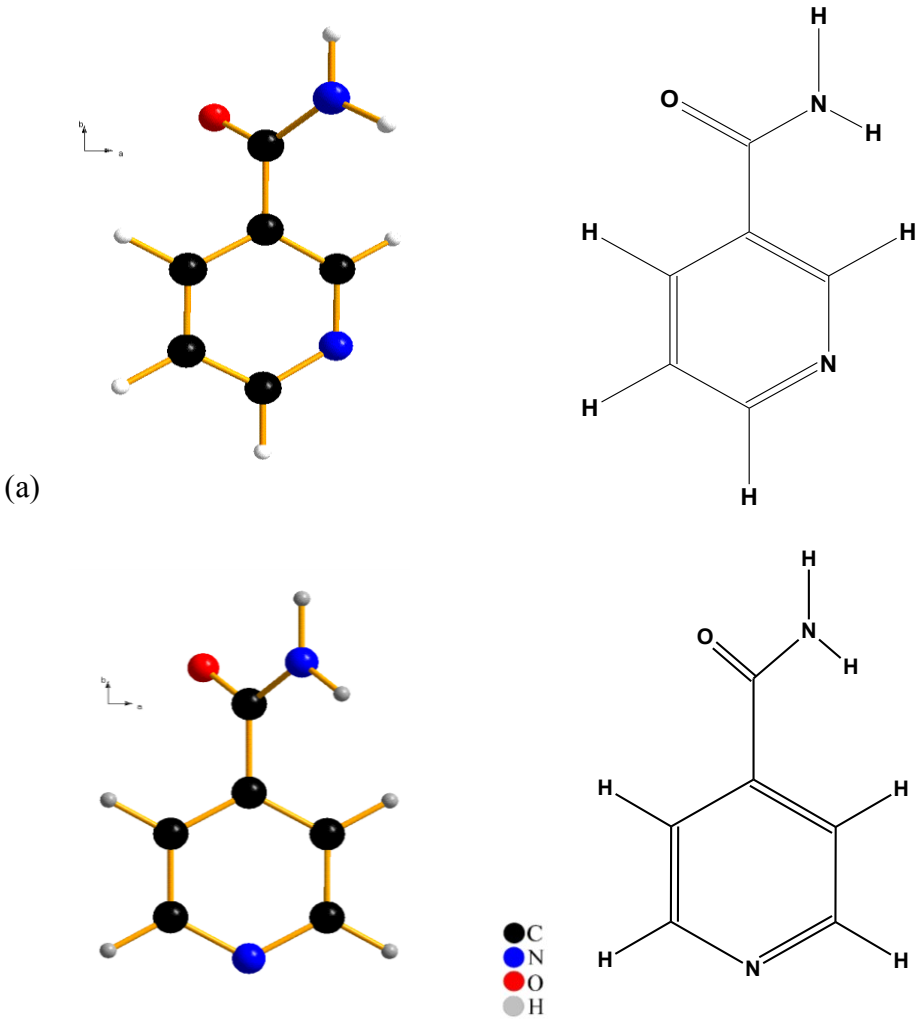

Figure 2.1: Molecularstructures of (a) Nicotinamide and (b) Isonicotinamide.

Nicotinamide and isonicotinamide (see figure 2.1) were used commonly throughout the project in crystallisation with dicarboxylic acids in the synthesis of binary co-crystals. The structures of the two molecules are structurally similar but differ in position of the N atom in the pyridine rings. Nicotinamide is also known as vitamin B_3. These two 'former' molecules were investigated in combination with the α,ω-dicarboxylic acids shown in figure 2.2 with the aim of investigating and comparing the structural behaviour of nicotinamide and isonicotinamide by study of the crystal behaviour and properties of materials formed[6, 21]. The alternation in melting points with increase in carbon chain in the dicarboxylic acids adducts was also investigated.

Carboxylic acids are known to act as good electron acceptors and electron donors and they often participate well in supramolecular reactions. Carboxylic acids also come under the category of GRAS (Generally Recognised as Safe) as defined by the FDA (the Federal Drug Agency)[22] and hence are potential co-crystal formers for combination with an API in pharmaceutical materials.

Figure 2.2:

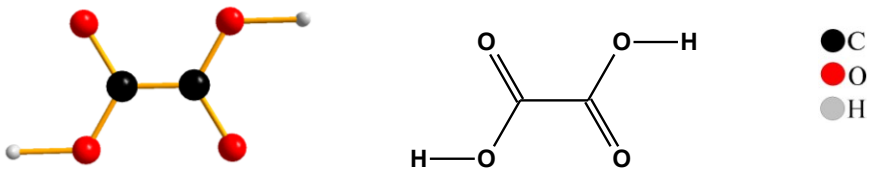

(a) Molecular structure of oxalic acid

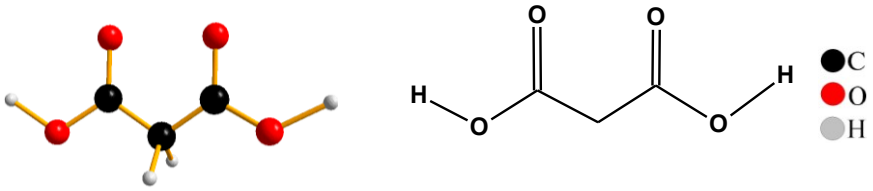

(b) Molecular structure of malonic acid

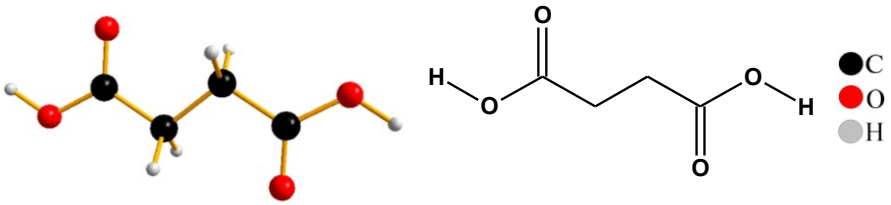

(c) Molecular structure of succinic acid

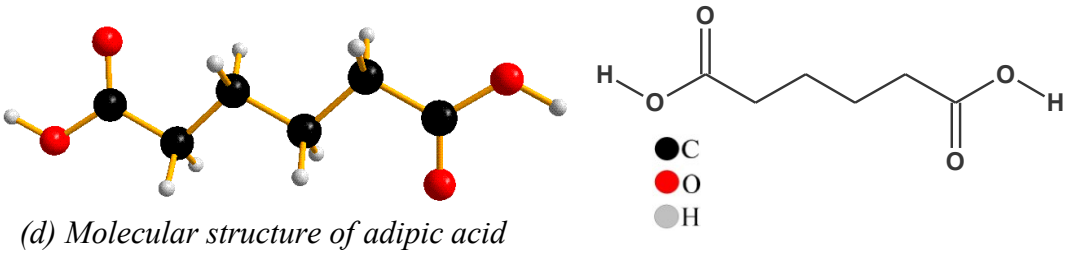

(d) Molecular structure of adipic acid

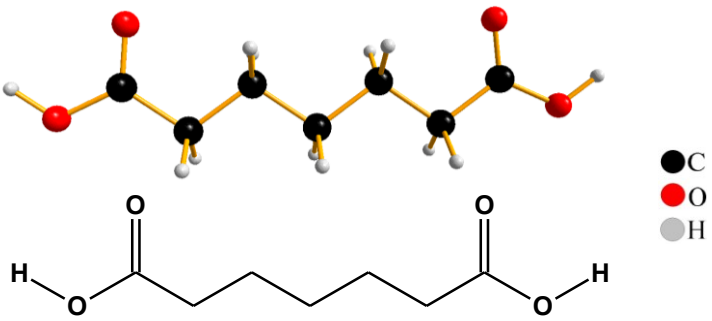

(e) Molecular structure of pimelic acid

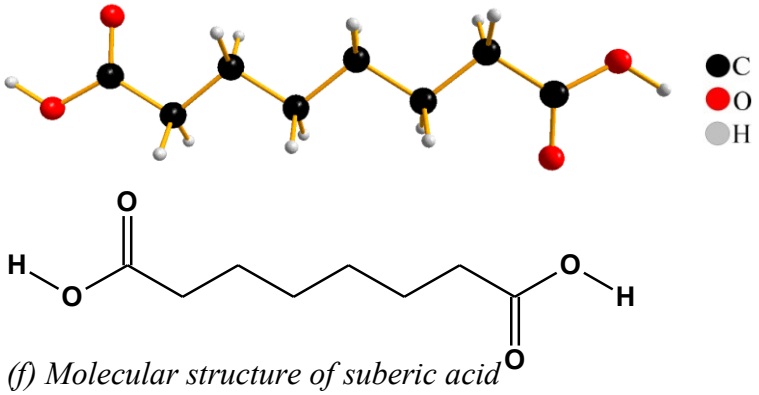

(f) Molecular structure of suberic acid

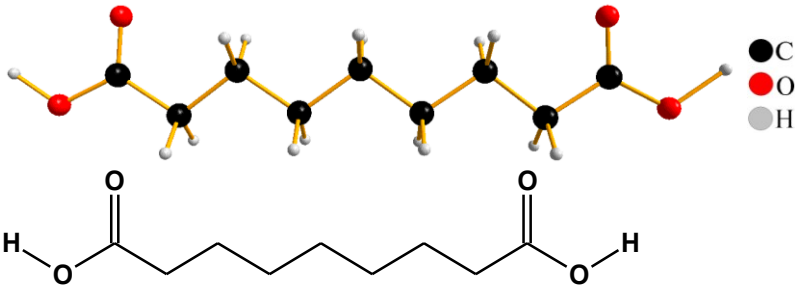

(g) Molecular structure of azelaic acid

2.1 Synthon flexibility

Crystal engineering of organic materials relies on the supramolecular building of crystalline solids based on the interaction of functional groups point of view. For the study of these crystalline materials, it is important to have a knowledge and understanding of intermolecular interactions between various functional groups[8, 23]. Functional groups such as carboxylic acids and amides are known to form robust synthons in the absence of other strong hydrogen bonding functional groups. The change in a common hydrogen bonding pattern of a particular functional groups can be observed, due to the presence of other functional groups in a molecule. An understanding of these interference effects is very important in crystal engineering and can be used in the design of preformed architectures. The factors to be considered are the matching of the strengths of donor and acceptor, cooperative effects of a synthon, balance between the number of donors and acceptor and solvation effects[24].

The effective and rapid synthesis of new materials is the main attraction in supramolecular chemistry with the ability to change physical properties e.g., solubility, crystal morphology, mechanical stability. Molecules with reliable functional groups are ideal candidates to engage in supramolecular heteromeric intermolecular interactions leading to successful co-crystallisation. This project deals with nicotinamide and alkyl dicarboxylic acid molecules with complementary functional groups (carboxylic acid, amide and *pyridine* N) and investigates the preferred formation of homomeric motifs or heteromeric synthons.

The presence of two carboxylic acid groups in the diacids potentially allows formation of products with different stoichiometric ratios of acid-amide components. By using a series of alkyl dicarboxylic acids, the effect of increased hydrophobicity and flexibility with systematic increase in carbon chain length can be related to any variation of stoichiometry in the resulting materials. These molecules would form synthons N···H-O, N-H···O, C-H···O and O-H···O intermolecular bonds when they are crystallised with nicotinamide and isonicotinamide molecules with potential pyridine and amide functional groups. There has been significant research going on co-crystallisation of dicarboxlic acids and APIs with complementary functional groups attracting pharmaceutical industries to rely on such molecules as potential

supramolecular reagents for crystallisation of pharmaceutical materials. Crystal structures of molecules with functional groups similar to isonicotinamide and dicarboxylic acids tend to display a few common intermolecular interactions, hence various combinations can be expected when such molecules are engaged for co-crystallisation (see figure 1.2.6.1).

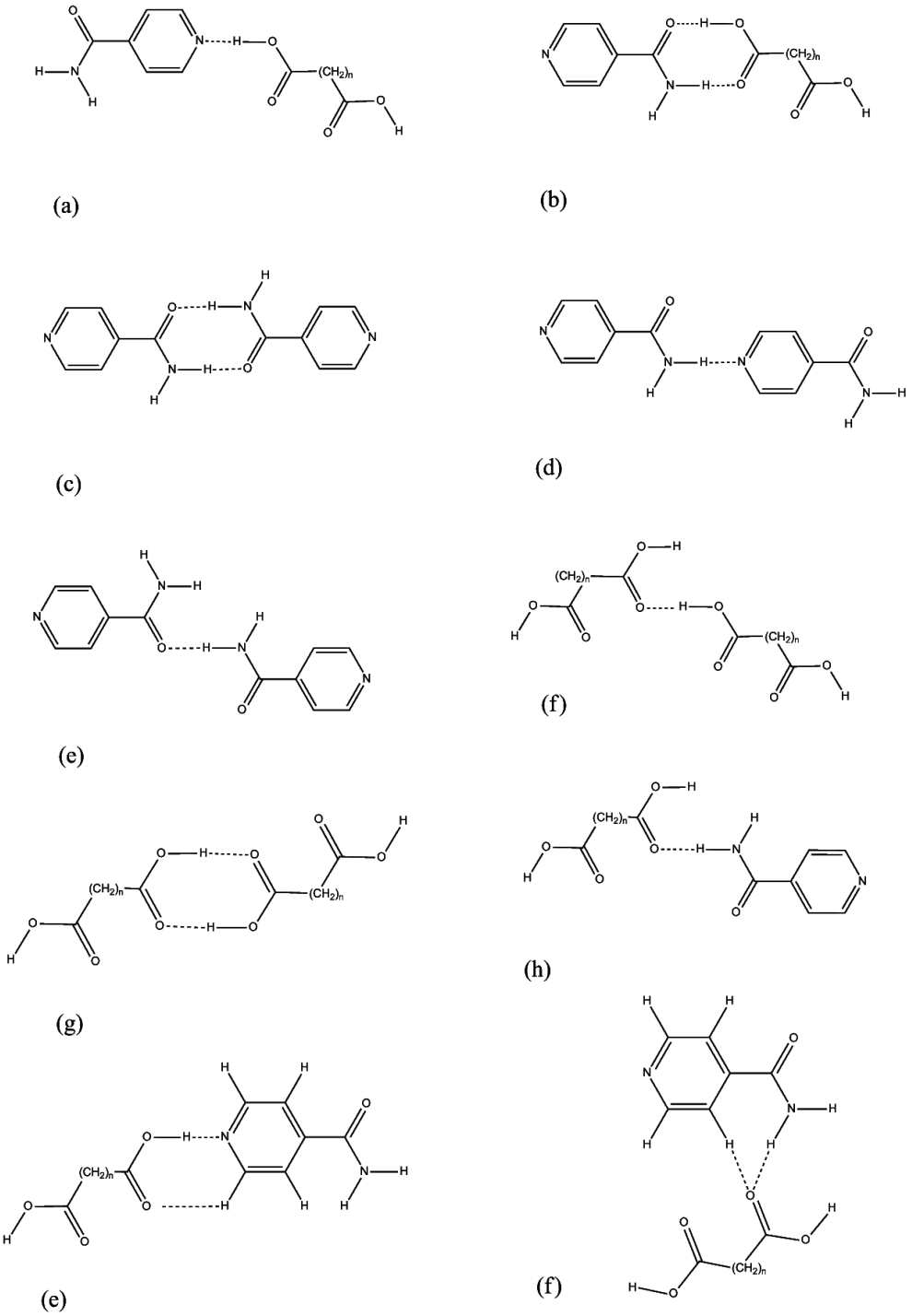

Figure 2.1.1: Schematic diagram showing potential supra-molecular synthons in co-crystals formed by isonicotinamide and di-carboxylic acids.

An important consideration while selecting organic molecules for potential co-crystallisation is to choose a crystallising agent that displays polymorphism. Polymorphic materials have the potential ability to form heteromeric intermolecular interactions, with the target molecule rather than homomeric interactions showing degree of structure flexibility. Aakeröy identified isonicotinamide, 2-amino-3-nitropyridine, 4-chlorobenzamide and maleic hydrizide as potential polymorphic molecules to form multiple hydrogen bonds and heteromeric synthons (see figures 1.2.6.2 (a-d))[17].

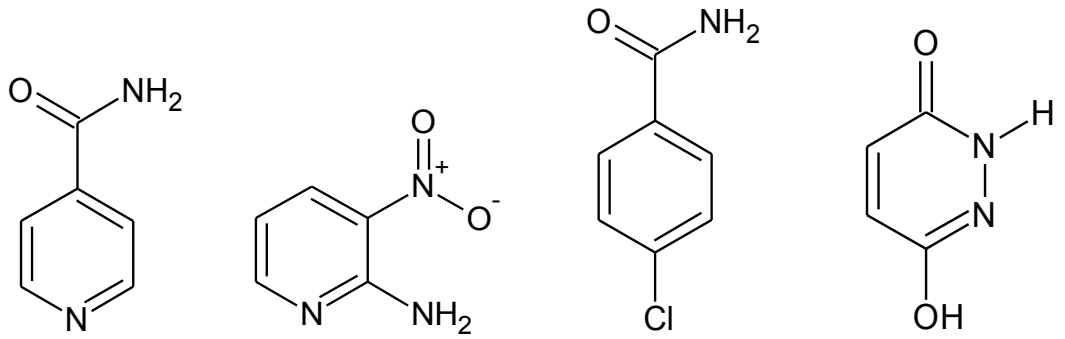

(a) (b) (c) (d)

Figure 2.1.2: Molecules capable of forming a variety of hydrogen bonded synthons : (a) isonicotinamide, (b) 2-amino-3-nitropyridine, (c) 4-chlorobenzamide and (d) maleic hydrazide.

One area of current interest in crystal engineering of organic materials is the synthesis of co-crystals using supramolecular reactions by establishing preferential hydrogen bonds. The formation of hydrogen bond interactions between molecules follows a hierarchical order; best donor to best acceptor; second best donor to second best acceptor[11]. In the example below, the best donor (carboxylic acid) and the best acceptor (heterocyclic ring) form a heteromeric motif while a homomeric motif is formed between the amide moieties (second best donors and acceptors) (see figure 1.2.6.3).

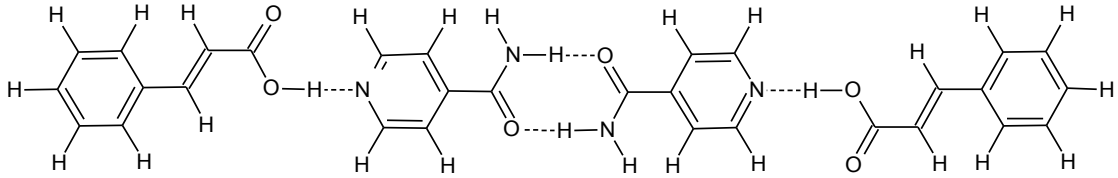

Figure 2.1.3: Carboxylic acid : isonicotinamide (1:1) co-crystal showing different intermolecular interactions between the molecules.

Aakeröy and co-workers[8] and Nangia[24] and co-workers have been amongst groups that have been successful in the exploitation of Etter's rule to design binary complexes of nicotinamide and isonicotinamide co-crystals with carboxylic acids[8]. In these structures, carboxylic acid interacts as strong proton donor and pyridine as strong acceptor. All the structures indicate that the acid-pyridine synthon is favoured over amide-acid and amide-amide motifs according to the hierarchy of the interactions[17]. However, there are several reports indicating that the result of crystallization experiments does not necessarily obey the hierarchy of interactions or the complementarities of the components. The final outcome of the crystallization depends on several other factors such as solvent, dilution, rate of evaporation and solvent of the components[23].

Analysis number of a crystal structures (and their intermolecular interactions) in the CSD through the crystallisation of di-carboxylic acids with heterocyclic N compounds allows for the prediction of a few common synthons and motifs based on the nature and behaviour of functional groups in the molecular structures (see figure 1.2.6.14). The acid – pyridine heteromeric synthon is a common intermolecular bond present in all crystal structures of this type (see figures 1.2.6.5-1.2.6.13). Hence, it is strong intermolecular bond among synthons formed by molecules with pyridine, carboxylic acid and amide functional groups (1.2.6.14 (a)). Amide – amide homomeric motifs are found in crystal structures with components in 1:2 stoichiometric ratios (1.2.6.14 (g)). Similarly, acid – amide heteromeric synthons are only observed in 1:1 crystal structures (1.2.6.14 (c)). No specific sequence was found with the presence of other synthons (1.2.6.14 (b – h)). Weak intermolecular bonds (1.2.6.14 (e, f)) are observed in all crystal structures as reinforcing on binding links often between the chains and ribbons found in these structures.

For effective and promising co-crystallisation, the former molecules should have potential hydrogen bond donor and acceptor groups with desired pK_a values for the formation of supramolecular bonds between the molecules. For the formation of a salt, a difference of $pK_a \geq 3$ is desirable between an acid and a base. The equilibrium pK_a values between former molecules is considered as an important criterion for the formation of a co-crystal. Almarsson and Zaworotko[25] illustrated salt and a co-crystal formation between saccharin and different former molecules with a wide range of

functional groups, and observed that the molecules with pK_a difference > 3 form salts (see figure 1.2.6.4) whereas structures with equilibrium pK_a values formed co-crystals.

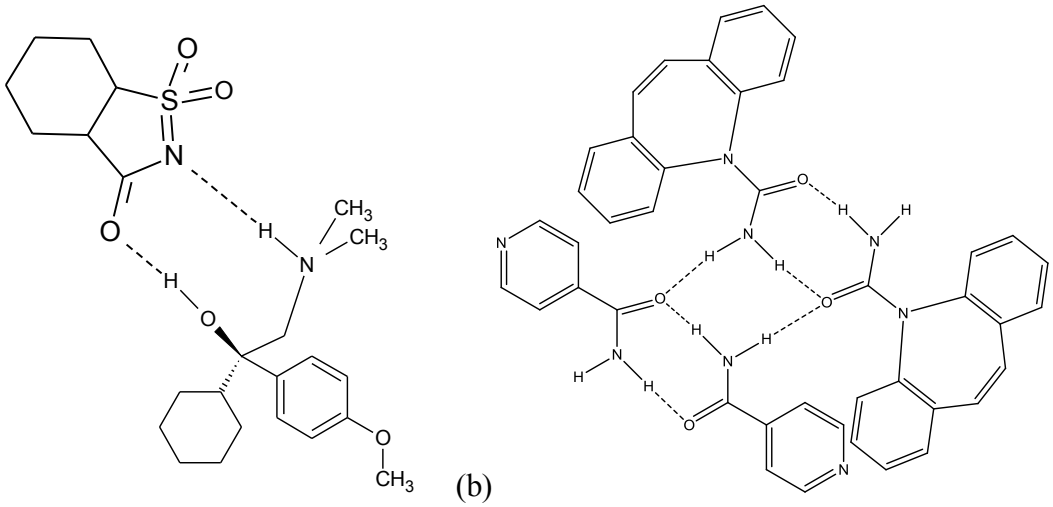

Figure 2.1.4: (a)Venlafaxine saccharinate showing $N^{(+)}$-H···N and O-H···O=C interactions between the two components and (b) Carbamazepine isonicotinamide showing N-H···O interactions between the two components.

The alternation in structural behaviour and properties with change in the number of methylene groups in α,ω-alkanedicarboxylic acids has also attracted attention for further investigation towards an understanding behaviour of such molecules. Vishweshwar et al. correlated the structures of α,ω-alkanedicarboxylic acids with the properties of the relative isonicotinamide co-crystals. They investigated co-crystals synthesized through the crystallisation of oxalic acid, malonic acid, succinic acid, glutaric acid and adipic acid with isonicotinamide. All products were obtained in a 1:2 stoichiometric ratio. Co-crystallisation of glutaric acid and adipic acid with isonicotinamide formed new materials in both 1:1 and 1:2 stoichiometric ratios[21]. Polymorphism has also been reported in the case of oxalic acid:isonicotinamide (1:2); the significant difference between the crystal structures of these polymorphs is due to differing conformation (cis and trans) of the oxalic acid molecule[26]. Fumaric acid is also of interest with a molecular structure similar to that of succinic acid[27]. Other materials that have been co-crystallised with dicarboxylic acids include cyclic amides 2-pyrrolidinone, 2-imidazolidinone, benzamide etc[21, 22].

In the oxalic acid : isonicotinamide (1:2) form I and form II co-crystals, the crystal structure is stabilized by O-H···N*(heterocyclic)* interactions, centrosymmetric homomeric amide motifs formed through N-H···O=C *(pyridine)* interactions, and C-H···O=C (carbonyl) and N-H···O=C(carbonyl) intermolecular interactions. Although the stable conformation of the oxalic acid molecule is *anti conformation (see figure 1.2.6.6)*, the oxalic acid molecule in one of the polymorphic forms exits in the *syn conformation (see figure 1.2.6.5)*.

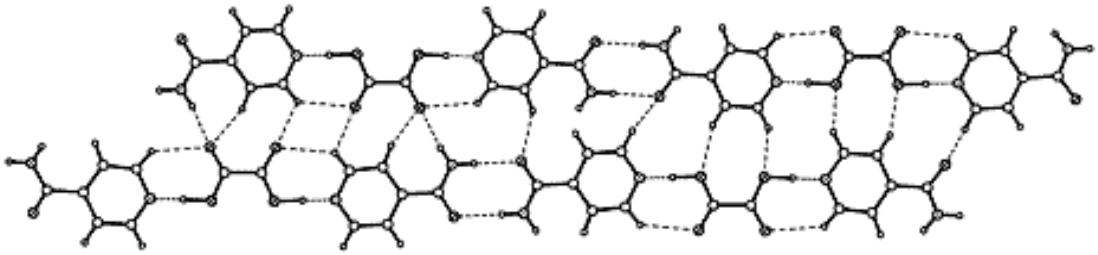

Figure 2.1.5: A view of the crystal structure of oxalic acid : isonicotinamide (1:2) form I co-crystal showing intermolecular interactions.

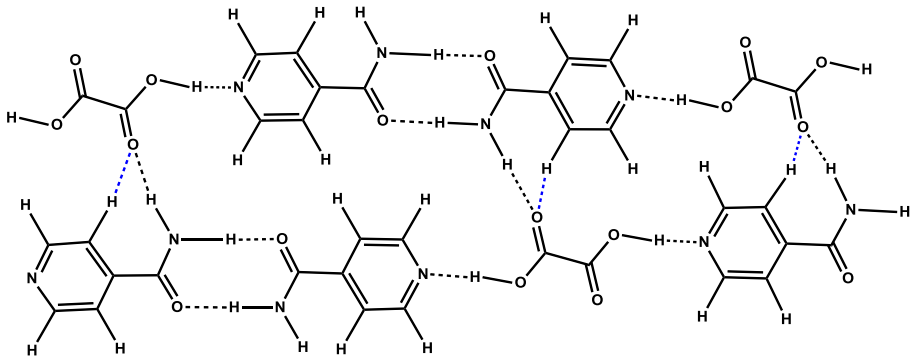

Figure 2.1.6: A view of the crystal structure of oxalic acid : isonicotinamide (1:2) form II co-crystal showing intermolecular.

The malonic acid : isonicotinamide (1:2) adduct is stabilized by different intermolecular bonds between the molecules. The tapes in the crystal structure are formed by O-H···N*(heterocyclic)* intermolecular interactions and these tapes are combined by (methylene)C-H···O(carbonyl) intermolecular bonds. There are also weak intermolecular bonds *(pyridine)*C-H···O=C (blue colour dotted) that reinforce the tapes shown in figure 1.2.6.7) along with the strong former intermolecular bonds.

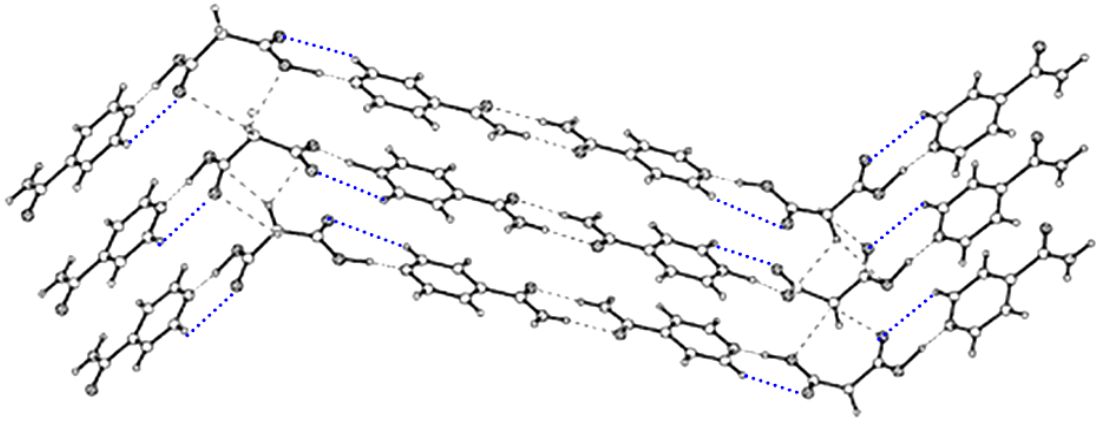

Figure 2.1.7: A view of the crystal structure of malonic acid : isonicotinamide (1:2) co-crystal showing intermolecular interactions.

The succinic acid : isonicotinamide (1:2) co-crystal is also stabilized through O-H···N*(heterocyclic)* heteromeric synthons, homomeric centrosymmetric motifs formed through N-H···O=C intermolecular bonds and N-H···O=C linking these tapes together. Along with strong intermolecular bonds, there is again a number of weak intermolecular bonds reinforcing the structure (blue colour dotted intermolecular bonds shown in figure 1.2.6.8).

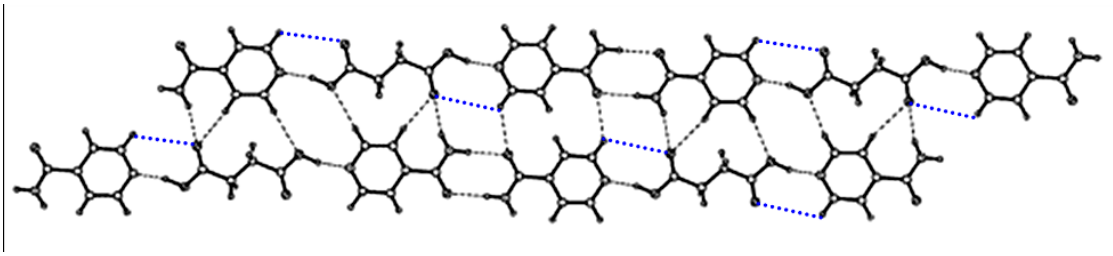

Figure 2.1.8: A view of the crystal structure of succinic acid : isonicotinamide (1:2) co-crystal showing intermolecular interactions.

The glutaric acid:isonicotinamide (1:1 and 1:2) co-crystals are stabilized through heteromeric synthons O-H···N*(pyridine)*, homomeric centrosymmetric motifs formed through N-H···O=C intermolecular bonds, *(pyridine)*C-H···O=C, N-H···O(COH) and N-H···O=C supramolecular bonds (see figures 1.2.6.9 and 1.2.6.10). The significant difference between the crystal structures of two stoichiometric ratios can be seen in the formation of amide dimers in 1:2 and heteromeric dimers (acid:amide) in 1:1. The molecular ribbons in 1:1 were linked by intermolecular bonds between carbonyl O and amide H. In 1:2, these ribbons are combined by intermolecular bonds between hydroxyl O and amide H.

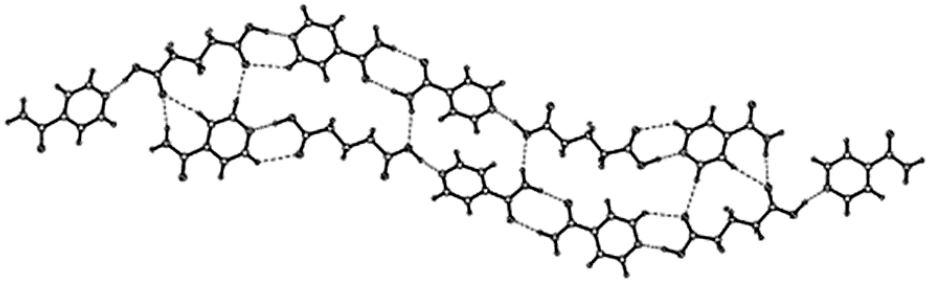

Figure 2.1.9: A view of the crystal structure of glutaric : isonicotinamide (1:1) co-crystal showing intermolecular interactions.

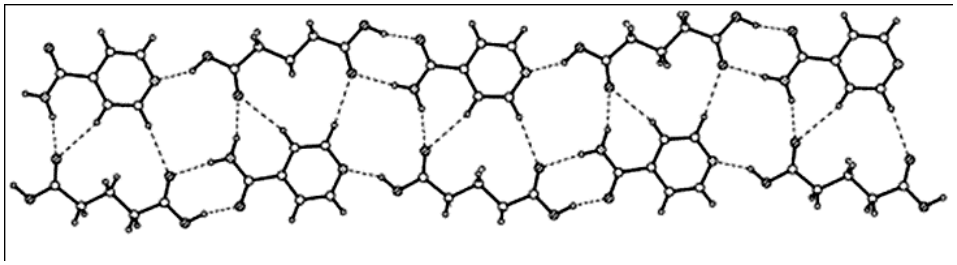

Figure 2.1.10: A view of the crystal structure of glutaric acid : isonicotinamide (1:2) co-crystal showing intermolecular interactions.

The co-crystals resulting from the crystallisation of adipic acid and isonicotinamide were also obtained in both 1:1 and 1:2 stoichiometric ratios and were stabilized through heteromeric synthons O-H···N*(heterocyclic)*, homomeric centrosymmetric motifs and heteromeric synthons formed through N-H···O=C synthons, *(pyridine)*C-H···O=C and *methylene* C(H)-H···O=C intermolecular bonds (see figures 1.2.6.11 and 1.2.6.13). The adipic acid in folded S-conformation in the crystal structure (1:1) is stabilized due to C-H···O=C intramolecular bonds within the molecule (see figures and 1.2.6.13). Along strong intermolecular bonds, there would be the possibility for the existence of weak *(pyridine)* C-H···O=C intermolecular bonds (blue colour dotted intermolecular bonds shown in figure 1.2.6.12). Similar strong intermolecular bonds can be observed in co-crystals formed through the crystallisation of oxalic acid, malonic acid, succinic acid, glutaric acid and adipic acid with isonicotinamide in 1:1 and 1:2 stoichiometric ratios. The molecular frameworks in 1:1 co-crystals are observed with heteromeric dimers (acid : amide) and 1:2 co-crystals with homomeric amide dimers. The common strong intermolecular bond appears in both stoichiometric co-crystals is O-H---N*(pyridine)*.

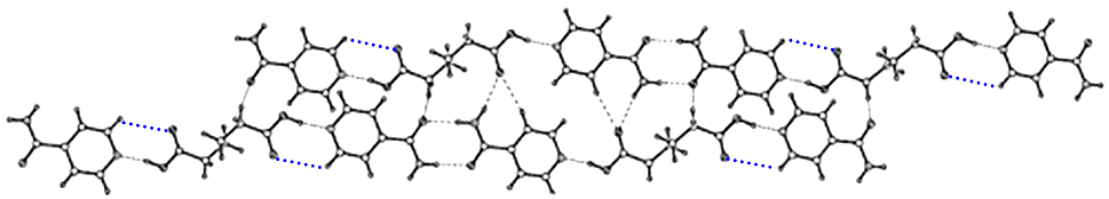

Figure 2.1.11: A view of the crystal structure of adipic acid : isonicotinamide (1:2) co-crystal showing intermolecular interactions.

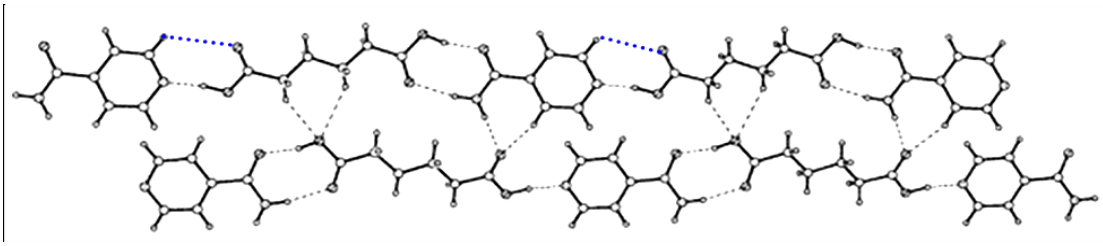

Figure 2.1.12: A view of the crystal structure of adipic acid : isonicotinamide (1:1) co-crystal showing intermolecular interactions.

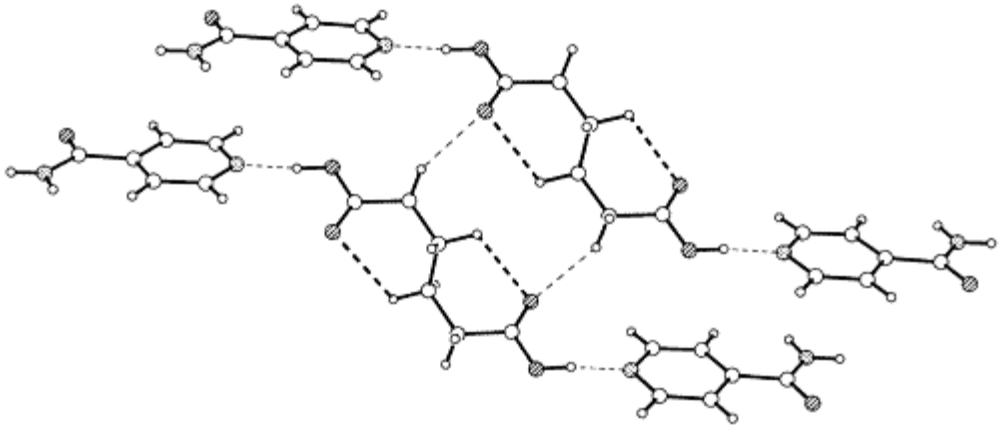

Figure 2.1.13: Folded S-conformer of adipic acid in adipic acid:isonicotinamide (1:2) co-crystal. The intramolecular C-H···O hydrogen bonds is shown with bold dash lines.

The summarization of a number of crystal structures (and their intermolecular interactions) in the CSD through the crystallisation of diacids with heterocyclic compounds implies possibility for the prediction of few common synthons and motifs relying on nature and behaviour of functional groups in the molecular structures.

2.2 Methods and Materials

Co-crystals are formed if different molecules with complementary functional groups form hydrogen bonds that are thermodynamically more favourable than those between like molecules of either component[28]. Individual components are obtained after crystallisation if the formation of these alternative bonding networks is not energetically favoured. Depending upon the composition of the resulting crystal structures, co-crystals can be further classified as polymorphic, solvated and hydrates[8]. The most energetically favoured crystal structures obtained through crystallisation can also differ by inducing different stoichiometries (ratio of starting materials), solvents or different crystallisation methods. The existence of more than one new co-crystalline material with the same composition or stoichiometric ratio is also polymorphism[12, 15]. Inclusion of one or more solvent molecule results in a solvated co-crystal. Similarly, inclusion of one or more water molecule results in a hydrate[29].

2.2.1 Solvent-mediated crystallization

The most common approach to the synthesis of co-crystals is solvent-mediated crystallisation in which two or more suspensions are obtained by dissolving stoichiometric amounts of starting materials in a solvent, mixing these together, and storage under optimized temperatures for co-crystallisation. The formation of the product depends on the relative solubility of the starting materials, experimental temperature and functional groups in the former molecules. The formation of a co-crystalline product can vary with concentrations of starting materials (stoichiometric ratios) and solvents and most likely a new co-crystalline form would be obtained unless co-crystal form is more stable than individual pure forms with minimal solubility. Although, sublimation, growth from the melt, sonic slurry and the grinding of solid formers in a ball mill are also suitable methodologies for the synthesis of co-crystals, solvent mediated transformation is simple, flexible and adaptable with many possible configurations for co-crystal synthesis[4, 30].

An important goal of solid-state pharmaceutical development is to optimize drug solubility while preserving drug activity. Co-crystals have emerged as a promising

means to modify solubility, dissolution, and other physicochemical properties of drug substances. Solubility is a complex parameter and in this work effects both this effectiveness of the co-crystal formulation in terms of drug solubility and bioavailability and in the initial synthesis of the co-crystal itself. Solubility has been cited to depend on the enthalpy of fusion, temperature of the solvent, melting point of the solid, hydrogen bonding in the solid and solvent, and other polar and non-polar forces in the solvent and the solute. It has long been known that hydrogen bonding networks, along with other intermolecular forces, are known to contribute to effect physical properties of solids[5, 30]. When two or more suspensions are obtained by the dissolution of stoichiometric amounts of starting materials in a solvent and mixed together, and storage under optimized temperatures for co-crystallisation, the concentration of solution slowly increases. At a certain concentration, crystallization would start the formation co-crystals, leading to equilibrium point where three forms (L+A, L+B, L+AB) coexist; where L is liquid, A and B are the initial solid components and AB is the co-crystal form. Phase solubility and triangular phase diagrams are used to represent the solubility and stability of co-crystals[3] (see figure 1.2.1) and can be used to optimise conditions for co-crystal formation rather than recrystallisation of the individual components[31].

Figure 1.2.1(a) shows a schematic triangular phase diagram at constant temperature for an API A, coformer component B, and solvent in which A is more soluble than B. At low concentrations of A and B in region L, a clear liquid exists. Overall compositions in the L+A, L+B, or L+AB region eventually equilibrate to comprise a liquid with a composition on the solubility line of A, B or AB respectively. Between these regions, mixtures of three phases can coexist (L+A+AB and L+B+AB). A composition in these regions eventually equilibrates to a liquid with a composition of the three-phase equilibrium point (the intercept of the pure component solubility line and co-crystal solubility line), and a solid mixture of AB crystals and A crystals (in the L+AB+A region) or AB crystals and B crystals (in the L+AB+B region).

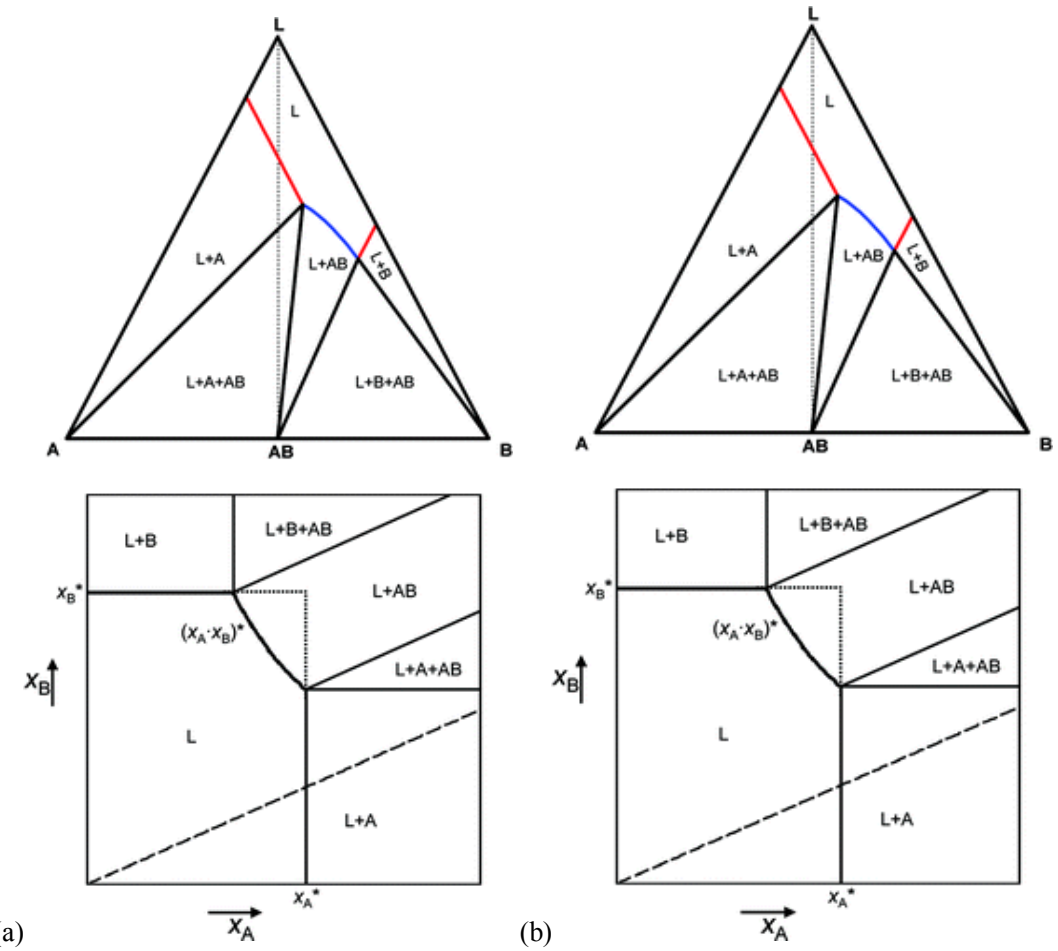

Figure 2.2.1.1: (a) A schematic ternary phase diagram for a highly soluble co-crystal system in solution at constant temperature. (b) A schematic phase diagram for slightly soluble components and co-crystal[30].

Figure (b) represents an alternative schematic phase diagram in which both components are slightly soluble. It shows a horizontal line for the coformer component solubility x_B*, a vertical line for the API solubility x_A*, and a curved line for the co-crystal solubility $(x_A.x_B)$*. Here it is assumed are that the solubility of each component is not affected by the presence of the other, except where a co-crystal is formed, and the solubility product $(x_A.x_B)$* of the co-crystal at a certain temperature is essentially constant. Both phase diagrams show a specific region (L+AB), in which only the co-crystal is in stable equilibrium with the solution. Both components A and B are needed in specific concentrations, defined by the boundaries of the (L+AB) region, in order for the co-crystal to be more stable than the pure component crystals and to be the sole solid phase present after equilibration.

A solution with overall composition inside the co-crystal region at the specified temperature will eventually co-crystallize as this is the most stable solid phase in the co-crystal region. Similarly, a suspension prepared from pure components with an overall composition inside the co-crystal region will also eventually co-crystallize. The use of such phase diagrams is a key tool in co-crystal synthesis.

2.2.2 Solvent drop grinding or liquid assisted grinding (SDG)

One approach used to circumvent unfavourable solubility issues that are often highlighted in the phase diagram as in section 1.2.1 is the use of mechanochemical methods. Binary co-crystals can be synthesized either by neat grinding of the two starting materials or in the presence of small amount of liquid phase or solvent (liquid assisted grinding or solvent drop grinding). SDG is a new promising and green process to accelerate the synthesis of co-crystals by grinding of starting materials with the addition of little solvent [32, 33]. It is anticipated that this approach will open new avenues in both the synthesis and characterisation of co-crystals, despite the limitations to characterize many materials obtained using this method by single-crystal X-ray diffraction. With this limitation in mind, this project also aims to explore the characterization of binary co-crystals made in this way by determination of crystal structures from PXRD (Powder X-ray diffraction data)[2, 29, 34]. This synthetic approach has the potential to produce co-crystals of new stoichiometry or a solvent-free adduct that cannot be prepared by traditional crystallisation approaches[33].

Co-crystals are often prepared by a traditional solvent mediated crystallisation approach and there are a number of reasons for the popularity of this approach. Solution crystallisation can yield single crystals with sufficient size, from which one may easily evaluate the crystal structure, crystal habit and surface features. However, there are several drawbacks to the solution crystallisation approach. The solubility of the starting components is one, as a suitable solvent for all starting materials must be identified before co-crystallisation may occur. Unexpected solvate formation and the large quantities of solvents necessary to prepare co-crystals in this way may also pose problems in forming desired the co-crystalline materials.

2.2.3 Salts and co-crystals

When an acid and a base are crystallized together using an appropriate solvent, the outcome would be salt or a co-crystal. The APIs having ionisable functional groups when crystallized with former molecules with complementary functional groups would form salts rather than co-crystals with non-covalent intermolecular bonds. The strategy behind the formation of a salt is an acid, a base and one or more solvents[9]. A salt is formed by transfer of proton from the acid to a base i.e., simple proton transfer between a donor and an acceptor and co-crystals are obtained through the formation of strong hydrogen bonding or non-covalent intermolecular bonds between a donor and an acceptor. For example, the synthons formed with as O–H···N intermolecular interaction is a co-crystal and one with O^{-}–H···N^{+} a salt (see figure 1.2.3.1). To determine the general differences between the reliability and predictability of the physical properties of salt and co-crystal forms, Aakeröy selected 85 crystal structures of which 61 are co-crystals and 24 are salts. (This study was confined to pyridine/benzoic acid and benzoate fragments). 58 out of 61 co-crystals (no solvates) and stoichiometrics are expected. 24 out of 85 structures were found to be salts resulting from a proton transfer from the acid to a nitrogen atom in an N-heterocyclic. Thirteen out of 24 compounds displayed the expected stoichiometry and primary intermolecular interactions. 9 out of 24 salts displayed an unpredictable stoichiometry resulting from the incorporation of carboxylic acid into the lattice.

(a)

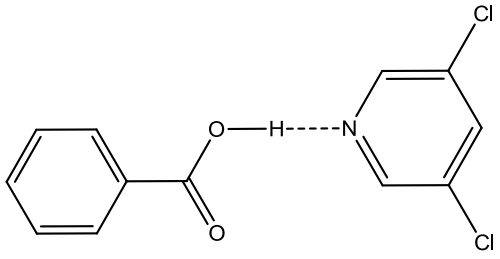

(b)

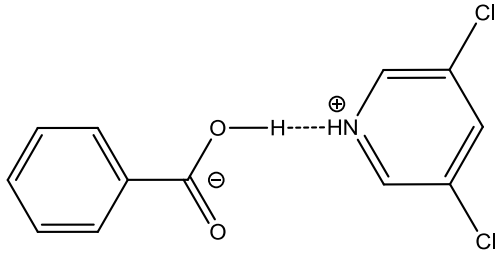

Figure 2.2.3.1: Formation of a supramolecular adduct and as ionised adduct of benzoic acid : dichloropyridine in (a) co-crystal and (b) salt forms.

Co-crystals and salts show dramatic difference in terms of crystal behaviour and physical properties. The molecules with ionisable centres can form salts with appropriate counter ions. Varying the salt forms changes properties such as solubility and dissociation rates. A salt form involves a three component system of an acid, base and one or more solvents. A salt is formed by transfer of a proton from an acid to a base and it requires atleast 3 pK_a units between them. In the example below (see figure 1.2.3.2), the carboxylate moiety is not readily satisfied with a single hydrogen donor, so, it tends to react further with other neutral carboxylic acid molecule. The neutral carboxylic acid is less powerful to bring another carboxylic acid. This example shows that the absence of functional groups such as amides in the starting components may lead to unexpected lattices. Such groups are capable of adding extra hydrogen donors.

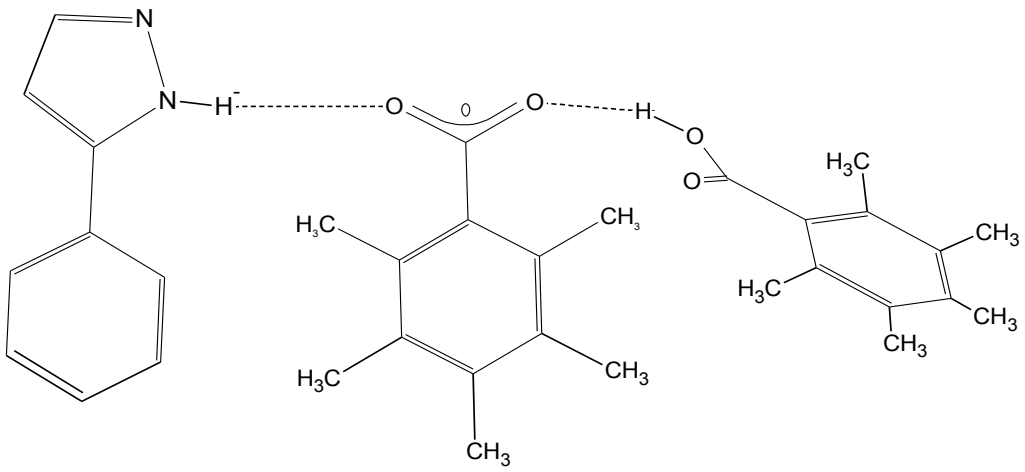

Figure 2.2.3.2: Example showing both proton transfer and supra-molecular synthons in 3-(4-pyridinium)-pyrazolepentamethylbenzoate pentamethyl benzoate : pentamethyl benzoic acid.

2.2.4 Co-crystal Solvates

The term 'solvate' defines the inclusion of one or more solvent molecules in the crystal structures and is sometimes called solvatomorphism. Solvatomorphism can be defined as the existence of a solvates with different crystal structures and same elemental composition along with inclusion of one or more solvent molecules in the crystal structure[35].

Solvents play a major role in the successful crystallization of starting materials (pure forms) to obtain different crystal structures. New materials formed through solvent mediated crystallisation can be either co-crystal, solvates, hydrates or salts, however the presence of solvent in many crystal structures can be considered as an advantage. Large crystal structures with empty cavities are often unstable and inclusion of solvent molecules can improve the stability of such crystal structures[35].

Solvent molecules play a role in the stabilization of crystal structures in different ways; the molecules can participate in hydrogen bonding as an integral part of the crystal structure network or as a space filler without strong interaction with other molecules in the crystal structure. Solvent molecules having ketone, hydroxyl and alkyl groups can act as bridges between polar and non polar regions in the crystal structures. It is interesting to note from the figures below that the proportion of solvates in the Cambridge Structural Database has dramatically increased in recent years (see charts 1.2.4.1 and 1.2.4.2).

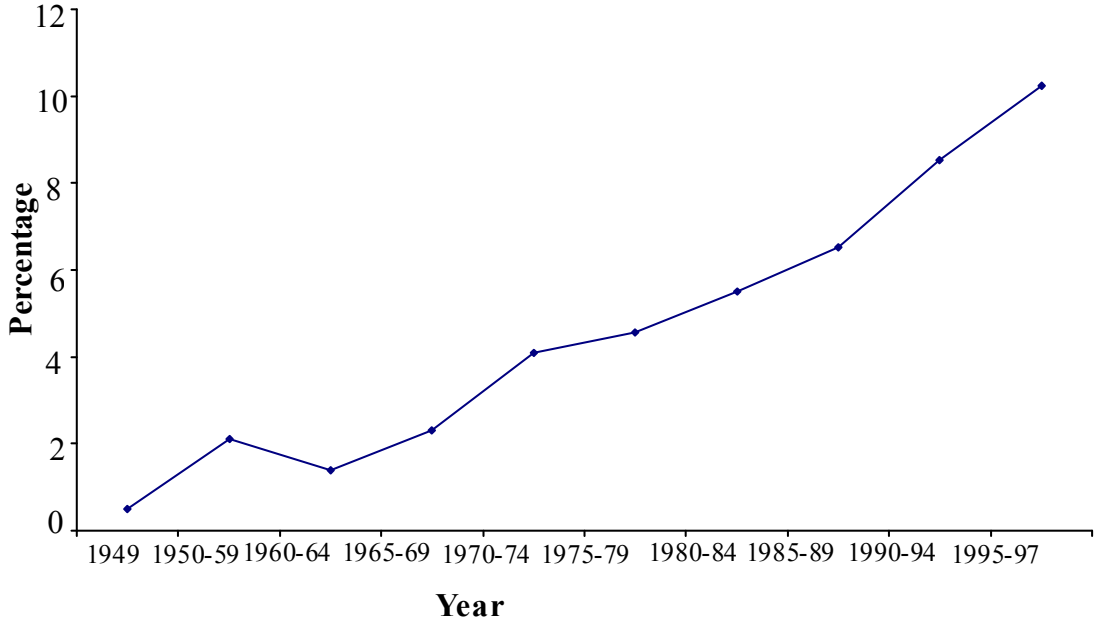

Chart 2.2.4.1: The percentage of published crystal structures which contain co-crystallized organic solvent molecules[36].

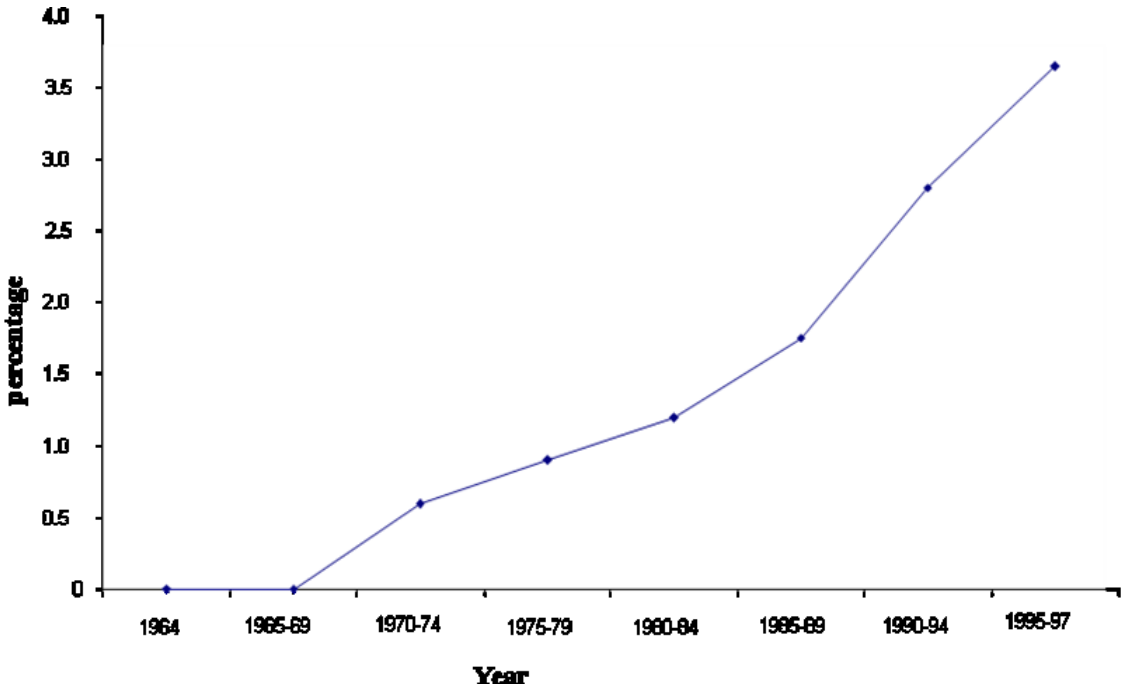

Chart 2.2.4.2: The percentage of solvates in which there are two or more different types of solvent molecules[36].

2.2.5 Co-crystal hydrates

Co-crystalline materials formed with inclusion of water molecules in their crystal structures comes under the category of co-crystal hydrates. These materials provide an alternative route to achieve high stability from high humidity conditions. In a recent paper[37], it was reported that neat grinding using the hydrated form of reactants and liquid drop grinding are proven to be more efficient compared to solvent mediated crystallization[37].

The properties of co-crystal hydrates are important for the API's which are very hard to obtain in anhydrous form. Different crystal structures were obtained from neat grinding and solvent drop grinding of theophylline and citric acid materials. Anhydrate co-crystal was obtained from neat grinding of citric acid and co-crystal hydrate from liquid drop grinding[29]. Theophylline:citric acid hydrate was obtained through solvent drop grinding method using water as solvent. The crystal structure is abanded with four membered centrosymmetric rings bonded together by O–H···O hydrogen bonds. The theophylline : citric acid hydrate was formed with O-H---N and

N-H---O intermolecular bonds formed with consecutive layers of theophylline and layers of citric acid and water (see figure 2.2.5.1). From chart 2.2.5.1, it is evident that there was a high initial interest in co-crystal hydrates in 1950s and gradual decrease over the following years.

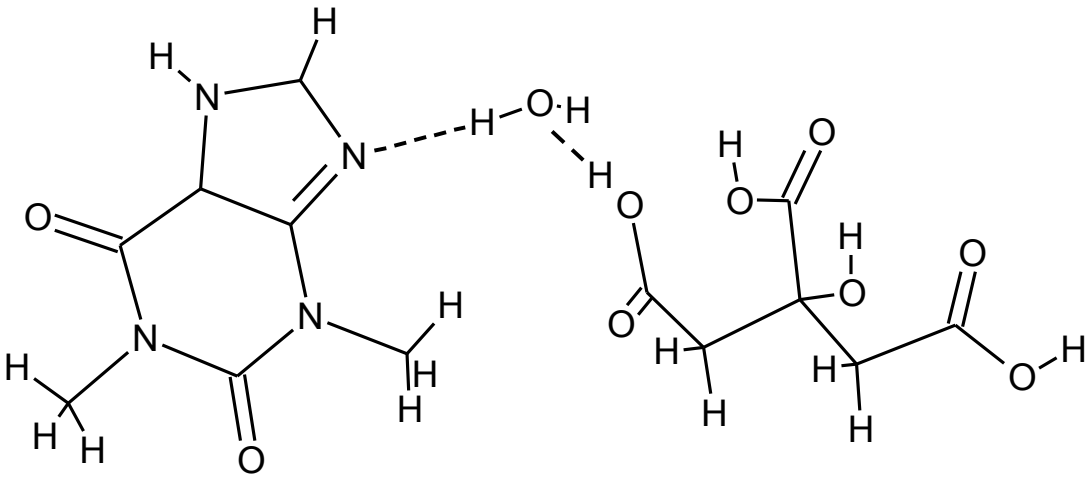

Figure 2.2.5.1: Theophylline:citric acid hydrate showing supramolecular adducts.

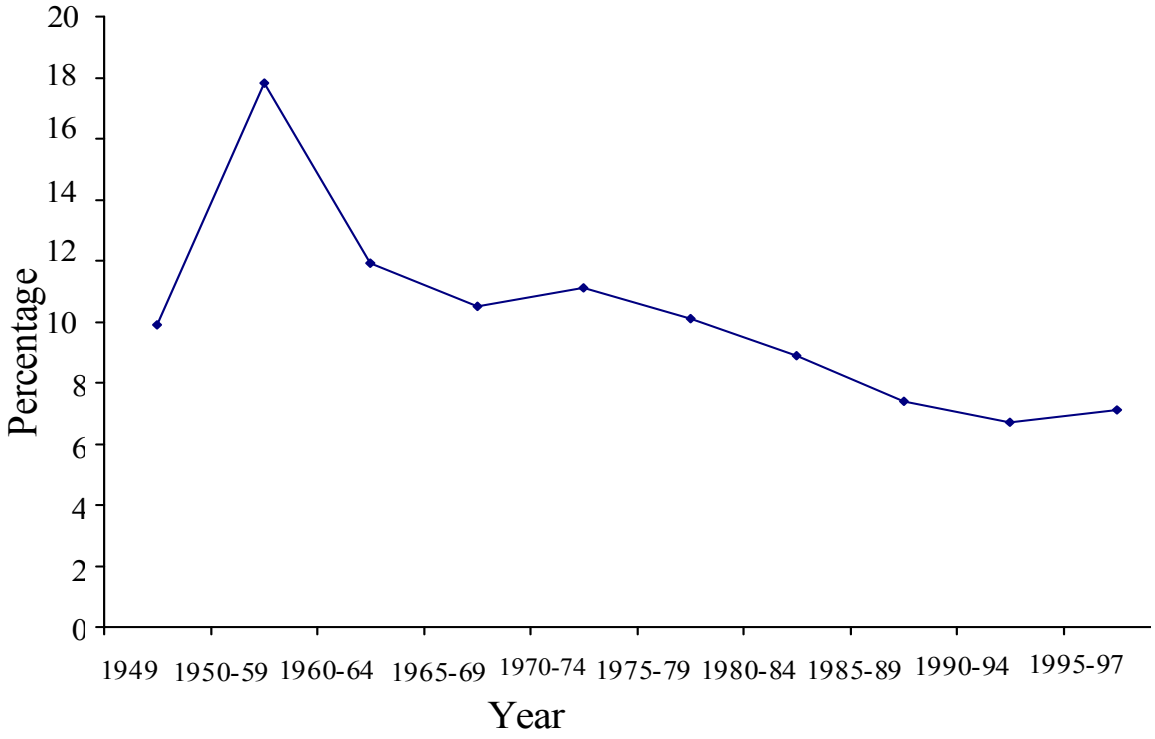

Chart 2.2.5.1: The percentage (in %) of the published co-crystal hydrates[36].

3. EXPERIMENTAL

3.1 Solution mediated crystallization

0.5 g of nicotinamide or isonicotinamide and the corresponding molar ratio of the dicarboxylic acid were dissolved individually in two conical flasks in the chosen 10ml solvent (methanol and ethanol) at room temperature. The solutions were stirred and warmed (if necessary) until the starting materials were completely dissolved. The solutions were filtered to avoid the inclusion of undissolved starting materials in the filtrate. The filtered solutions were mixed and left on the bench for crystallization under room temperature. The material obtained from crystallization was filtered and dried under suction. This experimental method was repeated using different solvents (methanol and ethanol) and stoichiometric starting ratios (1:1, 1:2 and 2:1).

3.2 Solvent drop grinding

0.25g of nicotinamide and isonicotinamide and the corresponding molar ratio of the dicarboxylic acid were ground together after adding a few drops of solvent (methanol and ethanol). The mixture was ground for 30 minutes at room temperature.

3.3 Powder X-ray diffraction data

The crystalline samples were ground and mounted in a flat disc of approximately 10mm diameter between transparent polyethylene tape. All data were collected at room temperature using a Bruker AXS D5000 or a Bruker D8 high resolution X-ray powder diffractometer with Ge-monochromated $CuK\alpha_1$ radiation with wavelength of λ=1.54056Å. Powder X-ray diffraction data were recorded between $5° \leq 2\theta \leq 60°$ or $5° \leq 2\theta \leq 90°$ for 30 minutes, for one hour or for 10 hours depending on the level of data analysis required. The step size was 0.0202°. The shorter data range was used to identify new materials and phase identification and for indexing. For structure solution and Rietveld refinement, the higher 2θ range was used. The powder X-ray diffraction data were collected in the form of a RAW file and converted to a UXD file for further analysis. The UXD file was then converted into .gsa and .xdd format files using Perl software for further analysis.

3.4 Single crystal X-ray diffraction data

The crystal selected from the sample was reduced to a crystal size of 0.18x0.16x0.08 mm^3 using a crystal habit known as Cut Slab. The data were collected on a Bruker APEXII CCD diffractometer with a Bruker FR591 rotating anode ($\lambda_{Mo\text{-}K\alpha}$ = 0.71072 Å) at 120 K in the range of 2.91°<2θ< 27.48° and with resolution between 7.00Å and 0.77 Å.

3.5 ^{1}H NMR spectra

0.03g of sample material was dissolved in 2ml of d^6 DMSO solvent as a reference in a 5mm diameter quad probe. The data was recorded at $300MH_z$ on a Bruker AC300 spectrometer.

3.6 Infra-red spectra

IR data was collected on a Perkin Elmer 100 FTIR spectrometer and recorded in the range of 400 to 4000 cm^{-1}.

4. METHODOLOGY

4.1 Indexing

Indexing of powder X-ray diffraction data by selection of accurate unit cell parameters is the crucial step on which the whole structure determination procedure depends. *XFIT*[38] is used to select peaks for input into the *CRYSFIRE*[39] indexing software suite. Initially, the 20 most intense peaks are selected and saved in a text file for input into *CRYSFIRE*. Alternatively, the first (lowest 2θ) 20 observable peaks can be used.

CRYSFIRE[39] is used to index the powder X-ray diffraction pattern[40] through the application of ten indexing algorithms. The results obtained from each indexing method are saved into a single summary file and listed in order of figure of merit F20[18]. The software *CHEKCELL*[41] was then used to verify the fit between the peaks selected and peaks generated by different unit cells obtained through indexing. The space group is then assigned based on the conditions for systematic absences (*hkl*) in the unit cell, or in a triclinic case, based on density considerations.

4.2 Le Bail pattern decomposition

The Le Bail[42] pattern decomposition method is a method used to refine the cell and other profile parameters without need for a structural model. *GSAS*[43] is a software package than can be used to apply Le Bail pattern decomposition to powder X-ray diffraction data. Lattice parameters, pseudo voigt peak shape (a combination of Lorenzian and Gaussian) and zero point error are all refined during this process. The fitness between the experimental and simulated powder X-ray diffraction patterns is measured in terms of R_{wp} (R-factor) and χ^2 [44]. The peak intensities also act as variable parameters in Le Bail decomposition, whereas for a Rietveld refinement these are defined by atomic positions. The Le Bail method increases the accuracy of direct space structure solution methods to determine the crystal structure by ensuring that the lattice parameters and profile parameters give the best possible fit[44].

4.3 Differential evolution (DE) structure solution

The next stage of crystal structure determination is the structure solution process, in this project; based on the differential evolution method. Many evolutionary algorithms are inspired by natural evolutionary processes and principles of biological evolution[40] and are used to explore the global minima on the fitness landscape[40, 45, 46]. These evolutionary techniques are now used widely in chemistry, nanoscience and bioinformatics[47]. Traditional methods (direct and Patterson methods) used to find structure solutions for organic materials in powder form are often unsuccessful[19, 48] and hence the alternative direct space approach was developed. The traditional methods need extraction of intensities of individual diffraction maxima. Due to peak overlap problem in X-ray powder diffraction data, it is often difficult for traditional methods to extract unambiguous values of the intensities *I* (hkl) of the individual diffraction maxima. In direct space approach, in order to solve crystal structures from powder diffraction data, trial crystal structures are generated in direct space and the suitability of each trial structure is assessed by direct comparison between the powder diffraction pattern calculated for the trial structure and its experimental powder diffraction pattern[49].

Differential evolution (DE) is relatively new algorithm technique originally used to solve the Chebychev polynomial fitting problem[50]. The DE approach was given highest preference in the International contest in evolutionary computation which does not use any specialised problem information[51]. It has proved to be highly efficient in a range of chemical contexts, including X-ray scattering[52, 53], protein crystallography[54], molecular docking[55], crystal epitaxy[56], disordered crystal structures[55], optimization of clusters[57] and direct space crystal structure solution of crystalline materials from powder diffraction data[45].

The differential evolution program used in the current project was implemented in the POSSUM[58] program suite. This program suite creates a control file which includes the details of the structural model(s), unit cell parameters and optimisation information used to direct the search and boundaries for the population hypersurface for the DE. In cases where specific crystallographic site symmetry is needed these values can be further constrained, enhancing the efficiency of the optimisation process

(see figure 4.2). The structural models are built on the basis that a crystal structure is the repetition of three dimensional models within the unit cell. The position and orientation of the three dimensional structural models are represented by various variables, e.g., the position (x**,** y, z) and orientation (θ, φ, ψ) and torsion angles to describe the molecular conformation (τ_1, τ_2,… τ_N). These variables are the allowed to vary between 0 and 1 for the position and the angles used to describe the molecular orientations will vary between 0° and 360°[59].

In DE, the initial population N_p is generated across the hypersurface, the size of which is directly proportional to the initial value given for N_p. The fitness of each initial trial structure is assessed by comparing the calculated powder diffraction pattern to the experimental powder diffraction pattern. This is expressed in terms of the R-factor (R_{wp}).

In a DE population, each offspring is produced from its parent and three random trial structures (see equation 3.1). The resulting child structure is the summation of the parent and difference between the parent and a random structure controlled by recombination (*k*) and the difference between two random structures controlled by mutation (*F*) as shown in the equation below. The parameters *K* and *F* can be varied between 0 and 1. With an increase in the value of K, the distance between the parent and the child structure will increase. The *F* value helps to maintain diversity in the population by including information from other individuals. The DE then uses the parameter boundary conditions to reset a child structure when a new offspring exceeds the boundaries of the fitness hypersurface.

$$\text{Child} = \text{Parent} + K\,(\text{Random}_1 - \text{Parent}) + F\,(\text{Random}_2 - \text{Random}_3) \longrightarrow (3.1)$$

K = Recombination

F = Mutation

Child = Child structure

Parent = Parent structure

Random_1, Random_2, Random_3 = Random structures

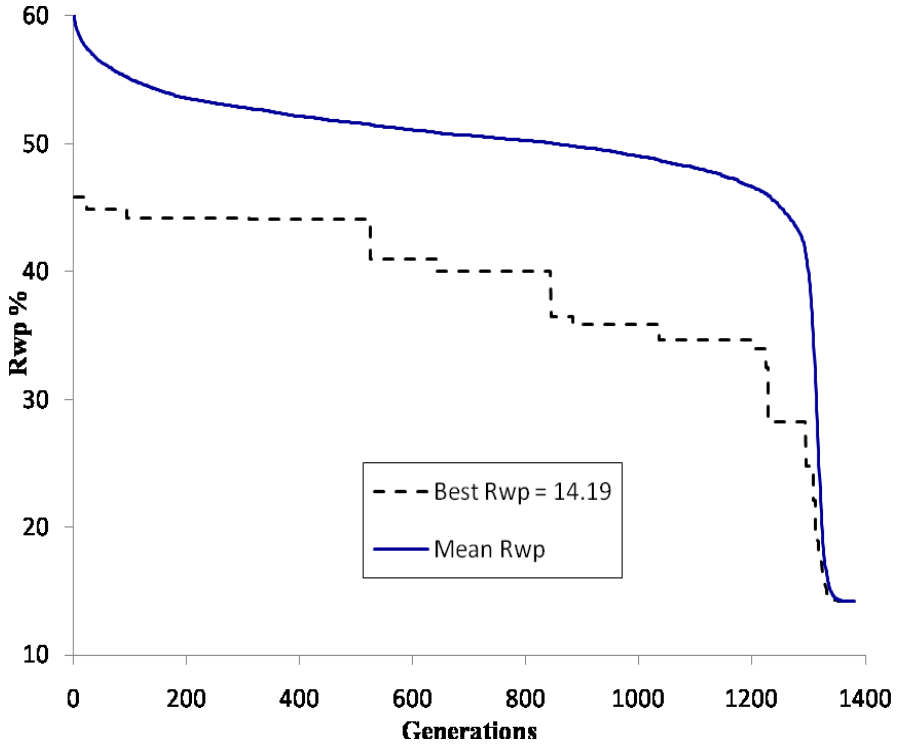

Figure 4.1: An example of an evolutionary progress plot for a DE calculation.

In the early stages of a search, the trial structures are dispersed widely across the fitness hypersurface. And hence the difference between the R-factors of the first few generations are expected to be large (see figure 4.1). As the search progresses, the population converges and the R-factor difference between the best member and the other members of the population in each generation decreases[60].

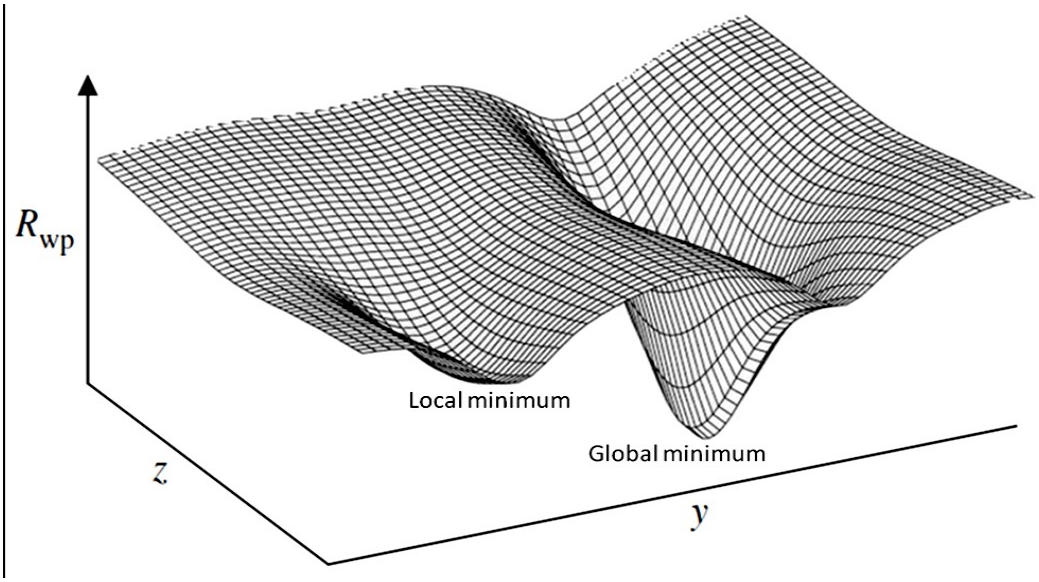

Figure 4.2: An example of a 2D hypersurface clearly showing the global minimum which represents the best structure solution[1]. A local minimum is also shown.

4.4 Rietveld refinement

The structure solution obtained from differential evolution is an approximate representation of crystal structure but should be close enough to the true structure to complete a quality crystal structure using Rietveld refinement. If all the atomic positions are within 1Å of the final refined structure, then the Rietveld refinement is usually successful[18]. Rietveld refinement in this work was performed using the *GSAS & EXPGUI* program package[43, 61]. During the refinement of structures, all bond lengths and angles are subjected to different restraints depending on the nature of the structures; the C-C bond lengths were restrained at 0.005Å and the C-H bonds restrained to 0.001Å. It is important to apply standard geometrical restraints in order to prevent excessive movement in atomic positions especially if an approximate structure solution has been obtained. Appropriate restraints are often imposed for successful refinement[60].

Rietveld refinement is based on the fitness between the experimental and calculated diffraction patterns measured in terms of R-factor (R_{wp}). By considering every point in the powder diffraction pattern as an individual intensity, the optimal fit between the calculated and experimental powder diffraction is obtained by applying least square minimisation methods[19].

4.5 Single crystal X-ray diffraction

The data collection was driven by *COLLECT*[62] and processed by *DENZO*[63]. An absorption correction was applied using SADABS[64]. The structures were solved in *SHELXS-97*[65] and were refined by a full-matrix least-squares procedure on F^2 in *SHELXL-97*. All non-hydrogen atoms were refined with anisotropic displacement parameters. All hydrogen atoms were added at calculated positions and refined by use of a riding model with isotropic displacement parameters based on the equivalent isotropic displacement parameter (U_{eq}) of the parent atom. Figures were produced using *ORTEP3* for Windows[66, 67] while structural analysis was carried using *PLATON*[68].

5. RESULTS

5.1 Oxalic acid and nicotinamide
5.2 Malonic acid and nicotinamide
5.3 Succinic acid and nicotinamide
5.4 Adipic acid and nicotinamide
5.4.1 Crystal structure determination using single crystal X-ray diffraction
5.5 Pimelic acid and nicotinamide
5.6 Pimelic acid and isonicotinamide
5.7 Suberic acid and nicotinamide
5.8 Suberic acid and isonicotinamide
5.9 Azelaic acid and nicotinamide
5.9.1 Determination and refinement of unit cell parameters from powder diffraction data
5.9.2 Determination of structure solution using differential evolution.
5.9.3 Crystal structure determination using Rietveld refinement.
5.10 Azelaic acid and isonicotinamide
5.11 Melting point alternations

5. RESULTS

A range of α,ω-di-carboxylic acids (HOOC-$(CH_2)_n$-COOH, where n= 0,1,2,4,5,6,7) have been investigated as potential former molecules to form co-crystals with nicotinamide (see figure 2.1(a)) and isonicotinamide (see figure 2.1(b)) using different solvents, different stoichiometric ratios and different methods of synthesis. The change in properties of these co-crystals is related to the sequential increase in the number of methylene groups in the di-carboxylic acid. The formation of new co-crystals was confirmed using powder X-ray diffraction and solid state infrared spectroscopy. The stoichiometric ratios of the former molecules within the crystalline products were confirmed using solution nuclear magnetic resonance spectroscopy (^{1}H NMR). Infrared spectroscopy (IR) was also used to investigate the presence of intermolecular bonds in these materials. The melting points of all new crystal materials were determined and found to lie between the melting points of the starting materials.

Indexing of the unit cells and Le bail pattern decomposition from powder X-ray diffraction were attempted for most of the new materials obtained. In addition, the crystal structures of two of the new co-crystal materials were determined. The crystal structure of the adipic acid : nicotinamide co-crystal was determined using single crystal X-ray diffraction data, whereas the crystal structure of the azelaic acid : nicotinamide co-crystal was determined from powder X-ray diffraction data.

5.1 Oxalic acid and nicotinamide

Oxalic acid (see figure 2.2 (a)) was crystallised with nicotinamide using a range of different solvents and synthetic methods in different starting molar ratios. The solid products were formed immediately after the solutions containing the individual components were mixed. The appearance of new materials obtained using different synthesising methods, solvents and stoichiometric ratios for nicotinamide and oxalic acid in this series of experiments are all white crystalline solids.

Crystallisation of oxalic acid with nicotinamide was done using different solvents (methanol and ethanol) in 1:1, 1:2 and 2:1 starting molar ratios. Solution crystallisation and solvent drop grinding (SDG) methods were both employed for the preparation of these new materials. Similar X-ray diffraction patterns were obtained for materials prepared using methanol and ethanol with 1:1 and 2:1 molar ratios illustrating formation of the same product (see figure 5.1.1). The X-ray powder diffraction patterns for the materials obtained from both 1:1 and 2:1 molar ratios are different compared to that 1:2. The product obtained from 1:2 also shows traces of peaks from the product with 1:1 ratio (or 2:1). It can be concluded from this data that it is a mixture of different new materials. Different synthetic approaches and molar ratios were used, but none of them were successful in the synthesis of this new material (from 1:2) in pure form. The same new materials (from 1:1 and 1:2) are formed reproducibly from both solution crystallisation (using both methanol and ethanol) and solvent drop grinding methods although in the latter case, starting materials were also present (see appendix A).

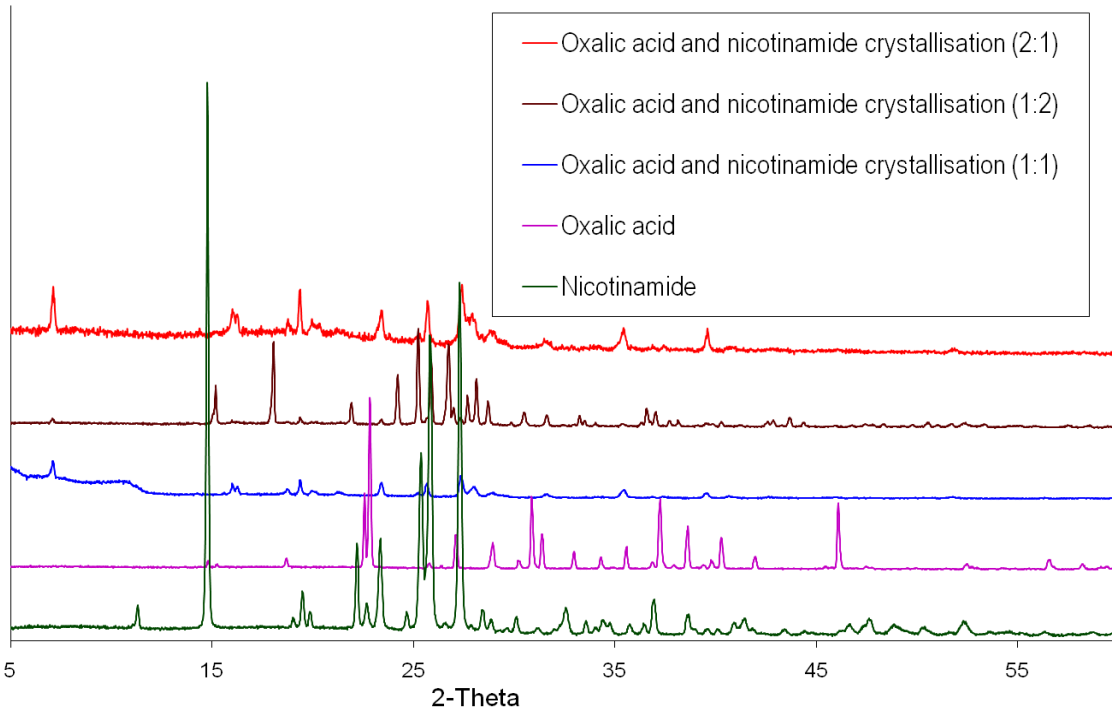

Figure 5.1.1: X-ray powder diffraction patterns of nicotinamide and oxalic acid and products of crystallisation using methanol.

From the NMR spectra and consideration of the ratio of integral values of the peak intensities for protons in different environments in nicotinamide and oxalic acid, it is evident that the new material obtained by crystallisation of the starting materials in the 1:1 and 2:1 molar ratios has the molecular formers crystallised in a 1:1 stoichiometric ratio (see figure 5.1.2). The other new material obtained (as a mixture) using starting materials in 1:2 stoichiometric ratio (see figure 5.1.3) indicates the presence of a 1:2 oxalic acid : nicotinamide ratio in the adduct. The ratio between the molecular components in the new materials is interpreted by comparing the integral values of individual peak intensities for the H atoms in the coformers. In the spectrum shown below (see figure 5.1.2), the B_1 peak is due to the two hydrogen atoms in the oxalic acid and the A_1 peak is due to the single H atom in the ortho position. The integral value for A_1 peak is approximately half that of B_1. This implies that the molecular components are in a 1:1 ratio. In the next spectrum (see figure 5.1.3), the integral values of both A_1 and B_1 peaks are approximately equal, hence representing two hydrogen atoms each. This can only be the case if for each oxalic acid molecule there are two nicotinamide molecules and hence the adduct has a 1:2 acid : amide ratio.

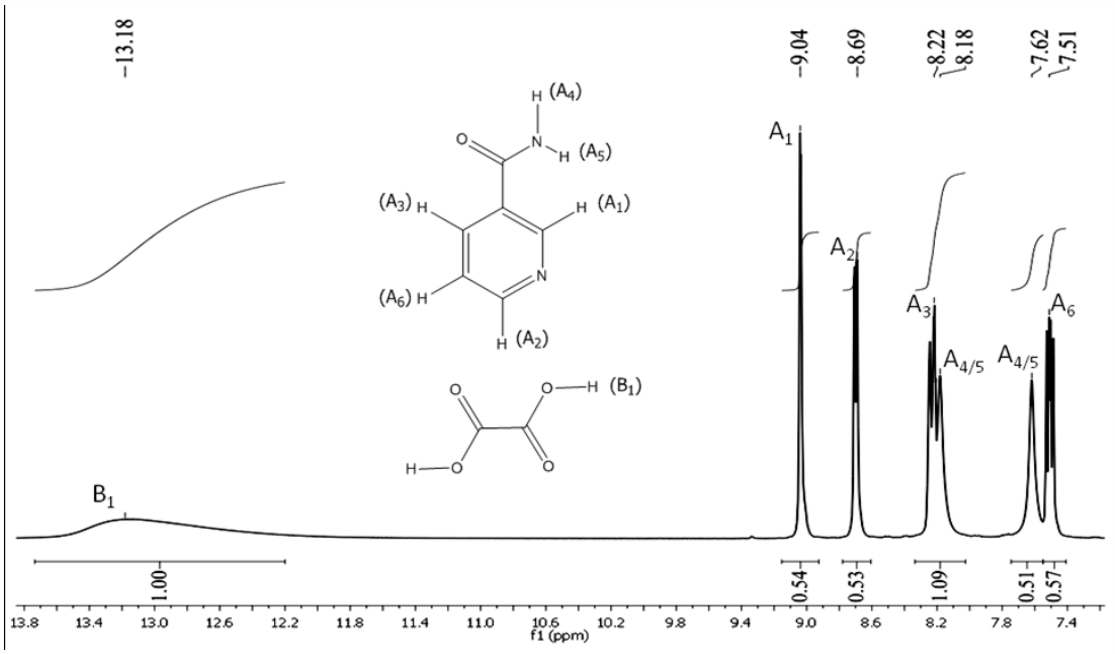

Figure 5.1.2: [1]H NMR of oxalic acid and nicotinamide adduct (from 1:1 starting ratio) using DMSO as solvent. ^{1}H NMR 300MHz (DMSO-d_6): δ = 13.18(s, 2H), 9.04(dd, 1H), 8.69(dd, 1H), 8.22(dt, 1H), 8.18(s, 1H), 7.62(s, 1H), 7.51(ddd, 1H).

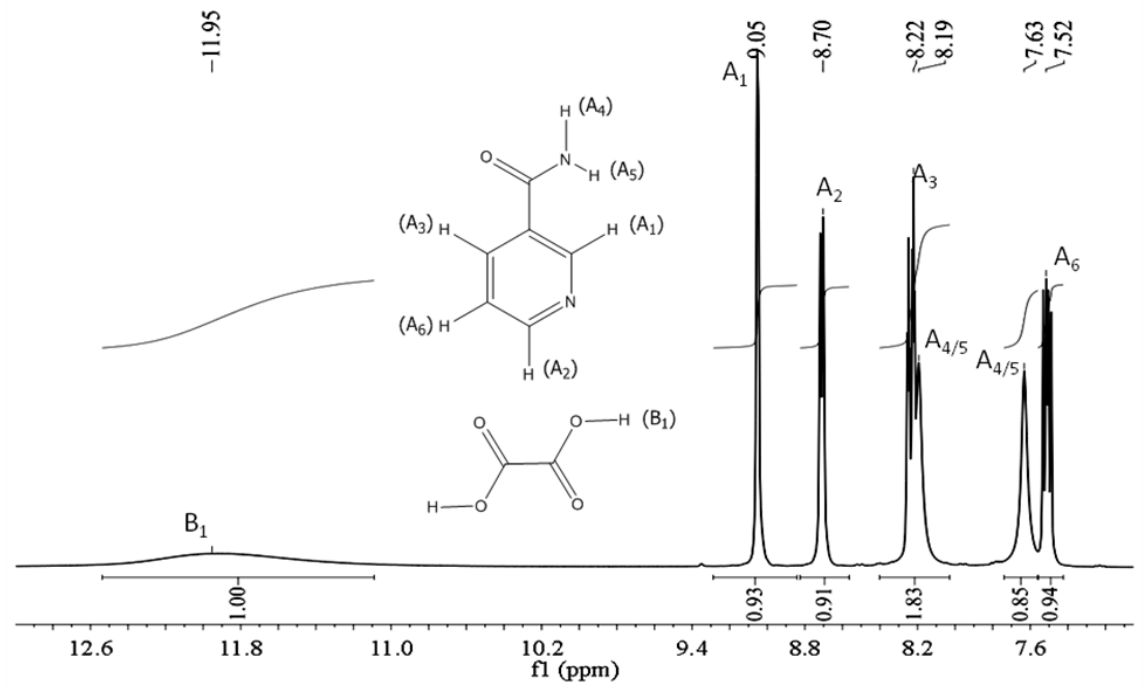

Figure 5.1.3: [1]H NMR for the product of oxalic acid and nicotinamide adduct (from 1:2 starting ratio) using DMSO as solvent. ^{1}H NMR 300MHz (DMSO-d_6): δ = 11.95(s, 2H), 9.05(dd, 2H), 8.70(dd, 2H), 8.19(dt, 2H), 8.17(s, 2H), 7.63(s, 2H), 7.52(ddd, 2H).

Solid state FTIR spectroscopy can be used to investigate whether the product formed is a co-crystal or a salt. The data from the product obtained from the crystallisation is compared to that from a mixture of the starting materials. The oxalic acid in the starting material is characterised with very broad peaks obtained for O-H stretching frequency with intense absorptions at 3470cm^{-1} and 3367cm^{-1}. The peaks at 3171cm^{-1} for the product show a downshift that may imply involvement in stronger intermolecular hydrogen-bonding. The peaks for C=O stretching vibrations at 1683cm^{-1} appear for both the starting mixture and product. The peaks at 3331cm^{-1} would belong to amide N-H stretching vibrations. The peaks at 3063cm^{-1}would belong to aromatic C-H stretchings. Symmetric out-of-plane aromatic C-H bending of the aromatic ring is at 710cm^{-1} and peaks for out of plane ring bending vibrations appear around 669cm^{-1}. In R. F. Evans and W. Kyaston[69], they showed that, if H is transferred from the acid to N within the hydrogen-bonding between the acid and pyridine ring, very broad peaks would appear around 2500±100cm^{-1} and for individual N^{+}-H bonds, peaks would appear at 3250±50cm^{-1}. None of these characteristics are observed so it is not conclusive whether or not the product is a co-crystal or salt as the two spectra do not match either as might be expected if a cocrystal was formed (see figure 5.1.4).

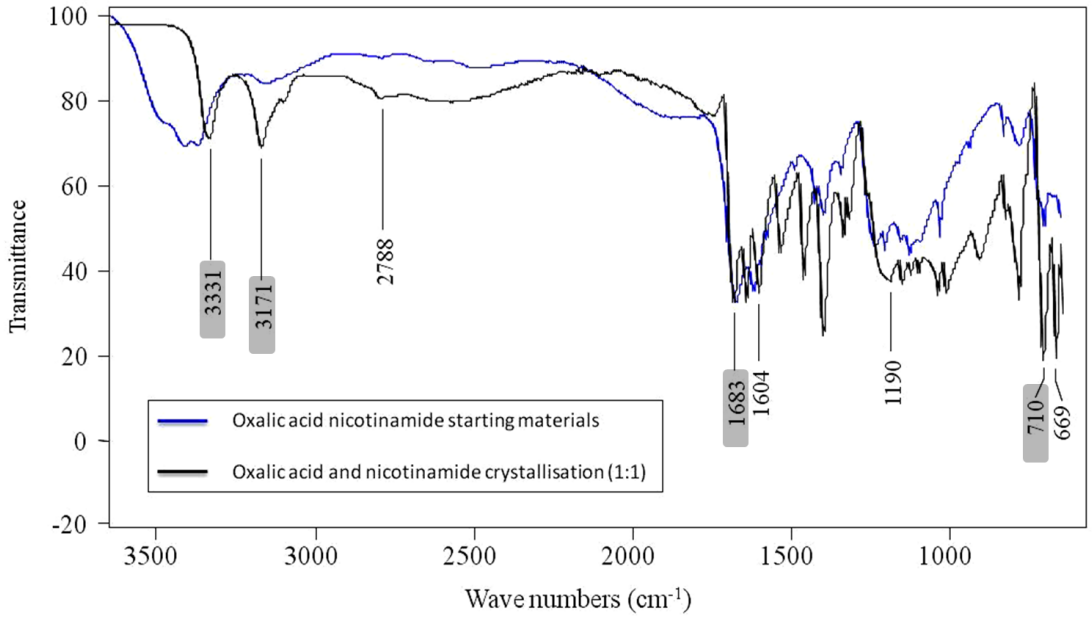

Figure 5.1.4: FTIR spectra for the product of oxalic acid and nicotinamide crystallisation (1:1).

Possible cell parameters were obtained for the 1:1 co-crystal by the indexing on the basis of the twenty most intense peaks in the powder diffraction pattern using the *CRYSFIRE* software suite. The possible cell parameters are chosen for Le bail pattern decomposition on the basis of stoichiometric ratio between the molecules obtained from NMR along with cell volume calculations and figure of merit (see Table 5.1.1). The space group was chosen on the basis of conditions for systematic absences in reflections for a unit cell with respective space group (see table 1). The accuracy of unit cell parameters and correct space group would be confirmed through Le bail pattern decomposition method (see figures 5.1.5). The unit cell refinement is also done simultaneously during the pattern decomposition process. The best fit between the experimental data (red) and simulated pattern (green) is quantified in terms of R-factor value (wRp) and χ^2. The lowest R-factor and χ^2 values obtained are 0.0956 and 0.3241 respectively.

Table 5.1.1

Indexed and refined cell parameters obtained for the product of oxalic acid and nicotinamide

	Figure of Merit / R_{wp} / χ^2	*a*(Å)	*b*(Å)	*c*(Å)	$\alpha(^o)$	$\beta(^o)$	$\gamma(^o)$	Cell volume (Å^3)	Space group
PXRD indexing	14.77	12.848	6.349	11.244	90.00	104.61	90.00	887.684	$P2_1/c$
PXRD Le bail fit	R_{wp}= 0.1129 χ^2=18.61	12.822	6.347	11.213	90.00	104.75	90.00	882.692	$P2_1/c$

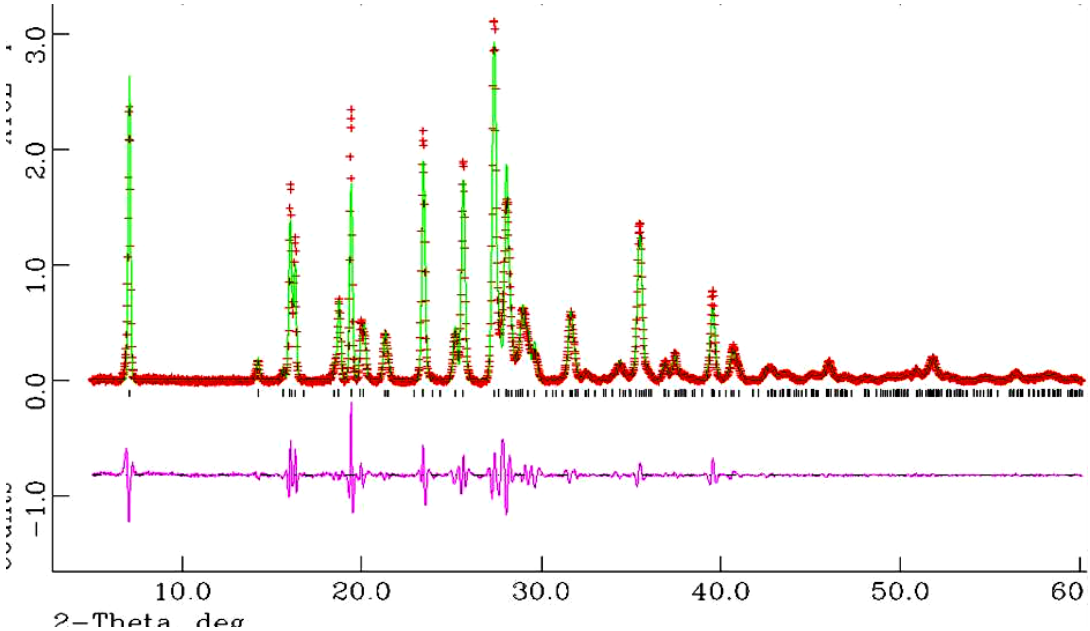

Figure 5.1.5: The Le bail profile fitting for the product of oxalic acid and nicotinamide crystallisation (1:1).

No further structural characterisation was carried out on this product.

5.2 Malonic acid and nicotinamide

Malonic acid (see figure 2.2(b)) was crystallised together with nicotinamide using different synthetic methods and solvents. All new materials were synthesized as white solid clusters. Crystallisation of malonic acid with nicotinamide was carried out in 1:1, 1:2 and 2:1 starting molar ratios, using different solvents (methanol and ethanol) both in solvent-mediated crystallisation and solvent drop grinding (see appendix B). The X-ray powder diffraction patterns for materials obtained from methanol and ethanol in 1:1 and 2:1 starting molar ratios shows the formation of the same product (see figure 5.2.1). For each stoichiometric ratio the new materials obtained using different solvents and synthesising methods are the same. However, it is evident that the new materials obtained from 1:1 and 1:2 stoichiometric ratios are different and differ from the starting materials (see figure 5.2.1).

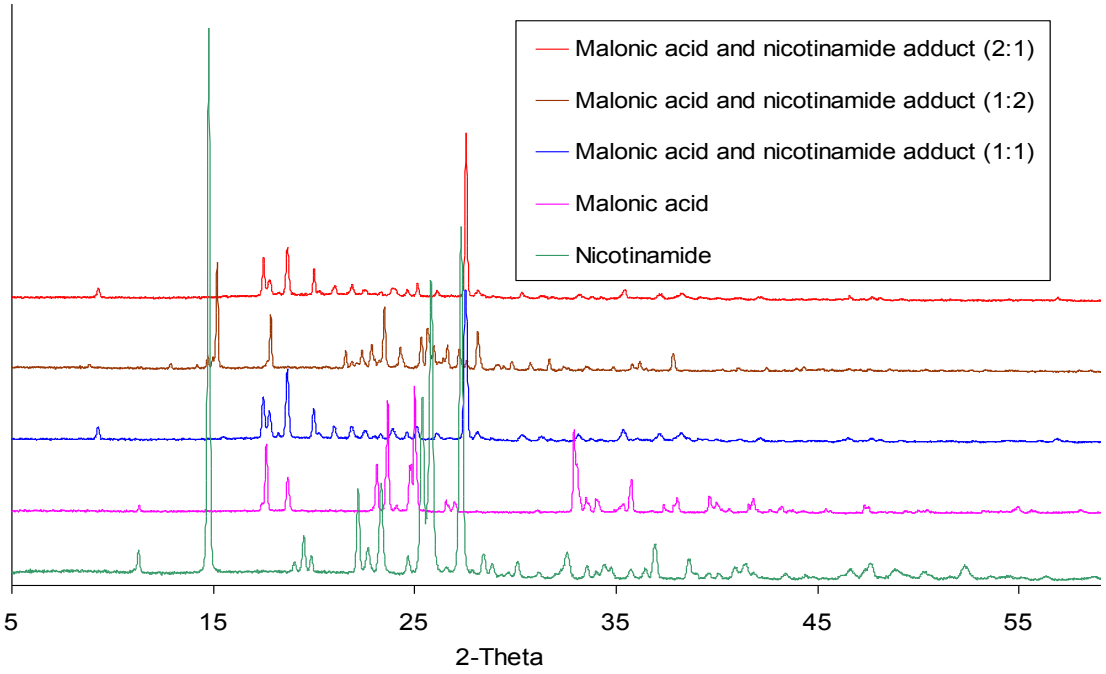

Figure 5.2.1: X-ray powder diffraction patterns of nicotinamide and malonic acid and products of crystallisation using methanol.

From the integral values of different peak intensities for protons in different environments on malonic acid and nicotinamide obtained from NMR spectra, it is evident that the new materials obtained from starting molar ratios of 1:1 and 1:2 are

obtained with approximate 1:1 and 1:2 stoichiometric ratios (see figures 5.2.2 and 5.2.3).

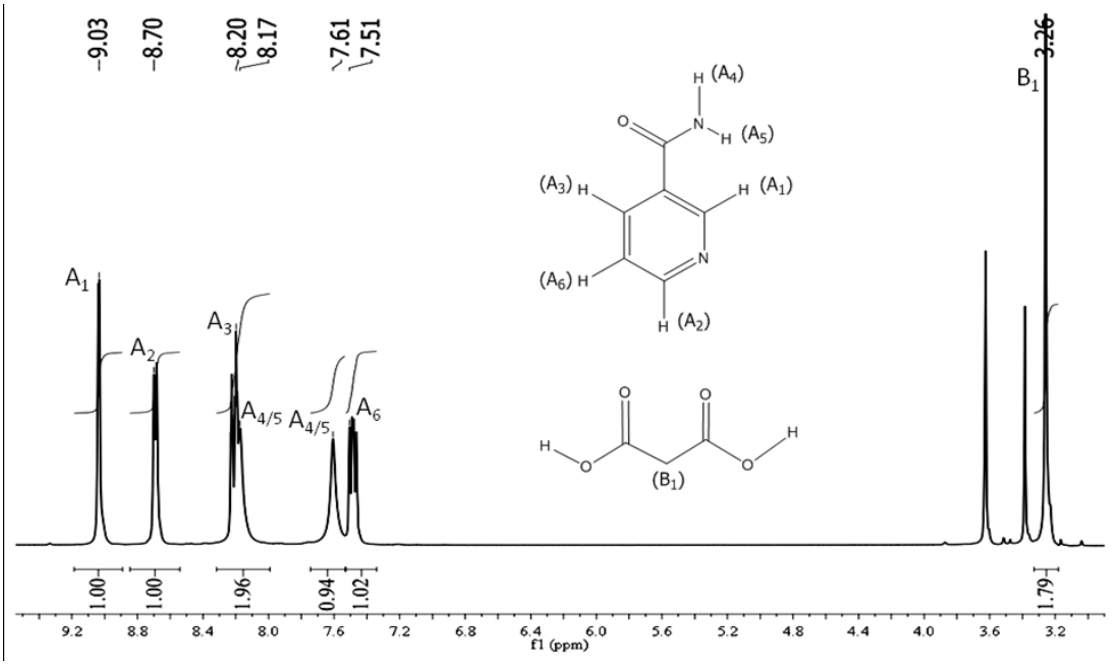

Figure 5.2.2: ^{1}H NMR of malonic acid and nicotinamide (1:1) crystallisation using DMSO as solvent. ^{1}H NMR 300MHz (DMSO-d_6): δ= 12.51(s, 2H), 9.03(dd, 1H), 8.70(dd, 1H), 8.20(dt, 1H), 8.17(s, 1H), 7.61(s, 1H), 7.51(ddd, 1H), 3.26(s, 2H).

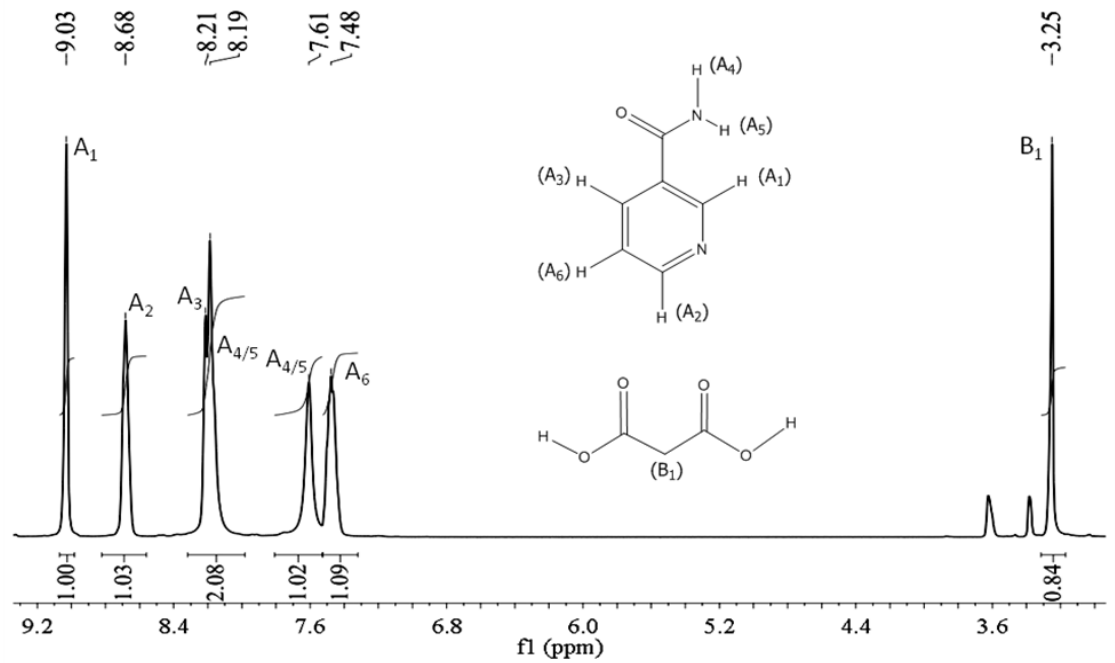

Figure 5.2.3: ^{1}H NMR of malonic acid and nicotinamide (1:2) crystallisation using DMSO as solvent. ^{1}H NMR 300MHz (DMSO-d_6): δ= 12.67(s, 2H), 9.03(dd, 2H), 8.68(dd, 2H), 8.21(dt, 2H), 8.19(s, 2H), 7.61(s, 2H), 7.48(ddd, 2H), 3.25(s, 2H).

The solid state FTIR data for the products (1:1 and 1:2) obtained from the crystallisation are compared to that from a mixture of the starting materials. For a discussion of characteristic peaks of nicotinamide, please see section 5.1. The C=O stretching frequency bands of the amide group can be observed between 1684 cm^{-1} and 1599 cm^{-1}. The peaks at 3368cm^{-1} (1:1) and 3374cm^{-1} (1:2) indicate N-H stretching frequency bands for the amide group in the product formed. The absence of characteristic high tone at 3000 cm^{-1} (O-H bond stretching frequency of a carboxylic acid) indicates the involvement of the carboxylic acid groups in intermolecular bonding. The peaks at 3173cm^{-1} (1:1) and 3171cm^{-1} (1:2) in both spectra may imply the involvement of O-H bonds in stronger hydrogen bonding. Interpretation of the IR spectra for different molecular fragments supports the presence of neutral intermolecular bonds. There are similarities between the spectra obtained for the product and starting materials, albeit the shift of some bands mentioned previously. This implies, although not conclusively, that there has been no proton transfer from the hydroxyl group to the heterocyclic nitrogen (see figures 5.2.4 and 5.2.5) and hence that in both cases a co-crystal rather than a salt has been formed.

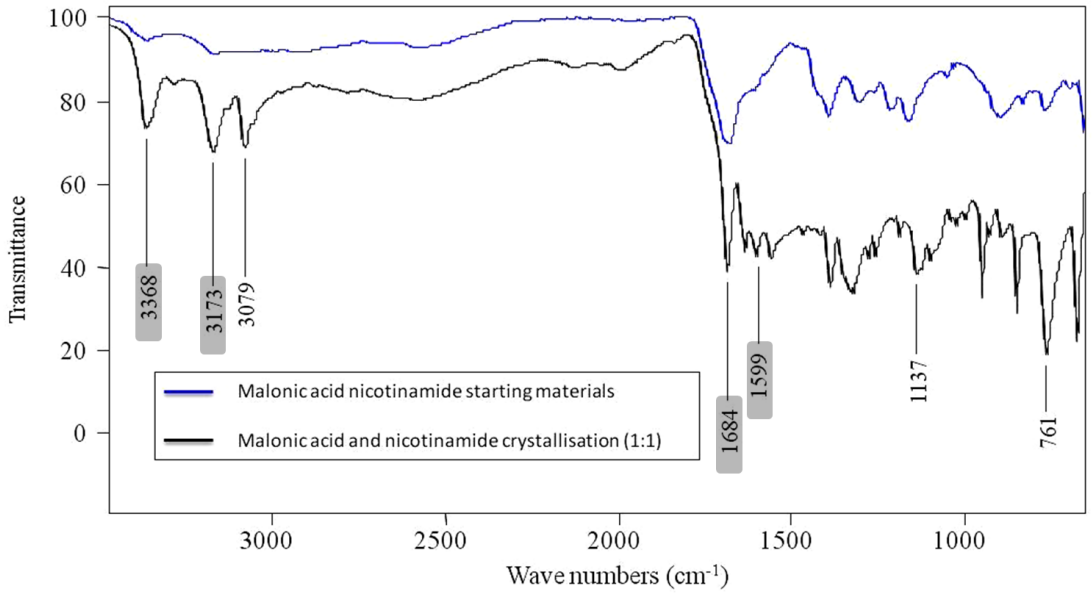

Figure 5.2.4: FTIR spectra of malonic acid and nicotinamide and the product of crystallisation (1:1).

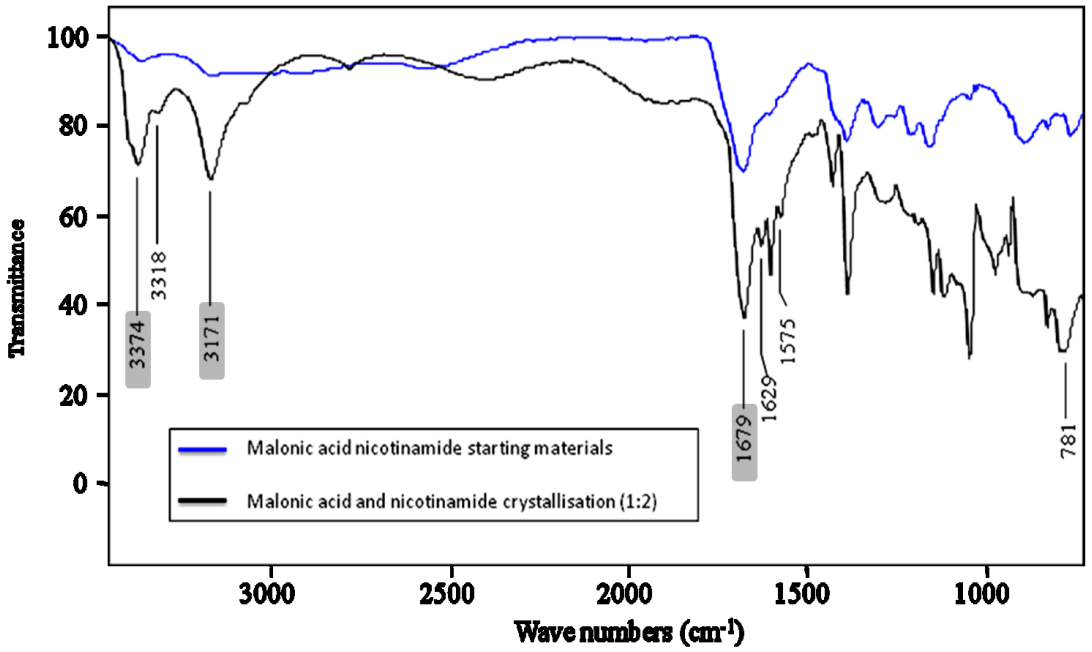

Figure 5.2.5: FTIR spectra of malonic acid and nicotinamide and products of crystallisation (1:2).

The X-ray powder diffraction pattern of the crystallised product (malonic acid: nicotinamide 1:1) was indexed using *CRYSFIRE*, on the basis of the twenty most intense peaks selected using XFIT. Possible cell parameters were assessed on the basis of stoichiometric ratios between the former molecules obtained from NMR. The most highly ranked unit cell (see table 5.2.1 and appendix C) indexed all twenty peaks successfully and was conducive with density considerations for a 1:1 ratio. These cell parameters were refined using Le bail pattern decomposition.

Table 5.2.1

Indexed cell parameters of malonic acid and nicotinamide:

	Figure of Merit / R_{wp} / χ^2	*a*(Å)	*b*(Å)	*c*(Å)	α(°)	β(°)	γ(°)	Cell volume (Å^3)	Space group
PXRD indexing	23	10.444	10.277	5.121	96.09	103.88	67.38	492	P1
PXRD Le bail fit	R_{wp}= 0.1085 χ^2=0.9889	10.431	10.234	5.102	96.12	103.87	67.32	492	P1

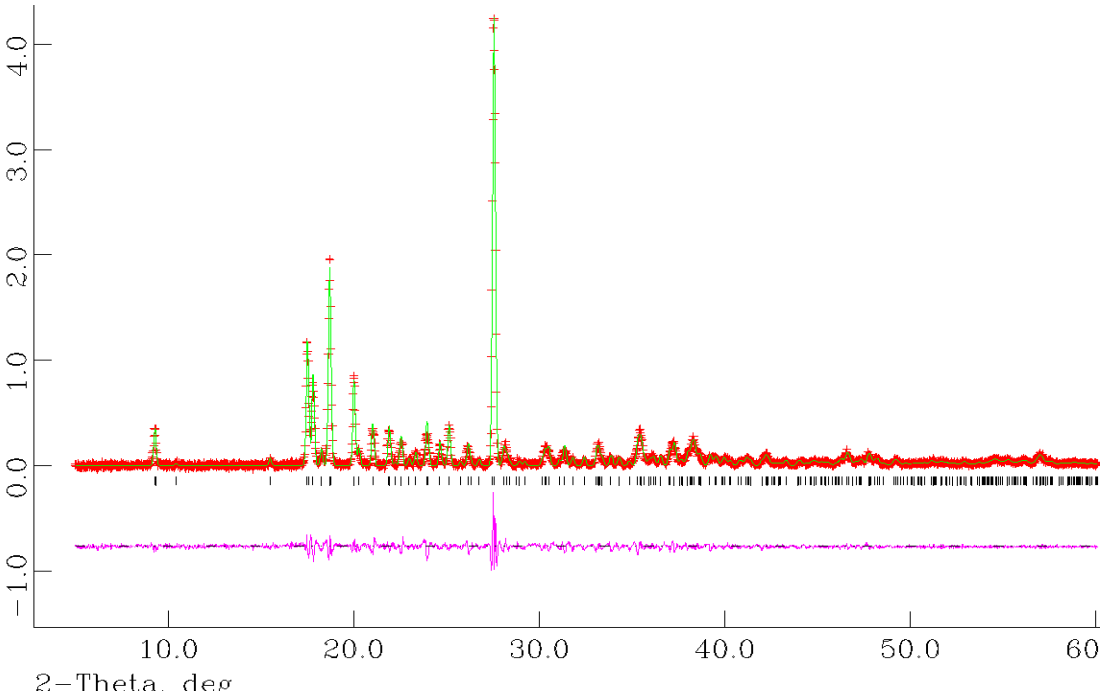

Figure 5.2.6: The Le bail profile fitting for nicotinamide and malonic acid crystallisation (1:1).

No further structural characterisation was carried out on this product.

5.3 Succinic acid and nicotinamide

Succinic acid (see figure 2.2(c)) was crystallised with nicotinamide in 1:1 starting stoichiometric ratio using different synthetic methods and solvents. All new materials were synthesized as white solid clusters. Crystallisation was performed using solvent mediated crystallisation and SDG methods in methanol and ethanol (see figure 5.3.1). The X-ray diffraction patterns for materials obtained from different synthesising methods and solvents shows the formation of the same new product (see appendix D), although there are clearly traces of succinic acid in the product from SDG.

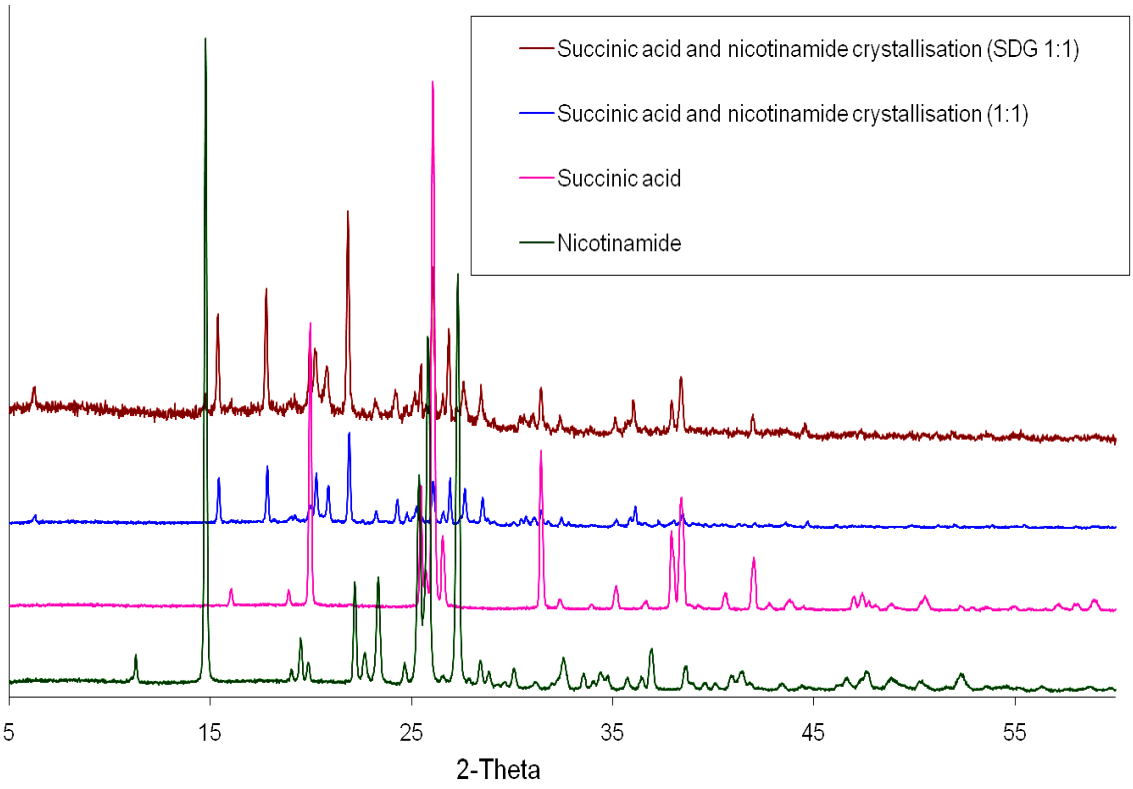

Fig 5.3.1: Powder X-ray diffraction patterns of succinic acid and nicotinamide and products of crystallisation from methanol.

From the integral values of different peak intensities for protons in different environments on succinic acid and nicotinamide obtained from NMR spectra, it is evident that the stoichiometric ratios in the product formed is 1:1 (see figure 5.3.2).

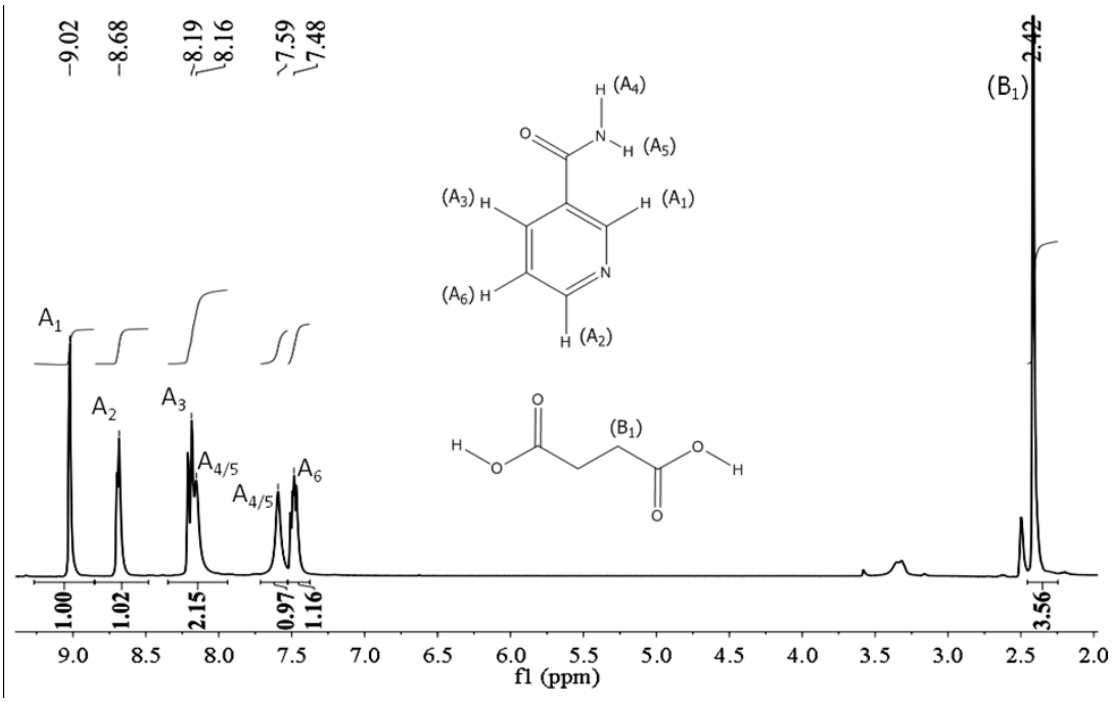

Figure 5.3.2: ^{1}H NMR of succinic acid and nicotinamide (1:1) crystallisation using DMSO as solvent. ^{1}H NMR 300MHz (DMSO-d_6): δ= 12.15(s, 2H), 9.02(dd, 1H), 8.68(dd, 1H), 8.19(dt, 1H), 8.16(s, 1H), 7.59(s, 1H), 7.48(ddd, 1H), 2.42(s, 4H).

The solid state FTIR data (figure 5.3.3) for the product obtained from crystallisation was compared to that obtained from the starting materials. The spectra for the new material succinic acid : nicotinamide (1:1) have few similar peaks to that in sections 5.1 and 5.2 showing characteristic IR bands of different molecular fragments in succinic acid and nicotinamide. The similarity between the spectra obtained for the product and the starting materials infers that the product could be a co-crystal. There may be indication of a two broad peaks at ~2474 cm^{-1} and 1912 cm^{-1}. This implies, although not conclusively, there has been no proton transfer from the hydroxyl group to the heterocyclic nitrogen and hence a co-crystal rather than a salt has been formed.

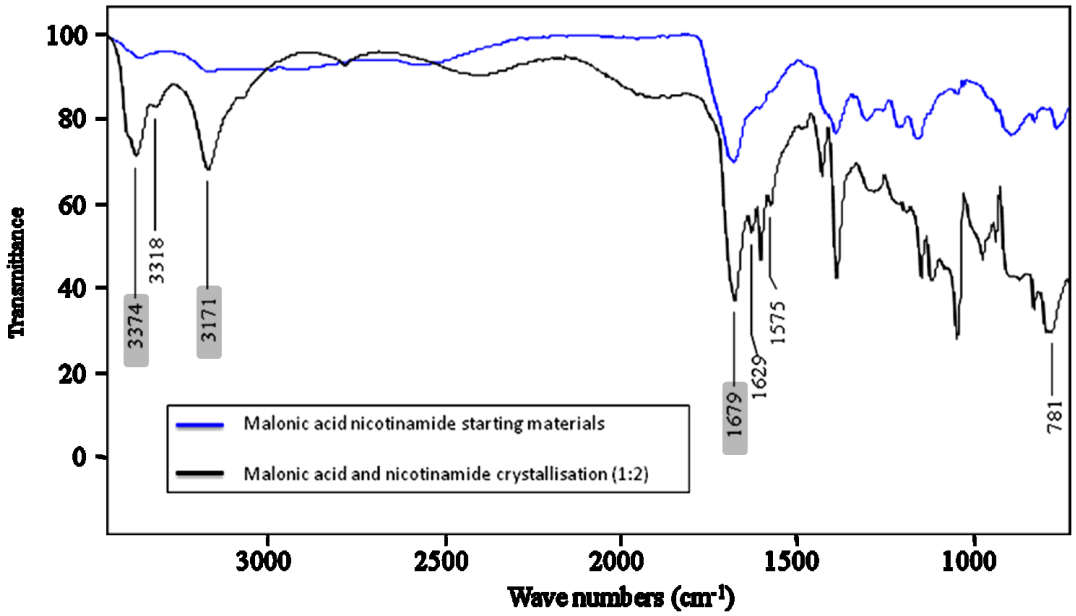

Figure 5.3.3: FTIR spectra of succinic acid and nicotinamide and products of crystallisation (1:1).

This material has not been indexed due to constraints of project time.

5.4 Adipic acid and nicotinamide

Adipic acid (see figure 2.2(d)) was crystallised with nicotinamide using different synthetic methods and solvents. All new materials were obtained as white solid clusters. Crystallisation of adipic acid and nicotinamide was attempted in 1:1, 1:2 and 2:1 starting molar ratios and performed with methanol and ethanol both in solvent-mediated crystallisation and solvent drop grinding (see appendix E). Similar X-ray powder diffraction patterns were obtained for different solvents and different starting molar ratios (e.g: adipic acid and nicotinamide 2:1), showing the formation of the same product (see figure 5.4.1). The new materials obtained from some different starting molar ratios, solvents and preparation methods were found to contain a mixture of product and adipic acid (starting material) (see appendix E).

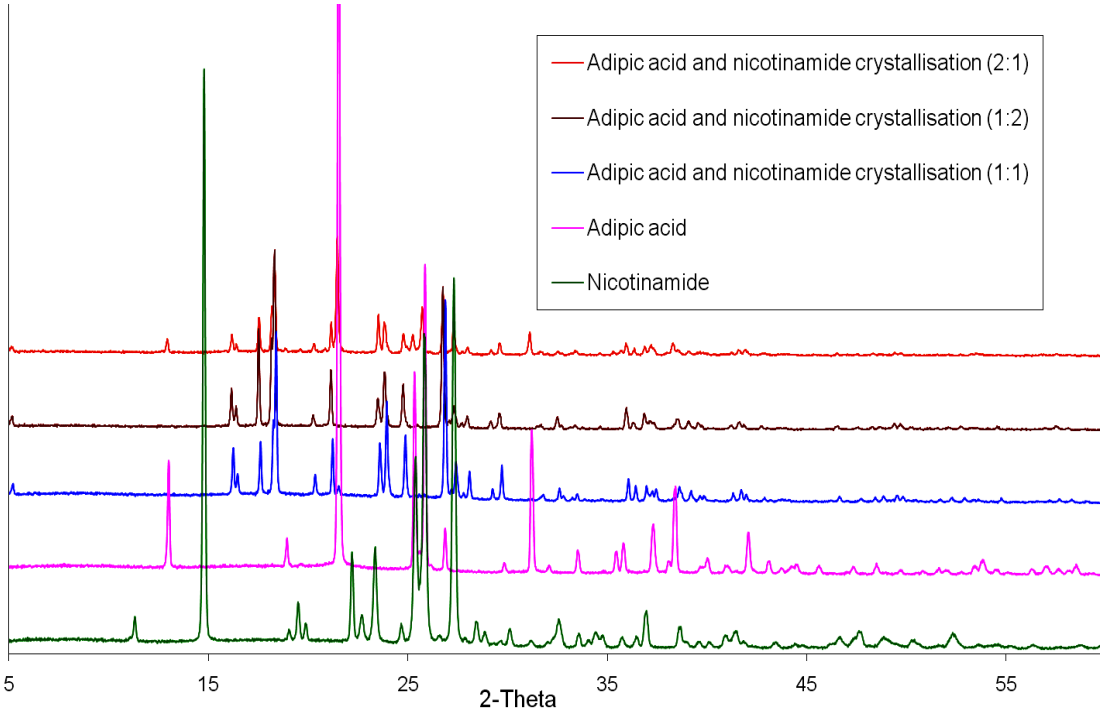

Figure 5.4.1: X-ray powder diffraction patterns of nicotinamide and adipic acid and products of crystallisation using methanol.

From the integral values of different peak intensities for protons in different environments on adipic acid and nicotinamide obtained from the NMR spectra, it is evident that the new material obtained from the 1:2 and 1:1 crystallisations has the molecular formers crystallised in 1:2 adipic acid : nicotinamide stoichiometric ratio (see figure 5.4.2).

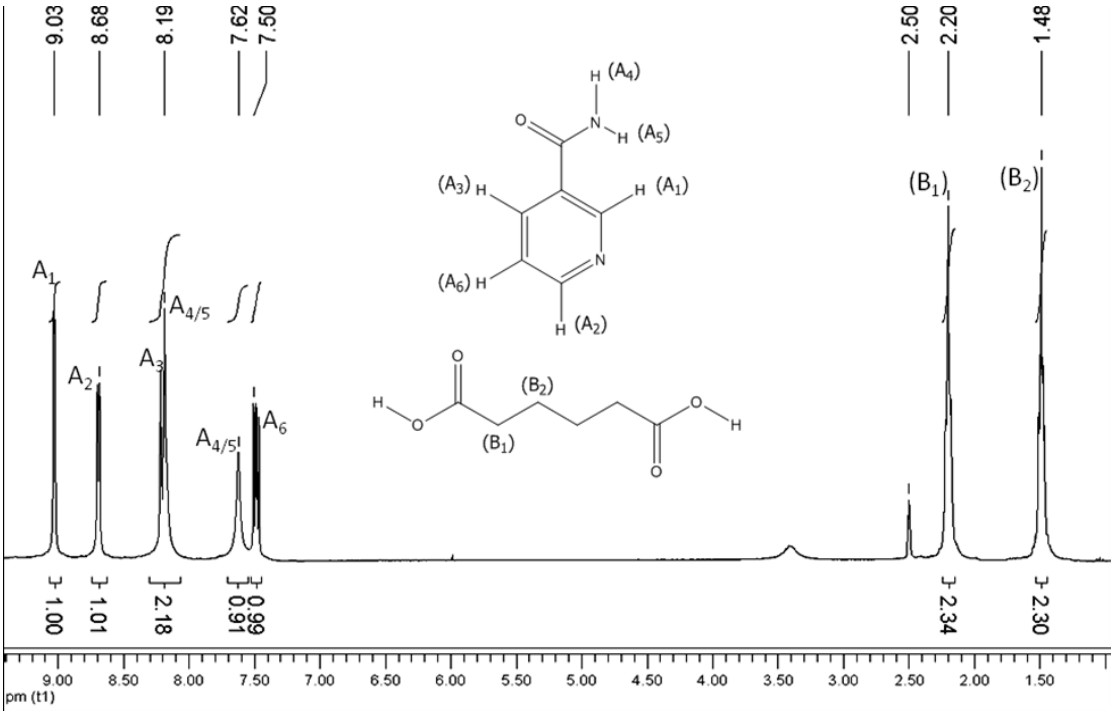

Figure 5.4.2: ^{1}H NMR of nicotinamide and adipic acid adduct using DMSO as solvent. ^{1}H NMR 300MHz (DMSO-d_6): δ = 12.03(s, 2H), 9.02(dd, 2H), 8.68(dd, 2H), 8.19(dt, 2H), 7.62(s, 2H), 7.50(ddd, 2H), 2.50(m, 4H), 2.30(m, 4H).

The solid state IR data for the new material obtained from crystallisation and the starting materials are compared. The spectra for the new material and the former products are similar. See sections 5.1 and 5.2 for the characteristic IR peaks of different molecular fragments in nicotinamide and adipic acid molecules. The similarity between the spectra obtained for the product and the mixture of starting materials (except for the shift of bands) supports the absence of salt formation and implies co-crystal formation (see figure 5.4.3) although not conclusively.

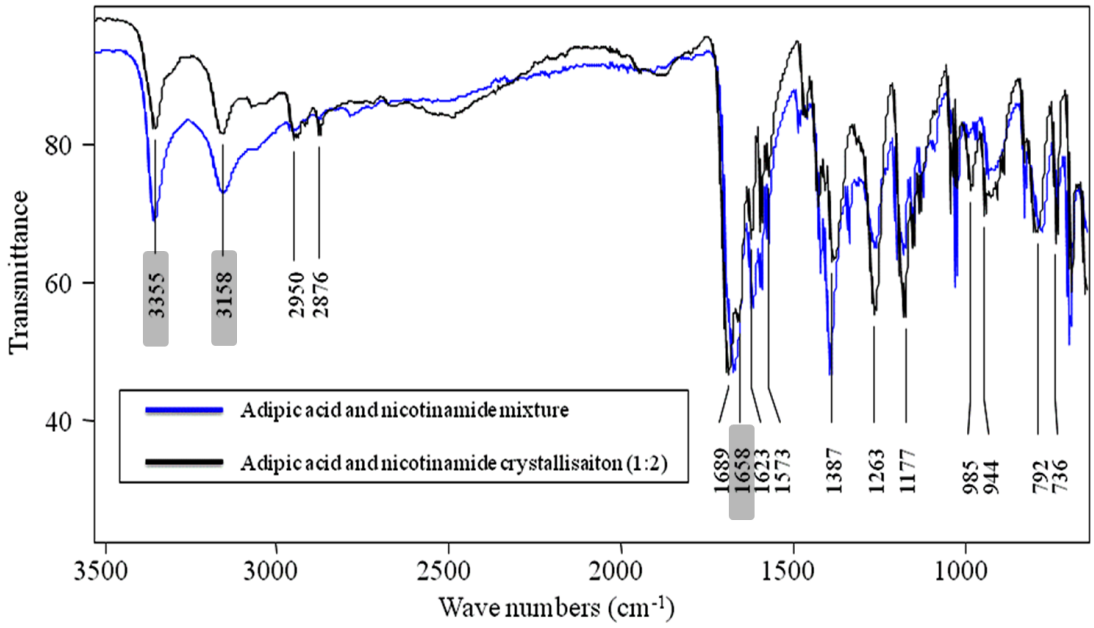

Figure 5.4.3: FTIR spectra of adipic acid and nicotinamide and product of crystallisation (1:2).

5.4.1 Determination of crystal structure from single crystal X-ray diffraction data (SXRD)

The crystal structure of the adipic acid : nicotinamide (1:2) co-crystal was successfully solved from single crystal X-ray diffraction data (see appendix F, G, H and see table 5.4.1). The unit cell parameters obtained from the powder X-ray diffraction data and single X-ray diffraction data are similar (see table 5.4.1) with the only difference being the expected contraction with temperature. The stoichiometric ratio of the adipic acid and nicotinamide established from NMR is confirmed as 1:2 by the single-crystal structure. Figure 5.4.1.1 shows the atom labelling used in this structure and clearly shows the adduct in neutral co-crystalline form with one half of the adipic acid molecule generating the other half through inversion symmetry.

The supramolecular structure of adipic acid : nicotinamide (1:2) is determined through four intermolecular hydrogen bonds; one soft C-H···O=C hydrogen bond and three strong hydrogen bonds, two N-H···O=C type and one O-H···N(heterocyclic) interaction (see table 5.4.2), such that all strong hydrogen-bond donors and acceptors are used in the intermolecular network(see figure 5.4.1.2 (I)).

The nicotinamide and adipic acid molecules are linked by a O-H…N(heterocyclic) hard hydrogen bond confirming that the components remain in their neutral form in cocrystal (rather than salt) formation. The carboxyl oxygen O4 at (*x*, *y*, *z*) acts as a hydrogen bond donor, via H4, to the heterocyclic N1 of the nicotinamide at (*x*, *y*, *z*), while this packing is reinforced by C6 in nicotinamide at (*x*, *y*, *z*) acting as a hydrogen-bond donor through H6 to the other carboxyl oxygen O3 also at (*x*, *y*, *z*). Propagation of these two hydrogen bonds through inversion symmetry within the adipic acid molecule generates the 1:2 adipic acid : nicotinamide building block in which the adipic acid molecule is capped at both ends by nicotinamide molecules at (*x*, *y*, *z*) and (-*x*, 2-*y*, 1-*z*).

Each nicotinamide molecule is connected to another through complementary N-H…O hydrogen bonds in which N2 at (*x*, *y*, *z*) acts as a donor via H2A to O1 at (-*x*, 2-*y*, 1-*z*) and O1 at (*x*, *y*, *z*) acts as an acceptor from N2 via H2A at (-*x*, 2-*y*, 1-*z*). The resulting amide-amide dimer (an $R^2_2(8)$ ring) links the 1:2 adipic acid : nicotinamide building

blocks together into an infinite zig-zag chain running in the [201] direction (see figure 5.4.1.2 (II)).

These chains are then linked together into a hydrogen-bonded sheet through the second N-H…O=C interaction forming a C(4) chain running parallel to the *a*-axis. The amide N2 at (*x*, *y*, *z*) forms this hydrogen bond through H2B to O1 at (1+*x*, *y*, *z*) while O1 at (*x*, *y*, *z*) also acts as an acceptor of H2B at (-1+*x*, *y*, *z*). Propagation of this hydrogen bond around the inversion centre at (0, 0.5, 0) results in the formation of infinite hydrogen-bonded ladders, running in the [100] direction, containing alternating $R^2_2(8)$ and $R^2_4(8)$ rings (see figure (I)).

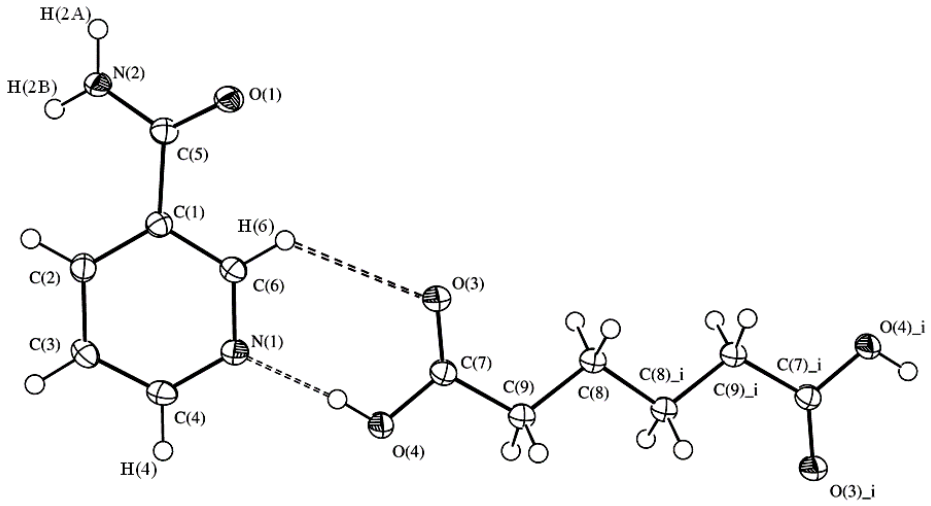

Figure 5.4.1.1: ORTEP diagram of the adipic acid : nicotinamide (1:2) co-crystal showing the strong hydrogen bond interaction between the two former molecules. Thermal ellipsoids are drawn at the 50% probability level.

Table 5.4.1

Summary of crystal data for adipic acid and nicotinamide co-crystal obtained from SXRD.

Empirical formula	$2(C_6 H_6 N_2 O), C_6 H_{10} O_4$
Fw	390.40
T [K]	120(2)
λ [Å]	0.71073
Crystal system	Triclinic
Space group	P -1
a[Å]	5.0261(2)
b[Å]	5.4280(3)
c [Å]	16.8981(10)
α[°]	98.147(2)
β[°]	91.072(3)
γ[°]	90.588(3)
V[Å^3]	456.24(4)
Z	1
D_m[mg/m^3]	1.421
Absorption coefficient	0.108 mm^{-1}
F(000)	206
Crystal size [mm^3]	0.18 x 0.16 x 0.08
2θ range [°]	3.65 to 27.48
Index ranges	-6<=h<=6, -7<=k<=7, -21<=l<=21
Reflections observed	7324
Independent reflections	2058[R(int) = 0.0331]
Completeness to theta = 27.48°	98.5%
Absorption correction	Semi-empirical from equivalents
Max. and min. transmission	0.9914 and 0.9808
Refinement method	Full-matrix least-squares on F^2
Data / restraints / parameters	2058 / 0 / 128
Goodness of fit on F^2	1.115
R [I > 2σ(I)]	R1 = 0.0468, wR2 = 0.1294
R indices (all data)	R1 = 0.0509, wR2 = 0.1327
Largest diff. peak and hole	0.340 and -0.284 e.Å^{-3}

Table 5.4.2

Intermolecular hydrogen bond parameters [Å, °] in the adipic acid : nicotinamide (1:2) co-crystal.

D-H···A	d(D-H)	d(H···A)	d(D···A)	<(DHA)
N(2)-H(2A)···O(1)(ii)	0.88	2.06	2.9260(16)	167.9
N(2)-H(2B)···O(1) (iii)	0.88	2.14	2.8851(17)	141.4
O(4)-H(4A)···N(1) (i)	0.84	1.85	2.6865(17)	174.2
C(6)-H(6)···O(3) (i)	0.95	2.70	3.3686(18)	127.9

Symmetry transformations used to generate equivalent atoms:
(i)-x,-y+2,-z+1 (ii) -x+2,-y+2,-z (iii) x+1,y,z

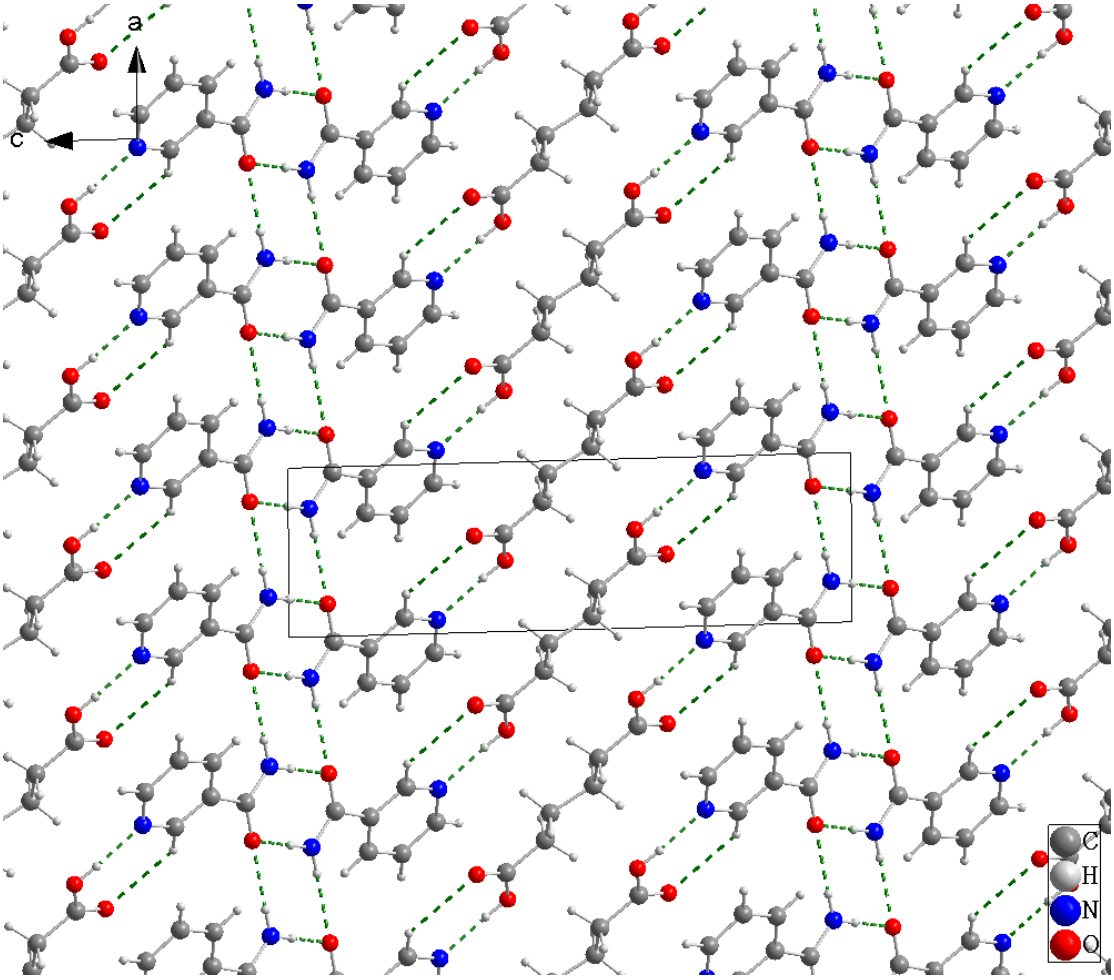

Figure 5.4.1.2 (I): A view of the crystal structure of adipic acid : nicotinamide (1:2) down [010] showing the intermolecular interactions between the molecules within a sheet.

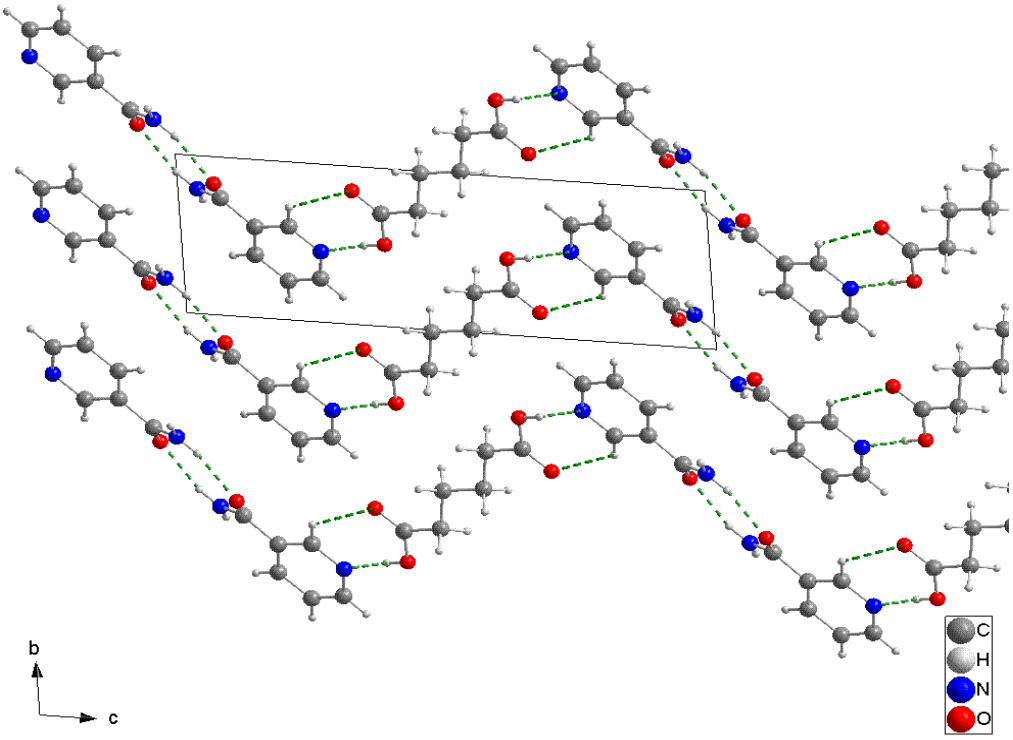

Figure 5.4.1.2 (II): A view of the crystal structure showing a projection down [100] illustrating the padding of sheets in adipic acid : nicotinamide (1:2) and zigzag sheets.

5.4.2 Determination of crystal structure from powder X-ray diffraction data (PXRD)

Once the crystallisation of a new adipic acid : nicotinamide (1:2) co-crystal was confirmed (using PXRD, NMR and IR), full crystal structure analysis was attempted from X-ray powder diffraction data. Possible unit cell parameters were obtained by indexing the 20 most intense peaks in the powder X-ray diffraction pattern selected using XFIT[38] software. *CRYSFIRE*[39] was then used to run different indexing programs and used to index the selected peaks (see appendix I). Possible unit cell parameters were chosen for further analysis on the basis of density considerations of the stoichiometric ratio of the co-crystal (obtained from NMR) along with cell volume and consideration of the figure of merit (see Table 5.4.3). Both space groups P1 and P-1 are possible for the structure: P1 would require both nicotinamide molecules and the adipic acid molecules to occupy general positions whereas in P-1 the second nicotinamide molecule would be generated by crystallographic symmetry and the adipic acid molecule would sit on the inversion centre. The accuracy of this chosen

unit cell can be confirmed through Le bail pattern decomposition. The refined unit cell and the fit between the calculated and experimental powder X-ray diffraction patterns by Le bail pattern decomposition are shown in table 5.4.3 and figure 5.4.2.1. The best fit between the experimental data (red) and simulated pattern (green) is quantified in terms of R-factor value R_{wp} and χ^2. The Le bail fit was then used as a starting point for the structure solution process from X-ray powder diffraction data (see figure 5.4.2.2).

Table 5.4.3

Cell parameters and space group from powder diffraction and single crystal data.

	Figure of Merit	*a*(Å)	*b*(Å)	*c*(Å)	α(°)	β(°)	γ(°)	Cell volume (Å^3)	Space group
PXRD indexing	57.61	5.505	17.128	5.039	90.16	90.67	96.75	471.88	P-1
PXRD Le bail fit	R_{wp}= 0.097 χ^2=0.92	5.493	17.103	5.034	90.93	96.78	89.71	469.27	P-1
Single crystal structure (120K)	R1 = 0.0468, wR2 = 0.1294	5.428 (3)	16.898 (10)	5.026 (2)	91.07 (3)	90.58 (3)	98.14 (2)	456.24 (4)	P-1

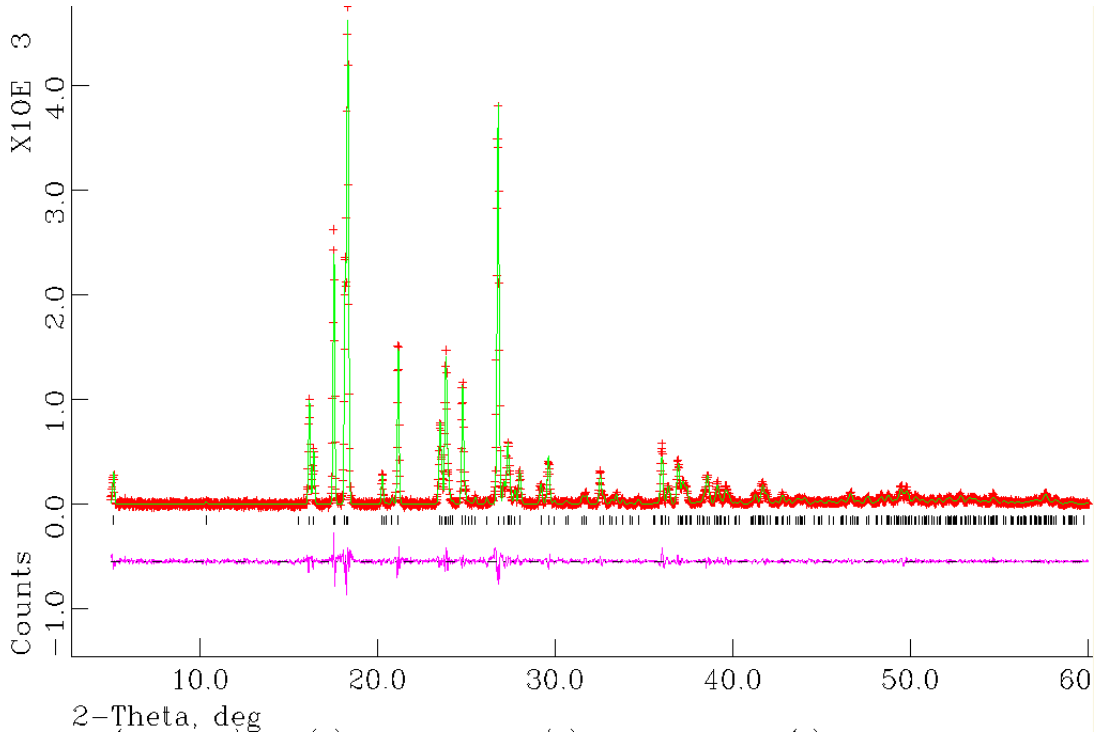

Figure 5.4.2.1: The Le bail profile fit for the adipic acid : nicotinamide (1:2) co-crystal.

Structure solution was carried out using the DE technique (implemented in the program POSSUM[58]). The adipic acid molecule was fixed at the inversion centre (0, 0, 0) such that one half of the molecule generated the other. The molecule was allowed to rotate around this pivot with torsional variation as shown (figure 5.4.2.2). The nicotinamide was allowed to translate and rotate with torsional flexibility as shown in (figure 5.4.2.2). In total, the structure solution had 11 degrees of freedom. The H atoms in amide and carbonyl functional groups are weak scatters and would increase the number of degrees of freedom needed in the global minimum search process, hence, these were not included in the structure solution. The DE was run using a population size of 35 and control parameters K = 0.99 and F = 0.3. The best solution obtained from 5 epochs gave a structure with R_{wp} = 0.1706. The evolutionary progress plot for this calculation is shown in figure 5.4.2.2.

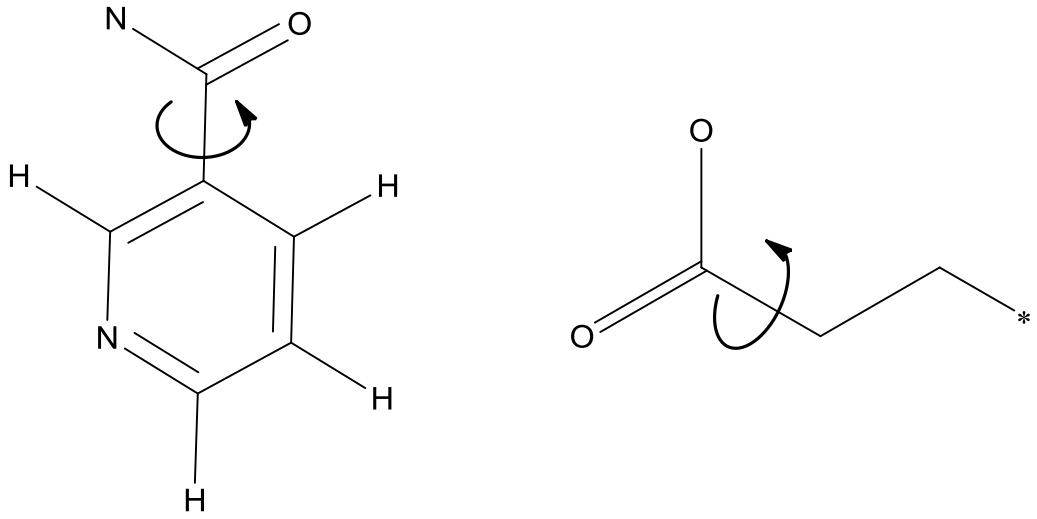

Figure 5.4.2.2: Molecular structures of nicotinamide and one half of adipic acid molecules showing the torsion angles used in the direct-space structure solution calculation.

Comparison between the structure solution obtained from PXRD and crystal structure obtained from SXRD shows the N and O atoms in the amide in the functional group of nicotinamide are swaped (see figures 5.4.1.2(I) and 5.4.2.3). This is not surprising as N and O have similar electron density and may not always be discriminated during the application of direct space methods from PXRD. Rietveld refinement was not carried out for this structure as the crystal structure was already rationalised from PXRD.

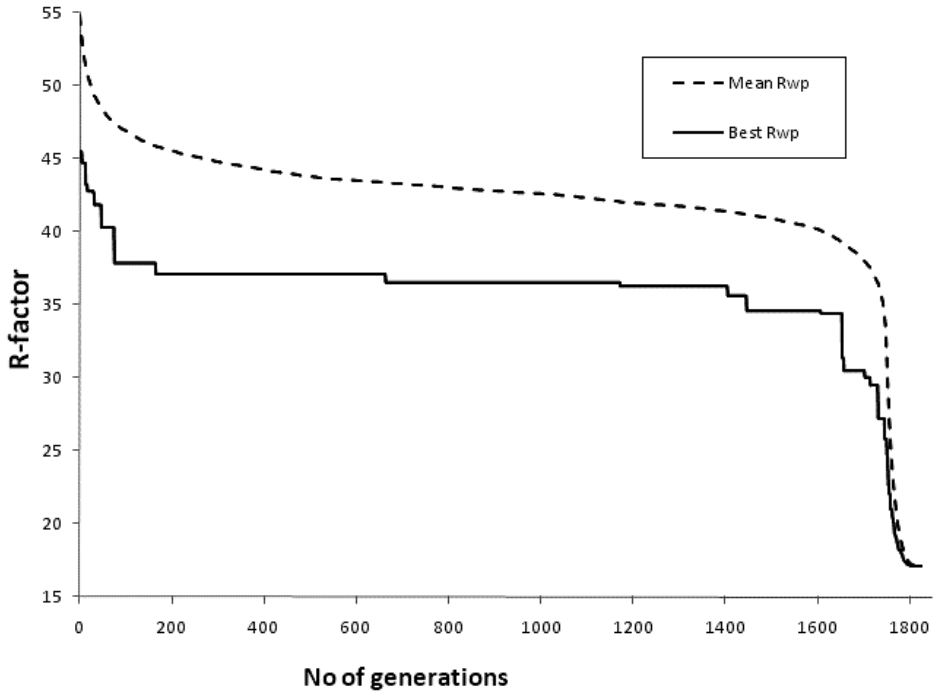

Figure 5.4.2.3: Evolutionary progress plot for the best DE calculations for the product of adipic acid : nicotinamide (1:2).

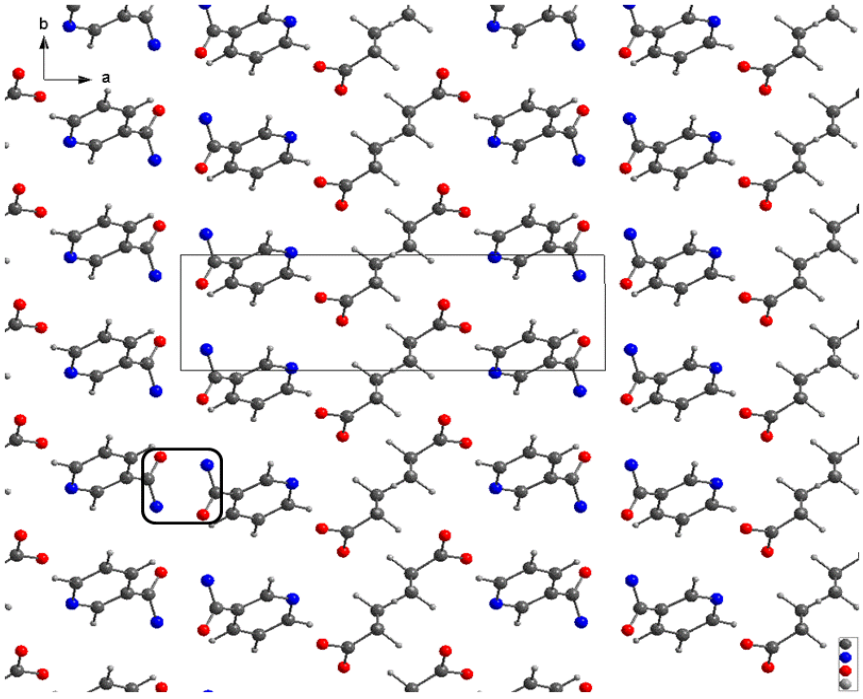

Figure 5.4.2.4: A view of the crystal structure of adipic acid : nicotinamide (1:2) showing the different amide conformation obtained from the structure solution from PXRD.

5.5 Pimelic acid and nicotinamide

Pimelic acid (see figure 2.2(e)) was crystallised independently with both nicotinamide and isonicotinamide. In the case of nicotinamide the crystallisation was carried out using methanol in a 1:1 starting molar ratio using traditional solvent crystallisation. The different X-ray powder diffraction patterns for the product formed and the starting materials illustrate the formation of a new material (see figure 5.5.1). This new product formed as a white crystalline solid.

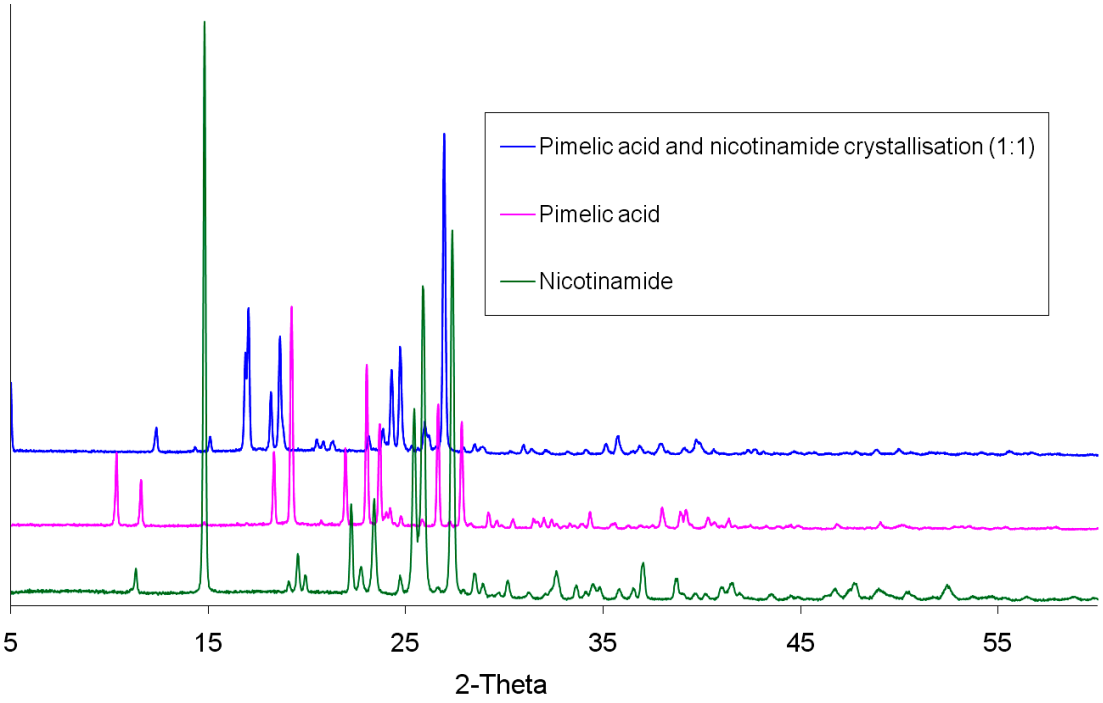

Figure 5.5.1: X-ray powder diffraction patterns for pimelic acid and nicotinamide and the product of crystallisation using methanol.

From the integral values of peak intensities for protons in different environments on pimelic acid and nicotinamide obtained from the NMR spectra, it is evident that the new material obtained from a starting molar ratio of 1:1 has a 1:1 stoichiometric ratio (see figure 5.5.2).

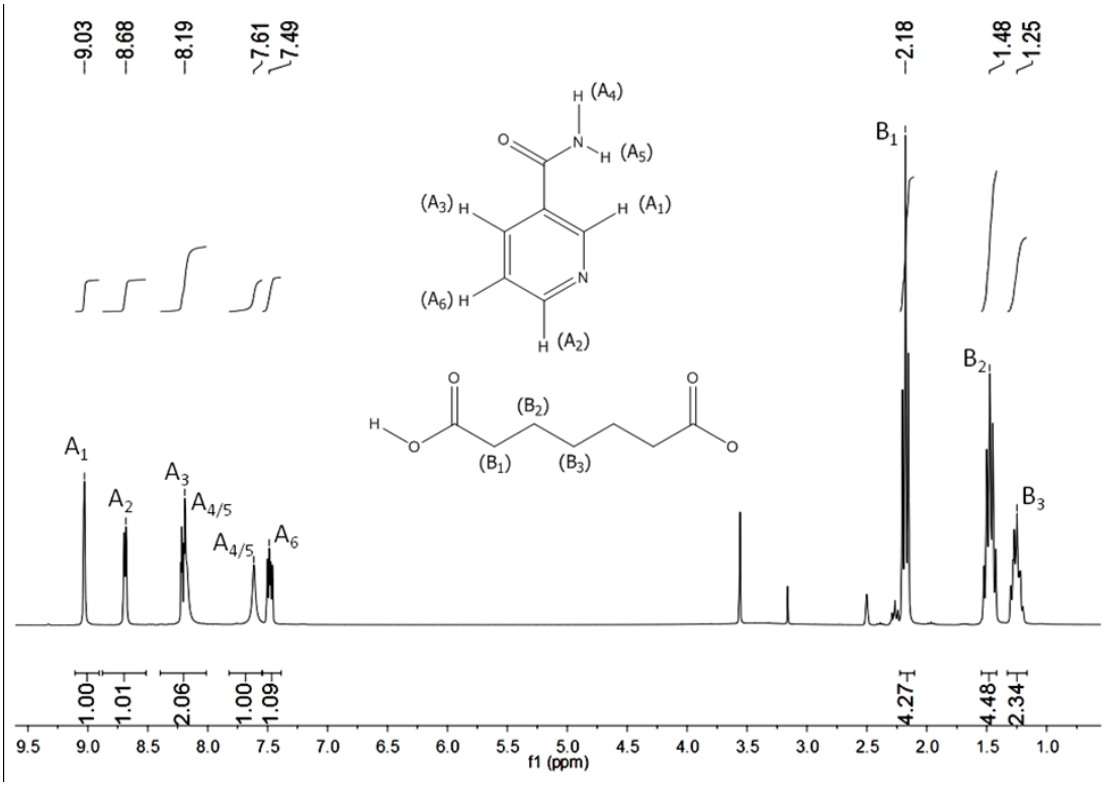

Figure 5.5.2: ^{1}H NMR of pimelic acid and nicotinamide crystallisation (1:1) using DMSO as solvent. ^{1}H NMR 300MHz (DMSO-d_6): δ = 12.60(s, 2H), 9.03(dd, 1H), 8.68(dd, 1H), 8.19(dt, 1H), 7.61(s, 1H), 7.49(ddd, 1H), 2.18(m, 4H), 1.48(m, 4H), 1.25(m, 2H).

The IR data for the new (1:1) material obtained from crystallisation and the starting materials are compared in figure 5.5.3. As in previous sections, there are characteristic IR peaks of different molecular fragments in nicotinamide and pimelic acid. The absence of a characteristic high tone at 3000 cm^{-1} for the O-H bond stretching of carboxylic acid shows the involvement of the carboxylic acid group in intermolecular bonds. Again there are similarities between the spectra obtained for the product and the mixture of starting materials apart from the shift of bands. There is an indication of broad peak ~2500cm^{-1} that may imply salt formation but this is not conclusive.

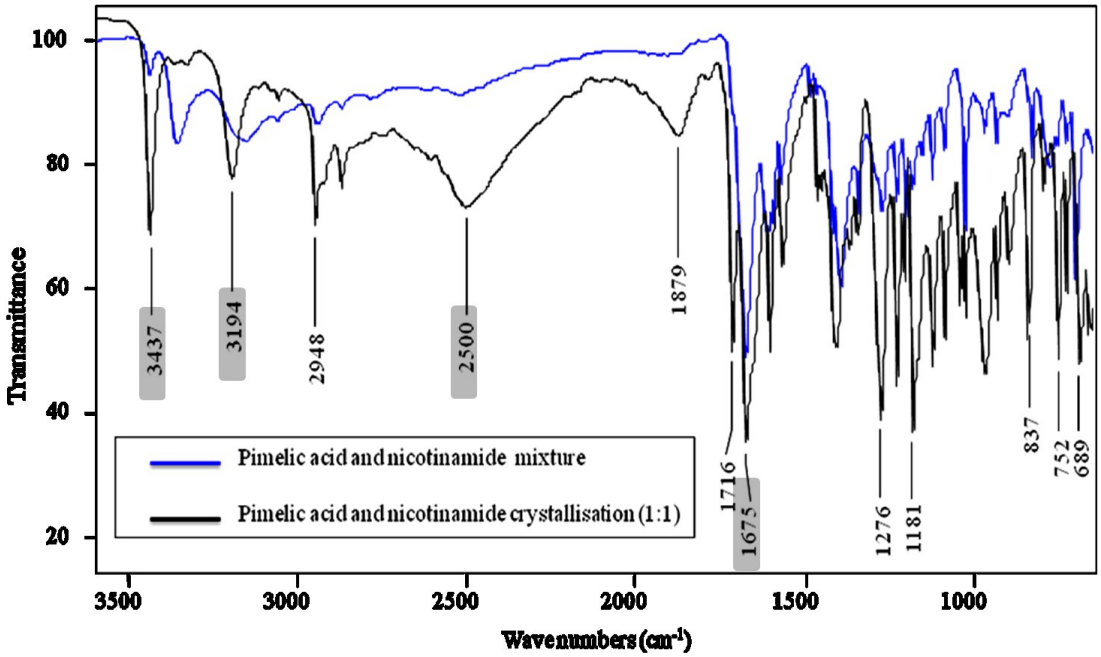

Figure 5.5.3: The FTIR spectra of pimelic acid and nicotinamide and the product of crystallisation.

No attempt has been made to index the pimelic acid : nicotinamide (1:1) adduct due to constraints of the project time.

5.6 Pimelic and isonicotinamide

Pimelic acid was crystallised with isonicotinamide using traditional solvent mediated crystallisation with methanol. This crystallisation was done in a 1:1 starting molar ratio and gave rise to white solid material. The X-ray powder diffraction pattern for the material formed was different in comparison to the starting materials showing formation of new adduct (see figure 5.6.1). However, there may also be some pimelic acid in this sample. Indexing of the new material would address this observation.

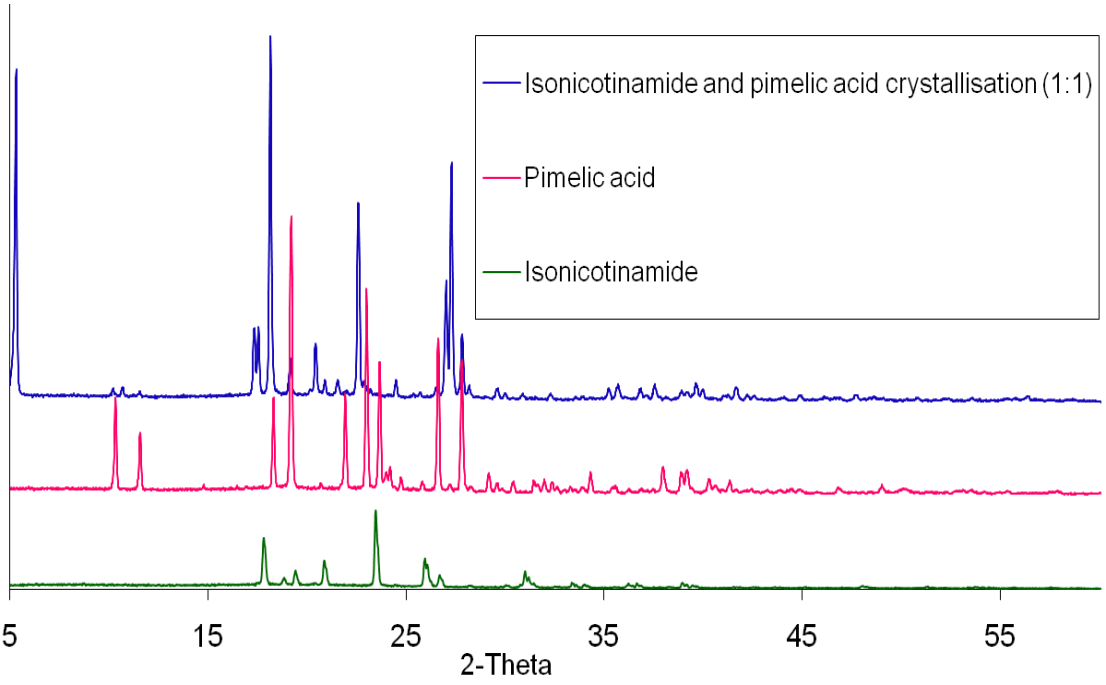

Figure 5.6.1: X-ray powder diffraction pattern for pimelic acid and isonicotinamide and products of crystallisation using methanol.

From the integral values of different peak intensities for protons in different environments on pimelic acid and isonicotinamide obtained from the NMR spectra, it is evident that the new material obtained from the starting stoichiometric ratios of 1:1 also has a 1:1 stoichiometric ratio (see figure 5.6.2).

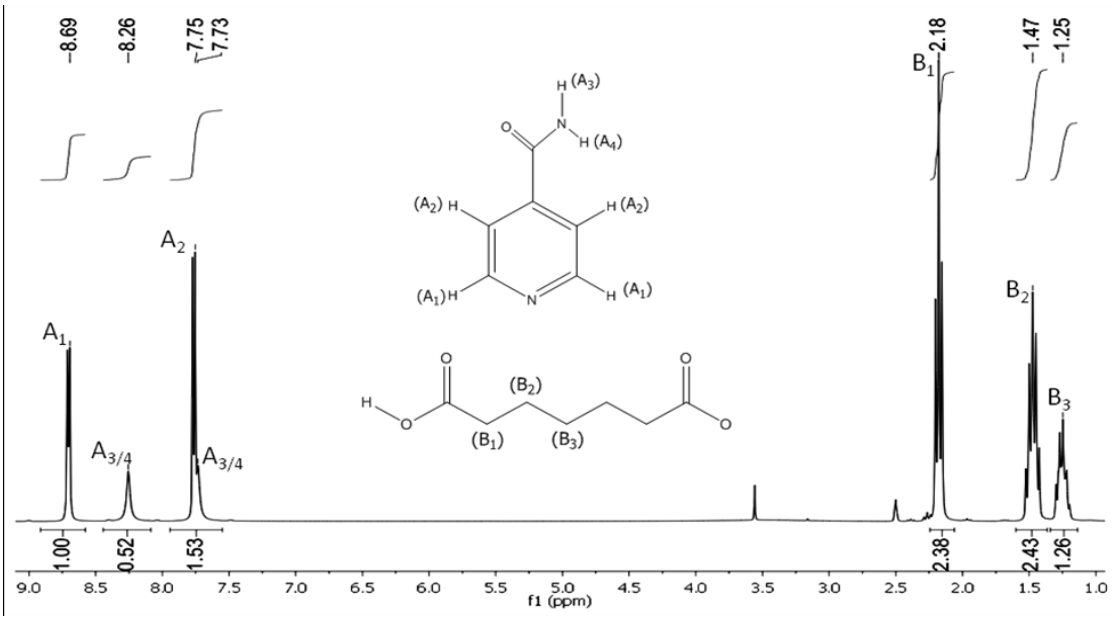

Figure 5.6.2: ^{1}H NMR of pimelic acid and isonicotinamide (1:1) crystallisation using DMSO as solvent. ^{1}H NMR 300MHz (DMSO-d_6): δ = 12.52(s, 2H), 8.69(dd, 2H), 8.26(s, 1H), 7.75(dd, 2H), 7.73(s, 1H), 2.38(m, 4H), 1.43(m, 4H), 1.26(m, 2H).

The solid state IR data for product obtained from crystallisation and mixture of starting materials are compared. As the structures for nicotinamide and isonicotinamide are similar, we would expect the IR spectra for these two compounds to look similar. The C=O stretching frequency bands of amide group can be observed between 1692 and 1548 cm^{-1}. The N-H stretching frequency bands of the amide group at 3354 cm^{-1} show the formation of intermolecular bonding and characteristic bands at 671 cm^{-1} and 721 cm^{-1} indicate the monosubstituted aromatic ring. The absence of a characteristic high tone at 3000 cm^{-1} for O-H bond stretching frequency of the carboxylic acid shows the involvement of the carboxylic acid in intermolecular bonding. Many features of these spectra are similar for the product and the starting materials. However, as in the case of pimelic acid : nicotinamide (1:1) there are indications of a broad band at ~ 2500 raising the possibility that this adduct could be in salt rather than neutral form. From 5.5.3 and 5.6.3 it is likely that both pimelic acid : nicotinamide and pimelic acid : isonicotinamide are in the same form.

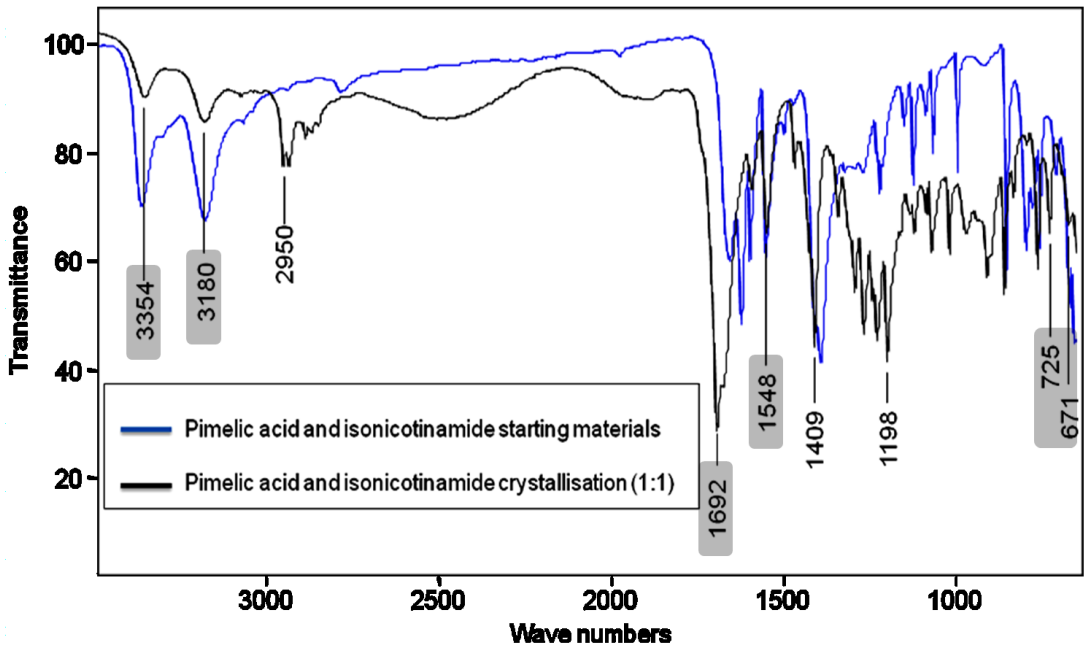

Figure 5.6.3: FTIR spectra of pimelic acid and isonicotinamide and the product of crystallisation.

No attempt has been made to index the pimelic acid : isonicotinamide (1:1) adduct due to constraints of the project time.

5.7 Suberic acid and nicotinamide

Suberic acid (see figure 2.2(f)) was crystallised with nicotinamide using different solvents with the components/starting molar ratios in different molar ratios. Crystallisation was carried out using methanol and ethanol and in 1:1, 1:2 and 2:1 starting molar ratios. Solvent mediated crystallisation and solvent drop grinding methods were employed. All new materials obtained from crystallisation were white solids. For each starting stoichiometric ratio, the same new material was obtained from different solvents and synthesis methods. From the powder X-ray diffraction data, it is evident that two new materials were obtained from the 1:1 (2:1) and the 1:2 stoichiometric ratios are different and differ from the starting materials (see figure 5.7.1).

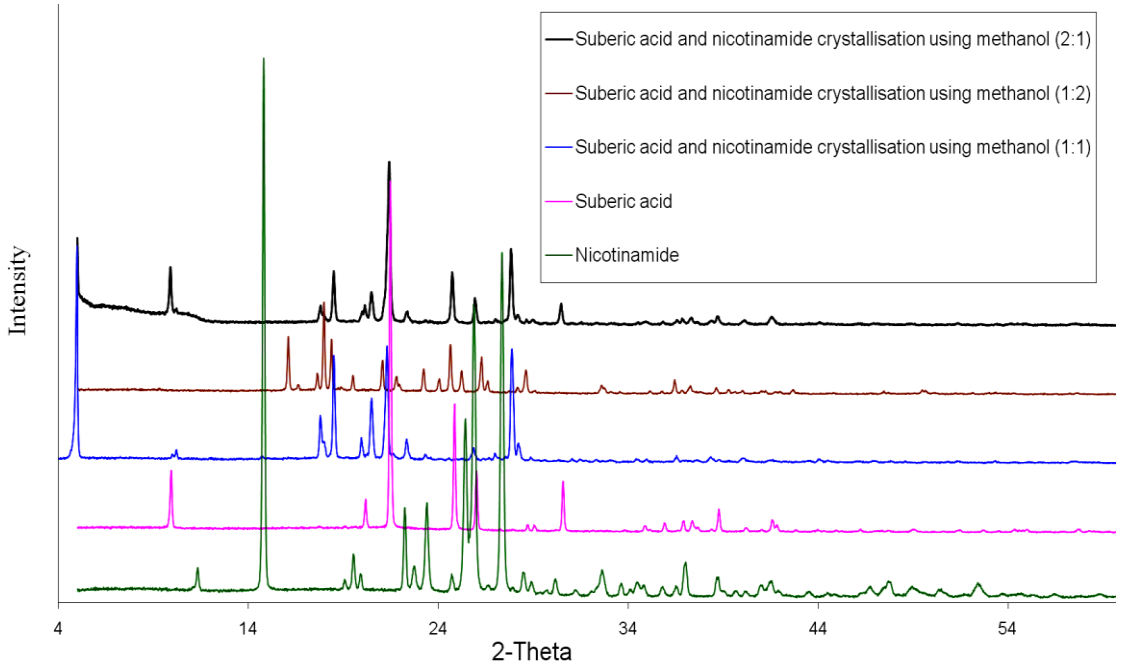

Figure 5.7.1: X-ray powder diffraction pattern for suberic acid and nicotinamide and products of crystallisation from methanol.

From the integral values of different peak intensities for protons in different environments on suberic acid and nicotinamide obtained from NMR spectra, it is evident that the new materials obtained by crystallisation of the starting materials in molar ratios of 1:1 and 1:2 are obtained with 1:1 and 1:2 stoichiometric adduct ratios (see figures 5.7.2 and 5.7.3).

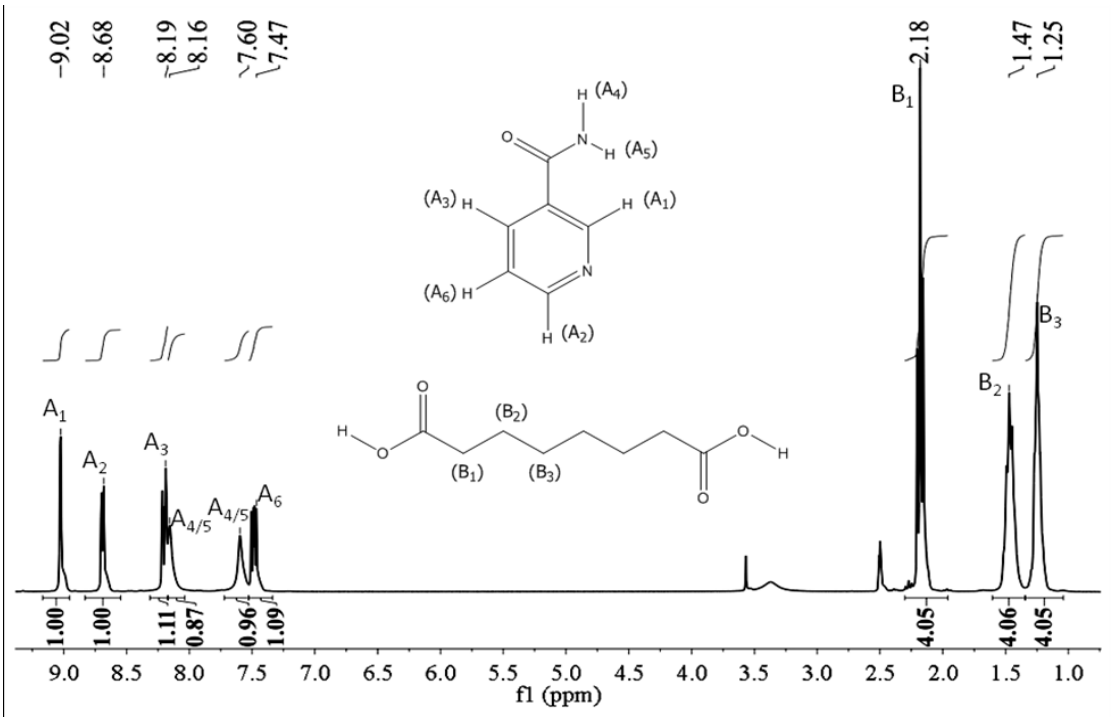

Figure 5.7.2: ^{1}H NMR of suberic acid and nicotinamide (1:1) adduct (from 1:1 starting ratio) using DMSO as solvent. ^{1}H NMR 300MHz (DMSO-d_6): δ = 11.97(s, 2H), 9.02(dd, 1H), 8.68(dd, 1H), 8.19(dt, 1H), 8.16(s, 1H), 7.60(s, 1H), 7.47(ddd, 1H), 2.18(m, 4H), 1.47(m, 4H), 1.25(m, 4H).

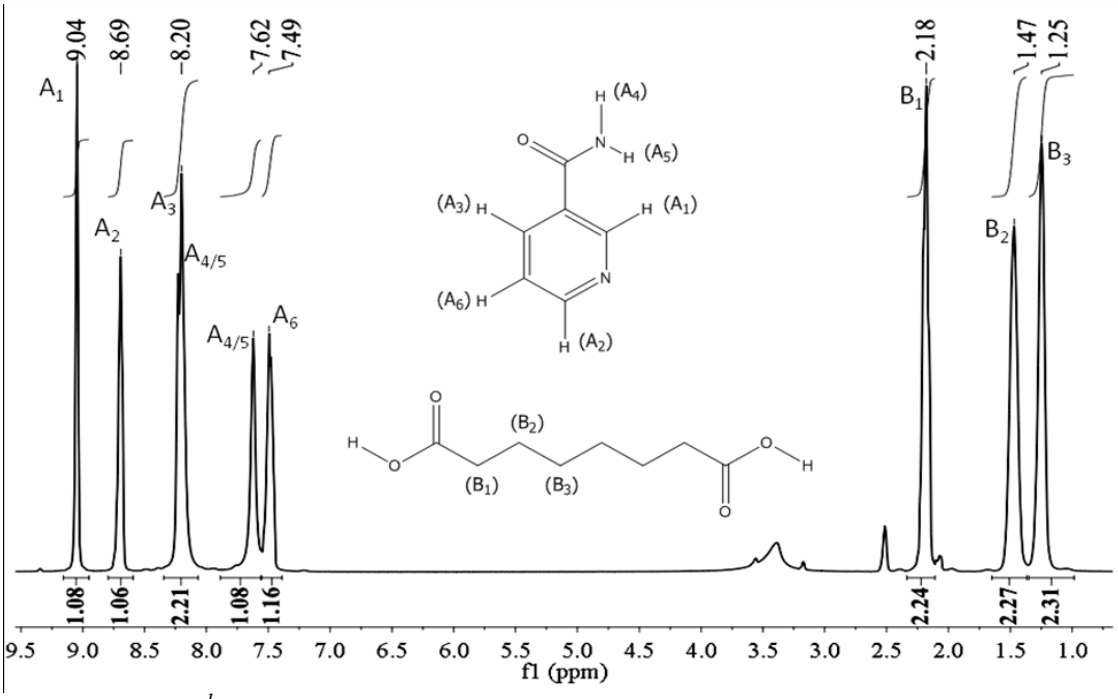

Figure 5.7.3: ^{1}H NMR of suberic acid and nicotinamide (1:2) adduct (from 1:2 starting ratio) using DMSO as solvent. ^{1}H NMR 300MHz (DMSO-d_6): δ= 11.99(s, 2H), 9.04(dd, 2H), 8.69(dd, 2H), 8.20(dt, 2H), 7.62(s, 2H), 7.49(ddd,2H), 2.18(m,4H), 1.47(m,4H), 1.25(m,4H).

The IR data for the product obtained from crystallisation (1:1) is compared to that from a mixture of starting materials (figure 5.7.4). The absence of characteristic high tones at 3000cm^{-1} for the O-H bond stretching frequency for a carboxylic acid shows the involvement of the carboxylic acid group in intermolecular bonding. For a discussion of the characteristic peaks of the starting materials, see sections 5.1 and 5.2. There are similarities between the spectra obtained for the products and starting materials, but there are also indications of a potential broad band at ~2454cm^{-1} and hence the discrimination between neutral co-crystal and salt form is again not clear.

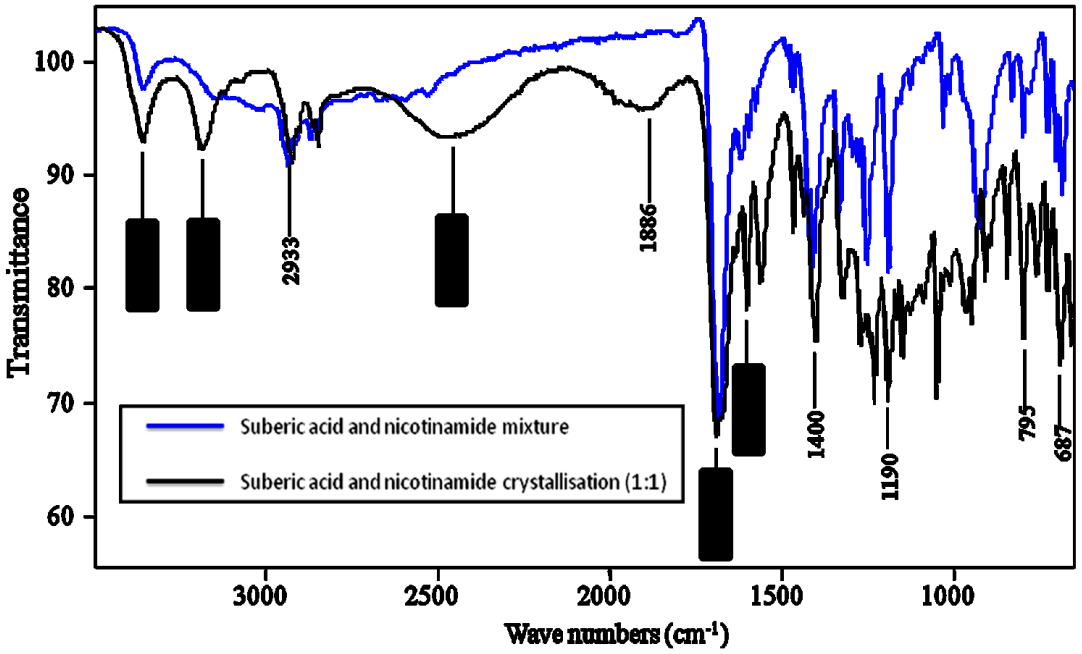

Figure 5.7.4: FTIR spectra for suberic acid and nicotinamide and product of crystallisation (1:1).

The IR data was not obtained for suberic acid : nicotinamde (1:2) adduct due to the time limitation and shortage of crystallised sample. No attempt has been made to index the suberic acid : nicotinamide (1:1 and 1:2) adducts due to constraints of the project time.

5.8 Suberic acid and isonicotinamide

Suberic acid was crystallised using traditional solvent mediated synthesis with isonicotinamide in methanol using a starting 1:1 molar ratio. The new material was formed as a white solid. The X-ray powder diffraction pattern for the material formed was different in comparison to starting materials, showing the formation of a new material (see figure 5.8.1).

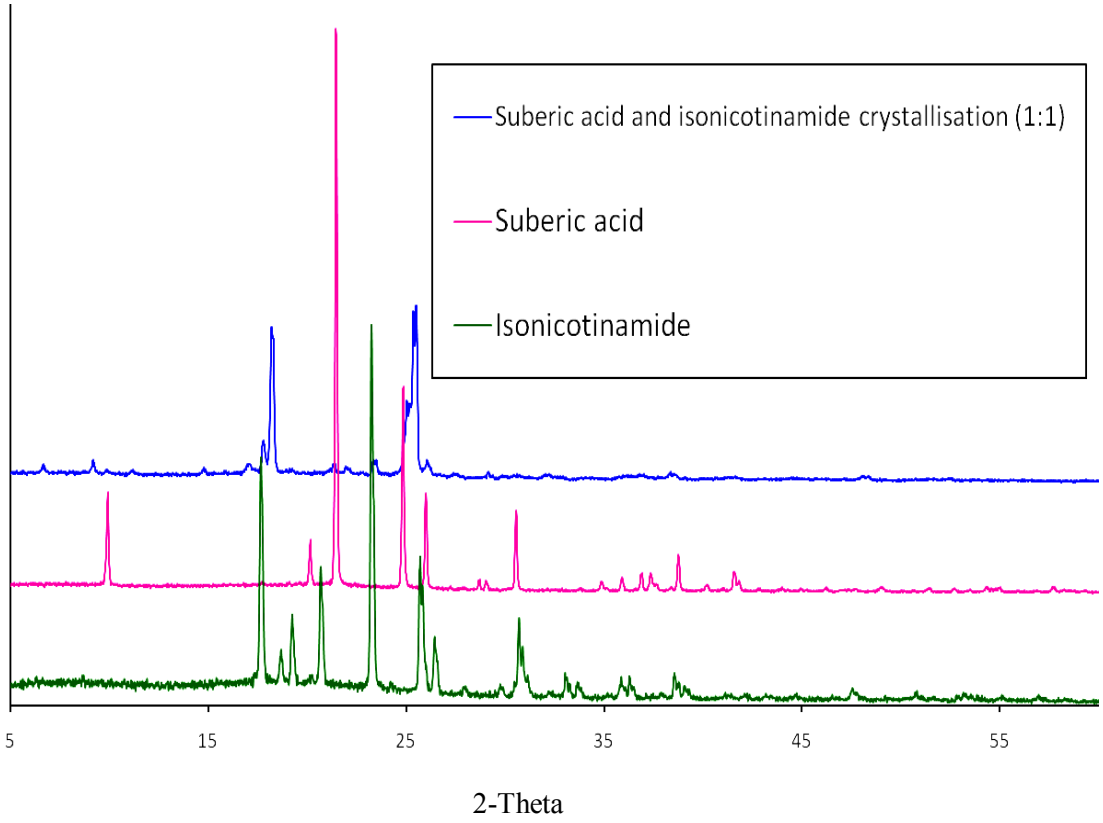

Figure 5.8.1: X-ray powder diffraction patterns of suberic acid and isonicotinamide and products of crystallisation using methanol.

From the integral values of different peak intensities for protons in different environments on suberic acid and isonicotinamide obtained from NMR spectra, it is evident that this new material contains the starting components in a 1:1 stoichiometric ratio (see figure 5.8.2).

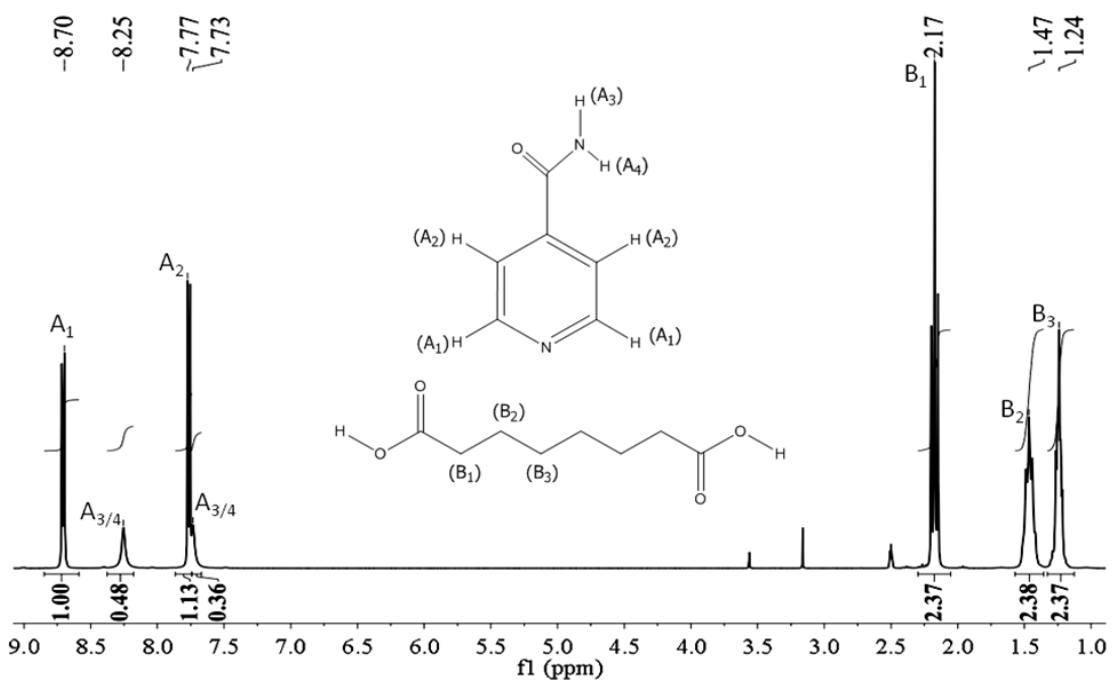

Figure 5.8.2: ^{1}H NMR of suberic acid and isonicotinamide adduct (from 1:1starting ratio) using DMSO as solvent. ^{1}H NMR 300MH (DMSO-d_6): δ = 12.01(s, 2H), 8.70(dd, 2H), 8.25(s, 1H), 7.77(dd, 2H), 7.73(s, 1H), 2.17(m, 4H), 1.47(m, 4H), 1.24(m, 4H).

The IR data for the crystallisation product (1:1) is compared to that from a mixture of the starting materials (figure 5.8.3). For a discussion of characteristic IR peaks of the starting materials, please see sections 5.2 and 5.6. The absence of characteristic high tones at 3000cm^{-1} for O-H bond stretching frequency for a carboxylic acid shows the involvement of the carboxylic acid group in intermolecular bonding. There are also indications of a potential broad band at ~2496cm^{-1} and hence the discrimination between neutral co-crystal and salt form is again not clear.

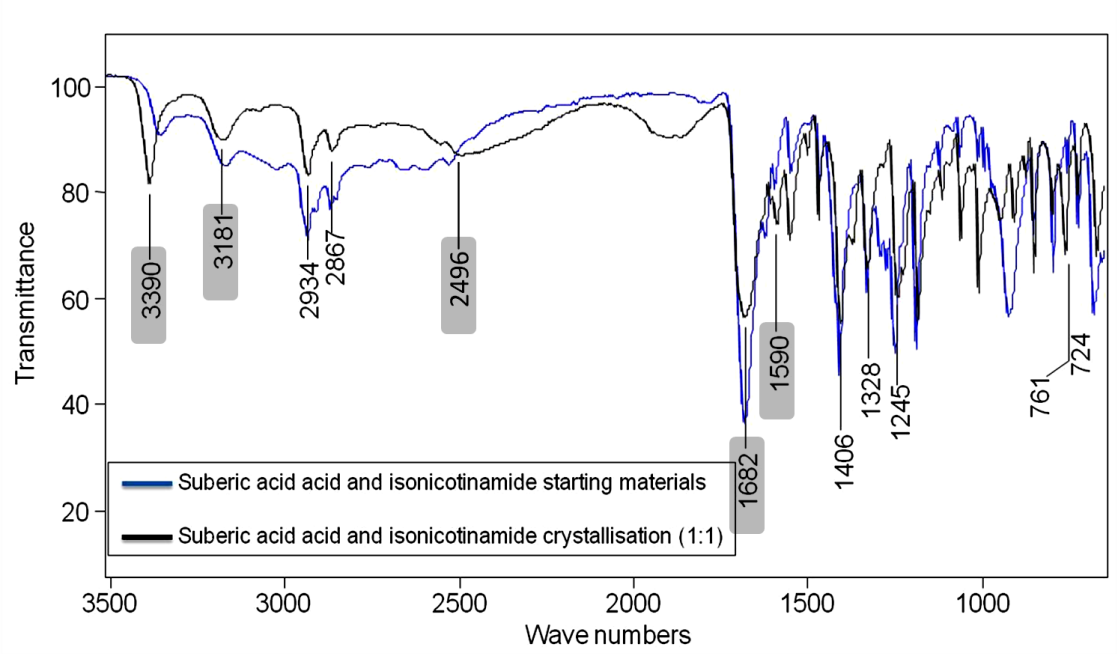

Figure 5.8.3: FTIR spectra for suberic acid and isonicotinamide and product of crystallisation (1:1).

No attempt has been made to index the Suberic acid : nicotinamide (1:1) adduct due to constraints of the project time.

5.9 Azelaic acid and nicotinamide

Azelaic acid (see figure 2.2(g)) was crystallised individually with both nicotinamide and isonicotinamide. In the case of nicotinamide, the crystallisation was carried out using methanol in 1:1, 1:2 and 2:1 starting molar ratios and performed using methanol and ethanol (in 1:1 only) both in solvent-mediated crystallisation and SDG methods (see appendix I). The different X-ray powder diffraction patterns for the product formed and the starting materials illustrate the formation of a new material (see figure 5.9.1). It is clear that other solvents also give the new product, but that in products from SDG mixtures of product and starting materials are obtained. The X-ray powder diffraction patterns obtained for all molar ratios, solvents and synthesizing methods are similar showing the formation of same product for different combinations. However, it is clear that in the 1:2 crystallisation, the new product is obtained in a mixture with some nicotinamide ; in the case of the 2:1 crystallisation there is azelaic acid also present. The presence of very little starting materials can be observed in the product obtained from 1:1 crystallisation

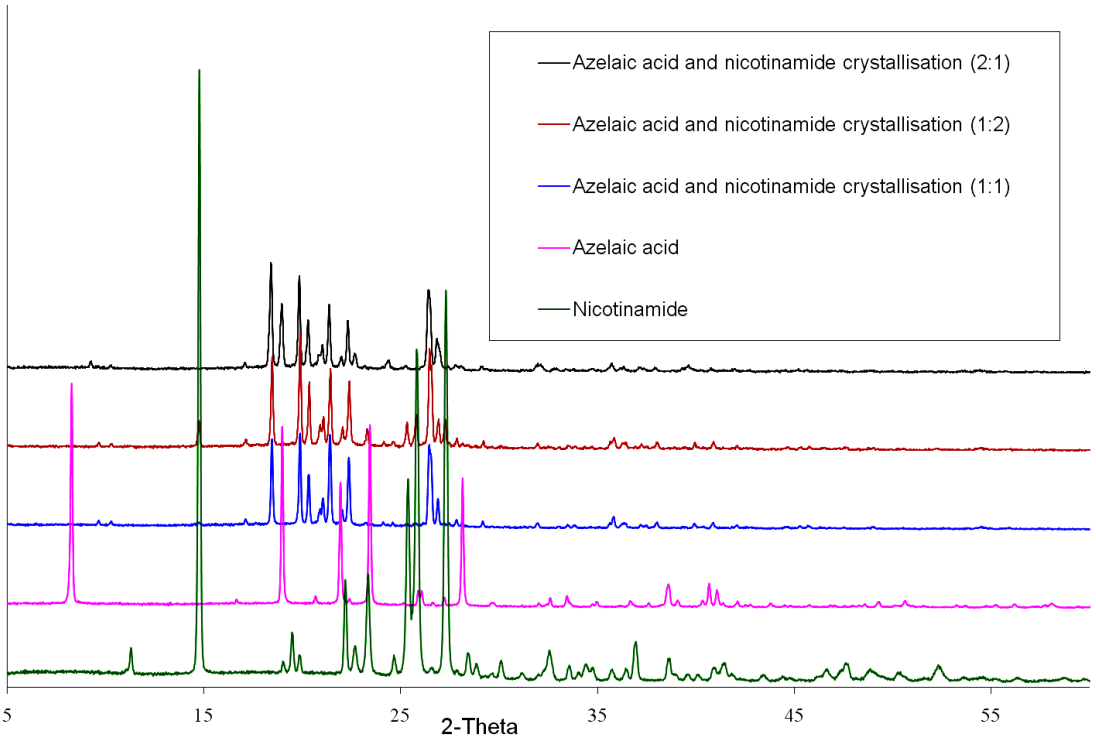

Figure 5.9.1: X-ray powder diffraction patterns for nicotinamide and azelaic acid and products of crystallisation using methanol.

From the integral values of different peak intensities for protons in different environments on azelaic acid and nicotinamide in the NMR spectra of the product obtained from 1:1 crystallisation, it is evident that the new material has a 1:1 stoichiometric ratio (see figure 5.9.2).

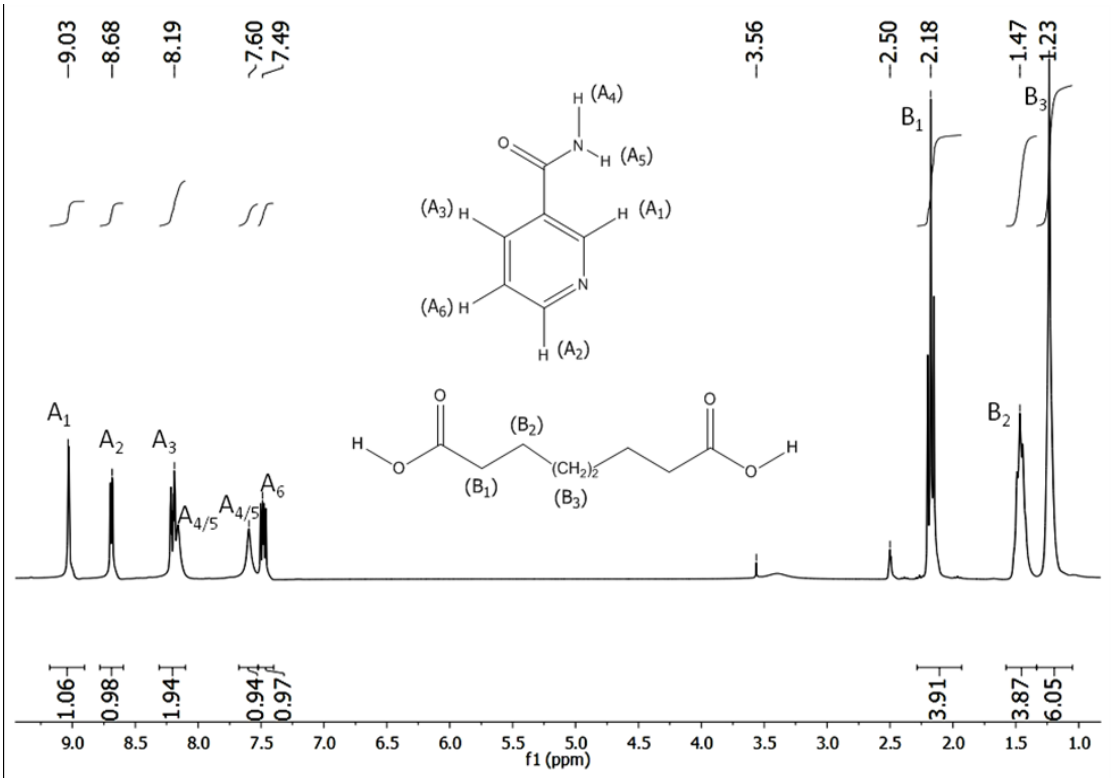

Figure 5.9.2: ^{1}H NMR for the product of nicotinamide and azelaic acid crystallisation using DMSO as solvent. ^{1}H NMR 300MHz (DMSO-d_6): δ = 11.97(s, 2H), 9.03(dd, 1H), 8.68(dd, 1H), 8.19(dt, 1H), 7.60(s, 1H), 7.49(ddd, 1H), 2.18(m, 4H), 1.47(m, 4H), 1.23(s, 6H).

The solid state IR data for the product is compared to that from a mixture of the starting materials. For a discussion of the characteristic peaks of nicotinamide, please refer sections 5.1 and 5.2. Interpretation of the IR spectra for different molecular fragments supports the presence of neutral intermolecular bonds. The similarities between the spectra obtained for the product and starting materials apart from shift of bands implies, although not conclusively, that there has been no proton transfer from the hydroxyl group to the heterocyclic nitrogen and hence the product formed would be a co-crystal rather than a salt. However, there is also a potential evidence of the broad peak at ~2466 cm^{-1} (see figure 5.9.3)

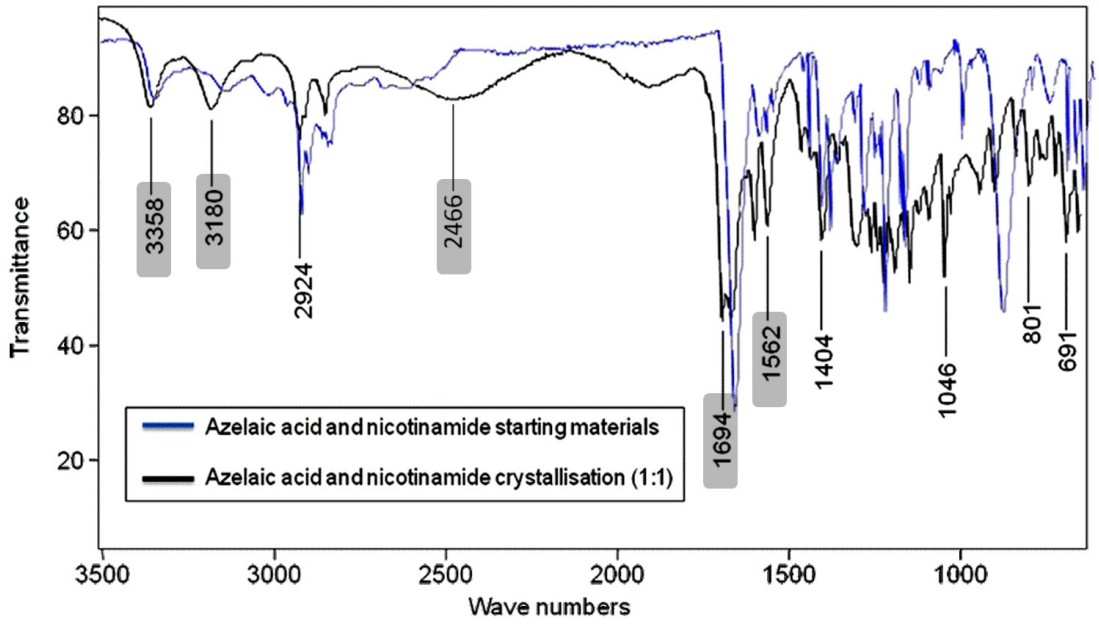

Figure 5.9.3: FTIR spectra of azelaic acid and nicotinamide and product of crystallisation (1:1).

5.9.1 Determination of unit cell parameters from X-ray powder diffraction data

The X-ray powder diffraction data was indexed using *CRYSFIRE*[39] on the basis of the 20 most intense peaks. Peaks were selected from the experimental PXRD using XFIT[38]. Additional information from the NMR was used to estimate the number of structural units in the asymmetric unit cell and help to identify the most probable unit cell with density considerations (see appendix L and table 5.9.1.1). Consideration of systematic absences gave the space group $Pna2_1$, as the most probable. This unit cell was then used as a starting point for Le bail profile fitting as shown in figure 5.9.1.1.

Table 5.9.1.1

Indexed and refined cell parameters obtained for the product of azelaic acid and nicotinamide:

	Figure of Merit	*a*(Å)	*b*(Å)	*c*(Å)	α(°)	β(°)	γ(°)	Cell volume (Å^3)	Space group
PXRD indexing	20	8.796	36.345	5.211	90	90	90	1665.95	$Pna2_1$
PXRD Le bail fit	R_{wp}= 0.0916/ 0.6565	8.881	36.795	5.258	90	90	90	1718.55	$Pna2_1$

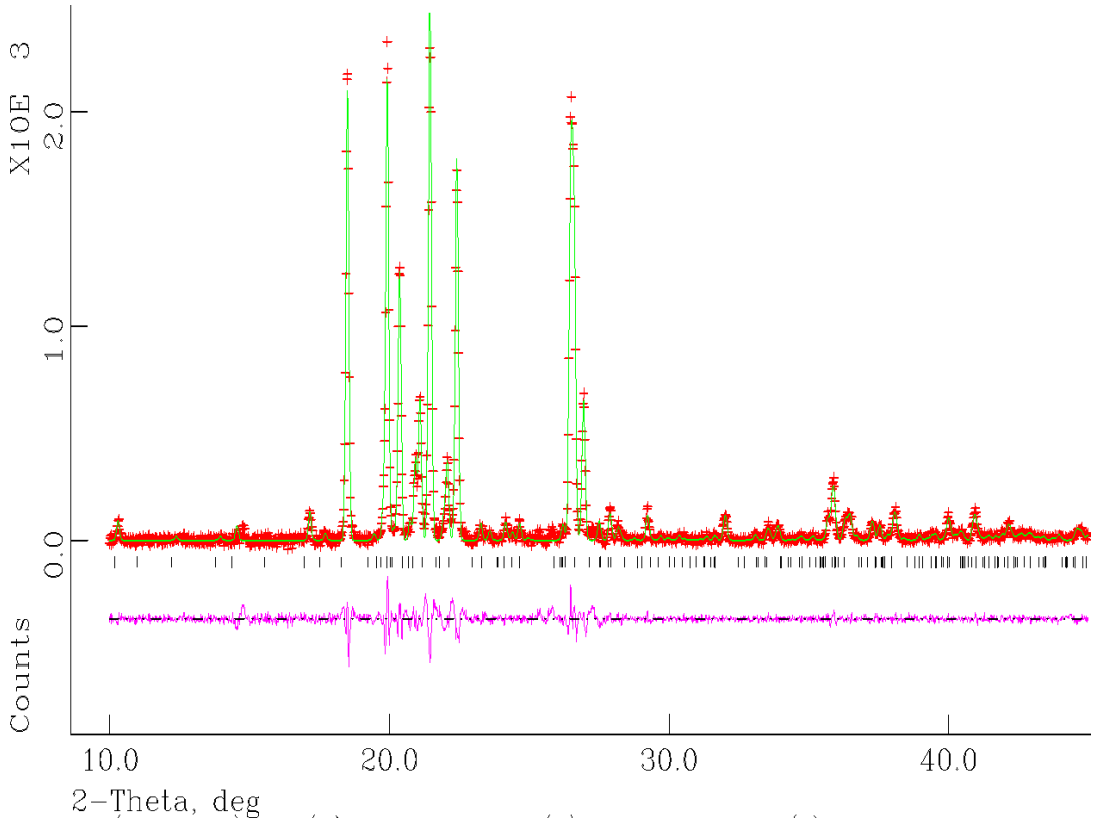

Figure 5.9.1.1: The Le Bail profile fitting for azelaic acid : nicotinamide (1:1) adduct. The greeen solid line shows calculated intensities and points superimposed on it are observed intensities. The difference between the calculated and observed intesities is shown by pink line. Reflection positions are also shown.

5.9.2 Determination of Structure Solution using Differential Evolution (DE)

The X-ray powder diffraction data used to run differential evolution calculations (using POSSUM[58]) for crystal solution was collected in the range $5° \leq 2\theta \leq 90°$. The maximum number of epochs set for each run was 5 and population size was $N_p = 35$. The rate of recombination (K) was set constant at 0.99 and a range of mutation rates (F) 0.2, 0.3, 0.4 and 0.5 used for structure solution. The structural models for solution comprised one molecule of azelaic acid and one nicotinamide excluding H atoms in amide and carboxylic acid functional groups.

The molecules were allowed free orientation and translation in the unit cell with torsion angles as shown. The no. of degrees of freedom was 15. The results for the different DE control parameters are shown in figures 5.9.2.1-5.9.2.4. In the case of F=0.2, the calculation clearly shows premature convergence of all the calculations, F=0.3 performed the best. The global minimum (the structure solution with R_{wp} = 0.146) has been found three times (other solutions with R_{wp} = 0.1419 and 0.1484). For F = 0.4, only one promising solutin was identified with an R_{wp} = 0.1535. In the case of F = 0.5, n o runs converged within the maximum generations allowed. The best structure solution (from F = 0.3, R_{wp} = 0.1416) was then used as a starting point for Rietveld refinement.

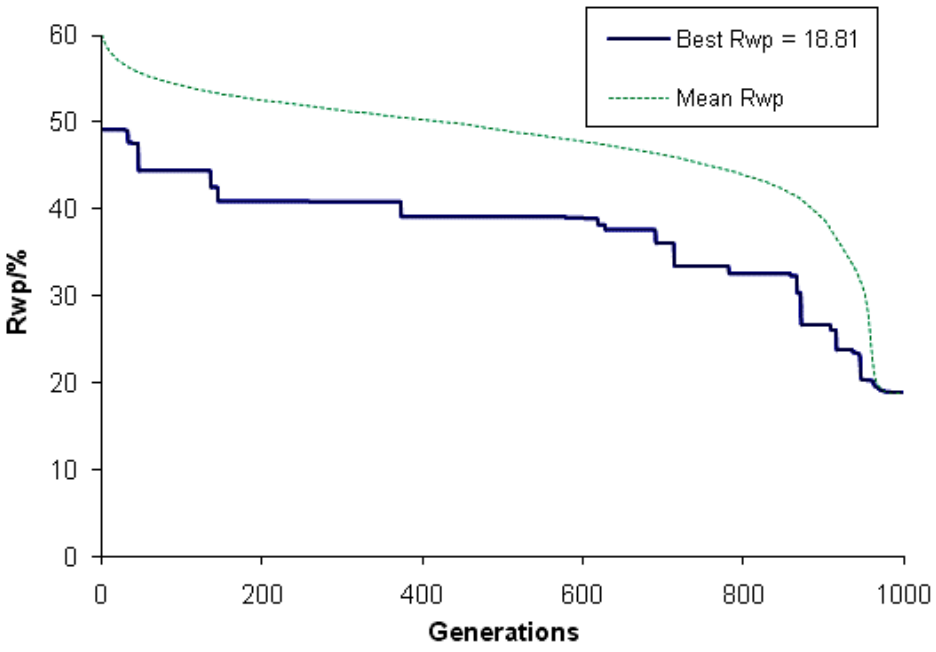

Figure 5.9.2.1: *Evolutionary progress plot for DE calculations for product of nicotinamide and azelaic acid crystallisation for N_p=35, K=0.99, F=0.2.*

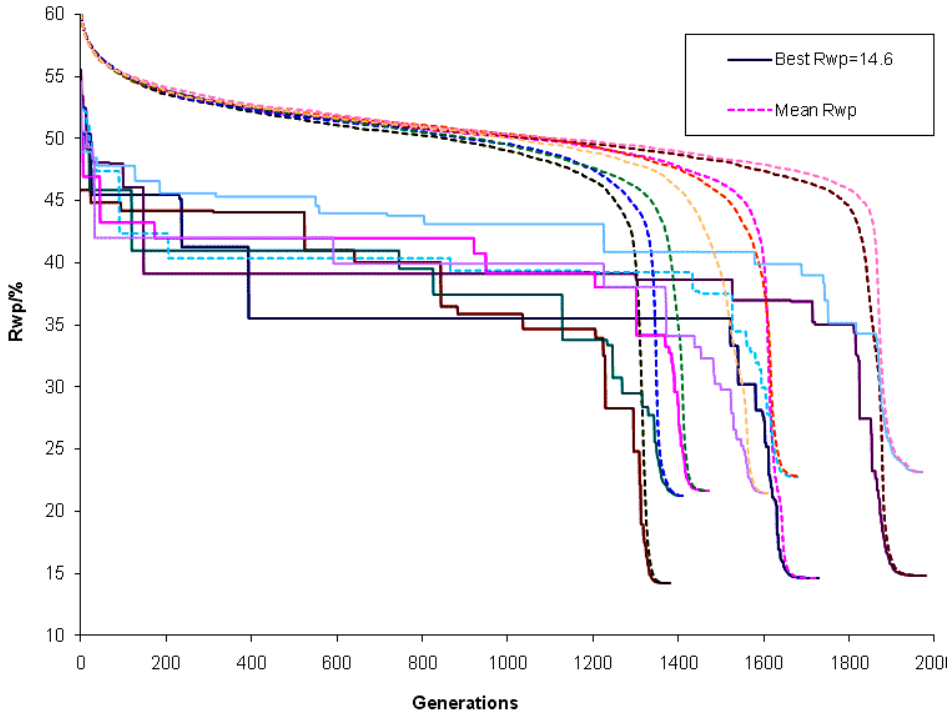

Figure 5.9.2.2: *Evolutionary progress plot for DE calculations for product of nicotinamide and azelaic acid crystallisation for N_p=35, K=0.99, F=0.3.*

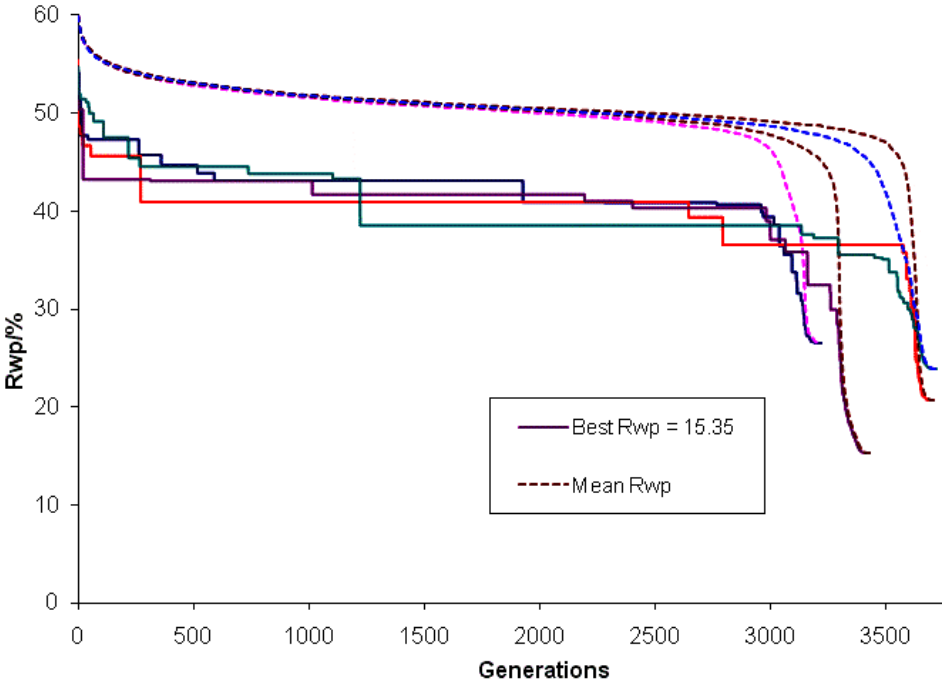

Figure 5.9.2.3: *Evolutionary progress plot for DE calculations for product of nicotinamide and azelaic acid crystallisation for N_p=35, K=0.99, F=0.4.*

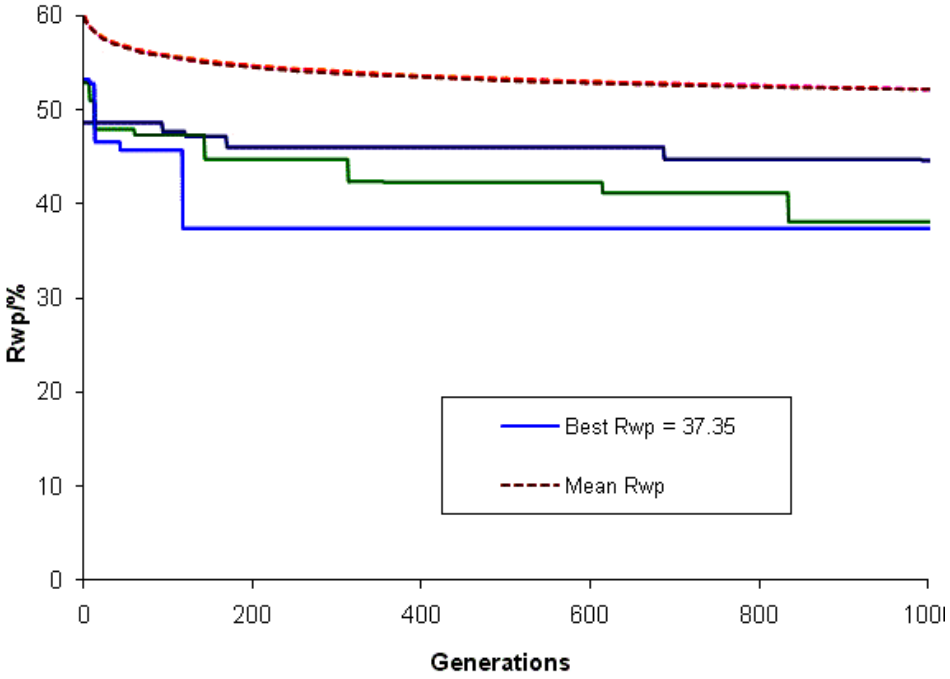

Figure 5.9.2.4: *Evolutionary progress plot for DE calculations for product of nicotinamide and azelaic acid crystallisation for N_p=35, K=0.99, F=0.5.*

5.9.3 Crystal structure determination using Rietveld refinement

Refinement of structure solution is carried out using the Rietveld[49] profile refinement. The crystal structure determination is completed after a suitable structure solution was obtained from differential evolution technique. The refinement is carried out using GSAS[43] & EXPGUI[61] software suites. During refinement, the intramolecular bonds in molecular fragments are subjected to various bond length and bond angle restraints. The C-C and C-H bond lengths are restrained about 0.005Å and 0.001Å respectively and the bond angles are restrained about 120° angle. The fitness of experimental and calculated diffraction patterns are compared point by point including selected profile parameters[19]. The lowest R-factor obtained for the structure solution of azelaic acid : nicotinamide (1:1) adduct is 14.6%. After the Rietveld refinement, the R-factor of crystal structure is further reduced to 11.6% (see figure 5.9.3.1).

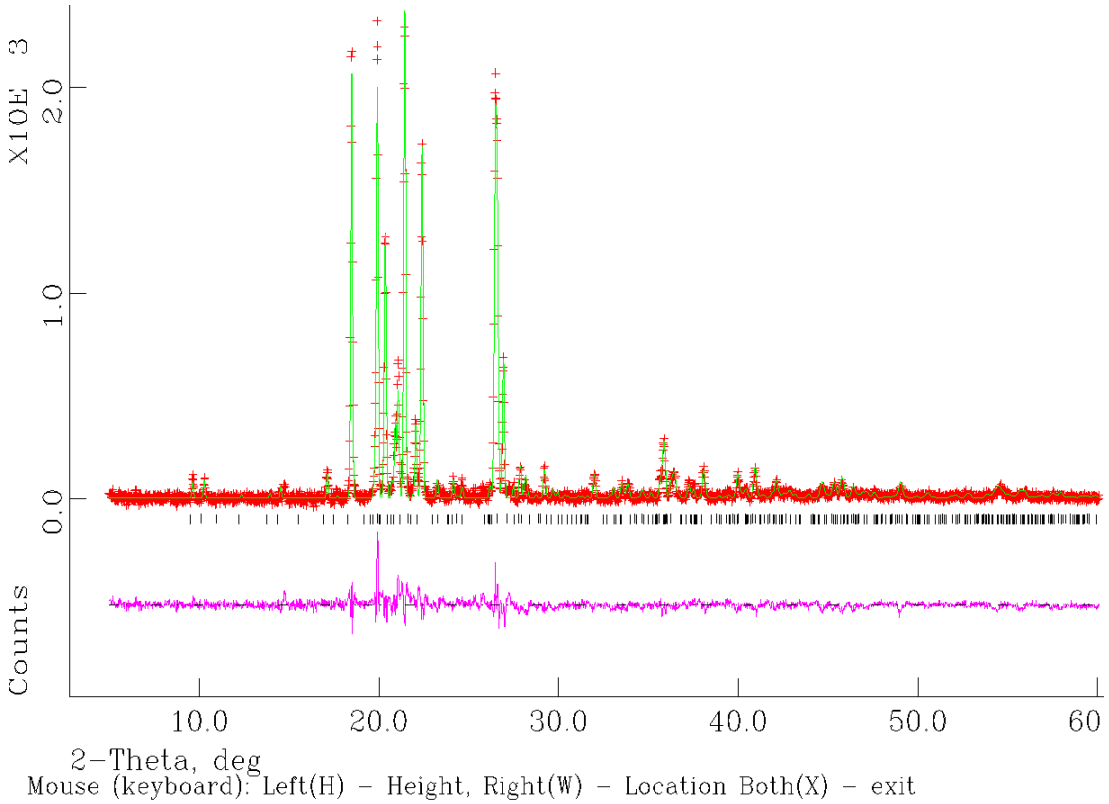

Figure 5.9.3.1: Rietveld refinement of the azelaic acid : nicotinamide (1:1) adduct. The green solid line shows the calculated intensities and the red crosses are observed intensities. The difference between the calculated and observed intesities is shown by pink line below. Reflection positions are also shown .

For the application of global optimization technique (DE) in directs space methods, the conformational flexibility of a molecular model is defined by the variation of a number of torsion angles. The H atoms in the carboxylic acid group are ignored the structure solution process and the carboxylate treated as the symmetrical functional group that is not discriminated in powder structures. Nicotinamide is a crystallographically unsymmetrical molecule with one flexible amide functional group, and so would require two variables to define the conformational flexibility in the molecule. As the H atoms in NH_2 group of the amide in nicotinamide are weak X-ray scatterers (producing little intensity at high diffraction angle), they are ignored during the execution of the structure solution process reducing the calculation to one conformational variable. However, there is a strong possibility that the N and C atoms in the pyridine ring and the N and O atoms of the amide functional group may have alternate conformation from the structure solution, compared to the correct crystal

structure. This is due to the similar electron densities of the atoms. Hence a number of possible conformations of nicotinamide have been modelled by replacing the nicotinamide with all possible conformations and evaluated to determine which ones give accurate and sensible intermolecular synthons and motifs in the crystal structure (see figure 5.9.3.2).

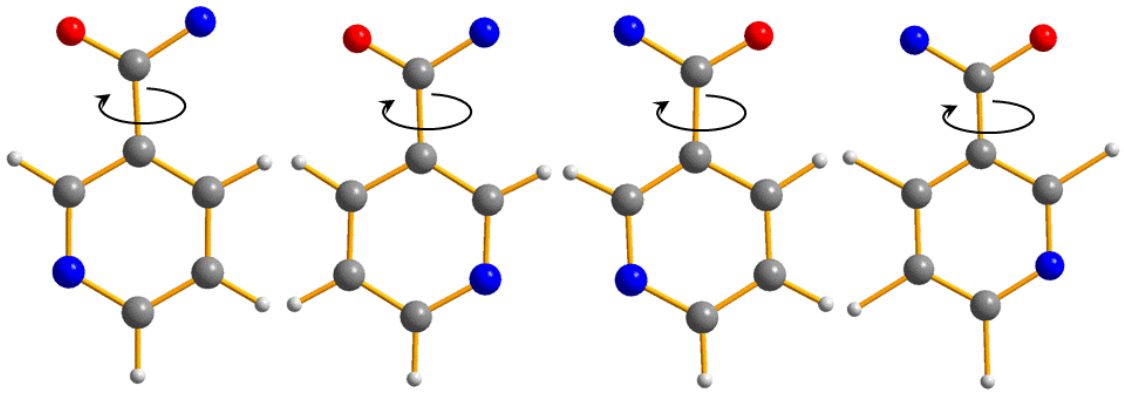

(a) (b) (c) (d)

Figure 5.9.3.2: Models of the nicotinamide molecule showing possible conformations of the pyridine ring in the structure (a) and (b) and the relative position of the amide group(c) and (d).

Figure 5.9.3.3 shows the molecular arrangement in the crystal structure as it is obtained from the structure solution process. Possible synthons were connected manually generating heteromeric motifs between the amide and carboxylic acid moieties. The pyridine N atom is the best hydrogen bond acceptor whereas the carboxylic acid is the best hydrogen bond donor expected to form strong *pyridine* N···H-O hydrogen bonding between the nicotinamide and azelaic acid molecules. It is also expected that combination of co-crystal formers would form multiple intermolecular bonds rather than zero dimensional supramolecular blocks throughout the crystal structure.

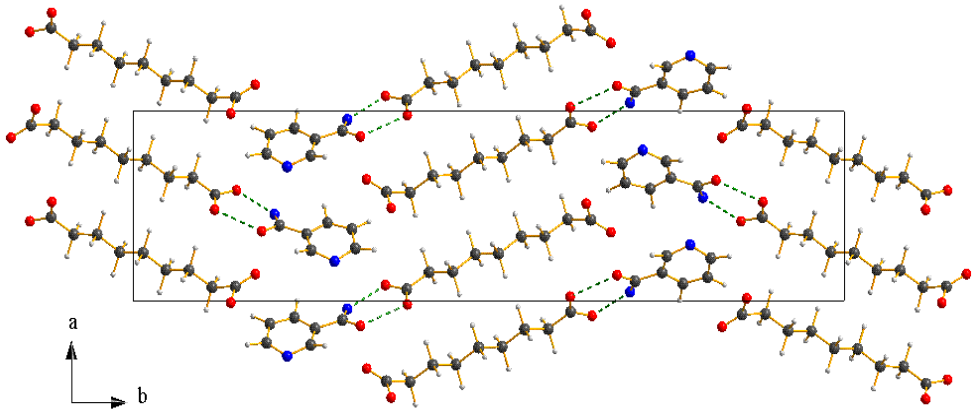

Figure 5.9.3.3: Projection on the [001] plane for the structural solution of the azelaic acid : nicotinamide (1:1) adduct.

A possible conformation of nicotinamide with the pyridine ring flipped by a 180° angle with respect to the amide functional group gives molecular structure with both N atoms on the same side with respect to axis passing through the molecule (see figure 5.9.3.2 (a)). The possible intermolecular bonds are connected between the molecules producing pyridine N···H-O synthons and heteromeric motifs between amide and carboxylic acid moieties constructing one dimensional long continuous chain along on b-axis throughout the crystal structure. The intermolecular bonds shown in the below structure solution are possible, unless the carbonyl groups in the azelaic acid are on the opposite sides with respect to the central axis passing through the carbon chain (see figure 5.9.3.4).

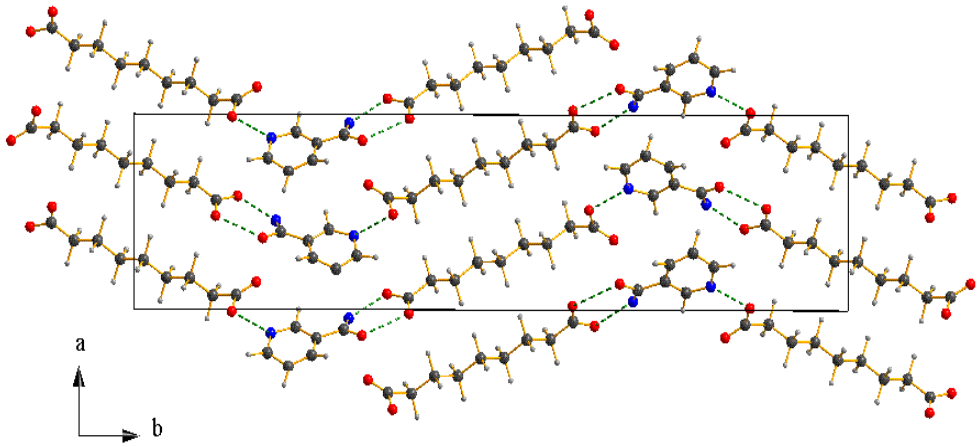

Figure 5.9.3.4: Project on the [001] plane for the structure solution of azelaic acid : nicotinamide (1:1) adduct.

Another possible conformation of the nicotinamide molecule obtained with the amide functional group flipped 180° angle with respect to pyridine ring implies a molecular structure with both N atoms on the same side with respect to the axis passing through the molecule (see figure 5.9.3.2 (c)). The possible intermolecular molecular interactions are interpreted producing aromatic C-H···O=C synthons and heteromeric motifs between amide and carboxylic acid moieties (see figure 5.9.3.5). The high probability of forming strong hydrogen bonds between pyridine N and carboxylic acid functional groups rather than weak hydrogen bonds (C-H···O=C synthons) implies that this crystal structure would be very unlikely to be formed.

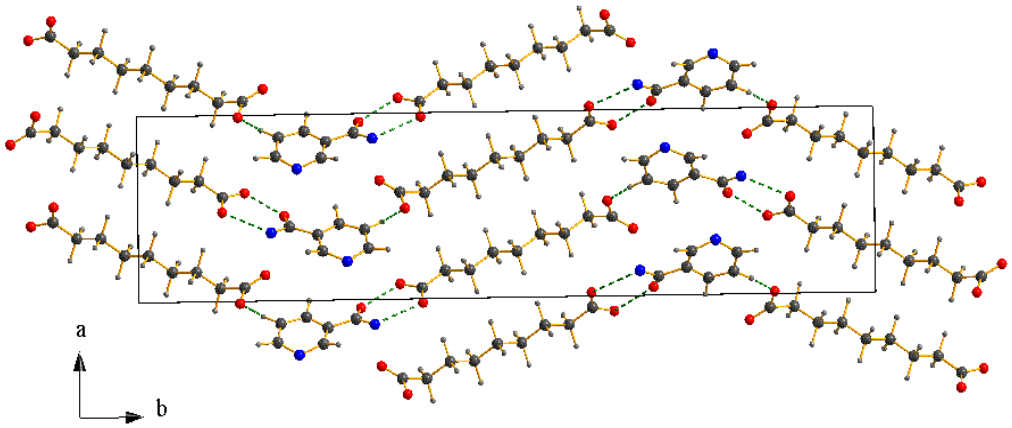

Figure 5.9.3.5: Project on the [001] plane for the structure solution of azelaic acid : nicotinamide (1:1) adduct with swapped atoms.

The conformation for nicotinamide molecule shown in figure 5.9.3.2 (d) was tried as another possibility in the crystal structure (see figure 5.9.3.6). The interpretation of possible intermolecular bonds in the structure solution produces pyridine N···H-O and N-H···O=C synthons and heteromeric motifs between amide and carboxylic acid moieties. Presence of strong hydrogen bonds between pyridine N and carboxylic acid functional groups and formation of maximum intermolecular bonds simultaneously satisfying stable conformations of molecular structures illustrates the formation of crystal structure with these specified intermolecular bonds would be more close to the correct crystal structure compared to the former possibilities (see figures 5.9.3.3-5.9.3.6).

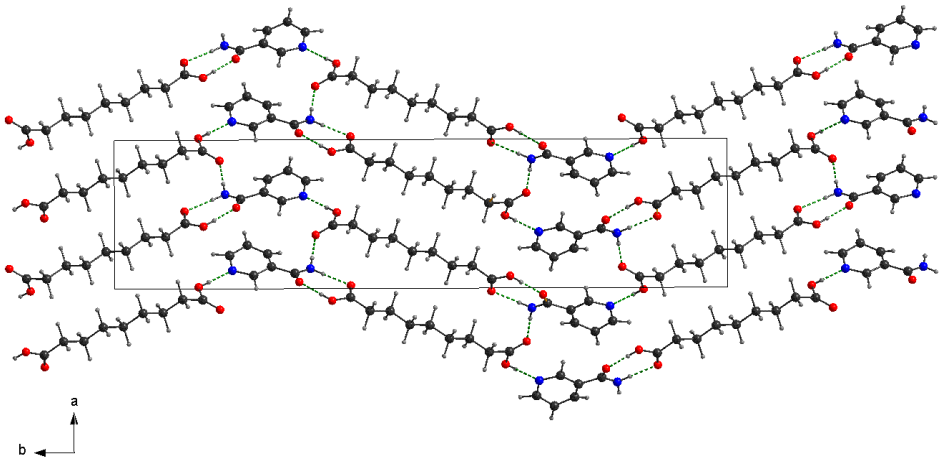

Figure 5.9.3.6: Projection on the [001] plane for the crystal structure of azelaic acid : nicotinamide (1:1) adduct showing $R_2^2(8)$ *and* $R_4^4(28)$ *rings in the unit cell.*

The adduct is assumed to be in neutral cocrystal rather than salt form as it is not possible to distinguish the proton position by X-ray powder diffraction. The moieties between nicotinamide and azelaic acid formed with amino N9 at (1-x, 1-y, -½) act as hydrogen bond donors via H1A at (1-x, 1-y, -½+z) to O10 and N9 at (1-x, 1-y, -½+z) acts as hydrogen bond donors via H1B at (1-x, 1-y, -½+z) to O21 at (1-x, 1-y, ½+z) produces $R^4_4(28)$. O22 at (1-x, 1-y, -½+z) acts as a hydrogen bond donor via H22A at (x, y, z) to O2 at (x, y, y), and combined with N9-H1A---O10 produces $R_2^2(8)$. The propagation of these hydrogen bonds produces C(14) spiral chains running through the unit cell can be observed. Four spiral chains running through the unit cell can be observed. Two spirals running along the (1, ½, z) and (½, 1, z) axes having opposite hand along (½, 0, -z) and (0, ½, -z) axes. O11 at (½-x, ½+y, -½+z) acts as a hydrogen bond donor via H11A at (½-x, ½+y, -½+z) to *pyridine* N2 at (½-x, ½+y, -½+z) and this hydrogen bond links the C(14) spirals together leading to continuous three dimensional framework throughout the crystal structure (see figure 5.9.3.1). All these intermolecular bonds combines to form large ring $R^8_8(60)$ and this ring is comprised with repetition of N9-H1A---O10 synthons for two times, O22-H22A---O2 for two times and O11-H11A---N6 for four times (see figure 5.9.3.6). From the extent of obtained crystal structure and IR spectral data, it is evident that the material obtained through the crystallisation of azelaic acid and nicotinamide (1:1 starting ratio) would be a co-crystal rather than a salt although not conclusively.

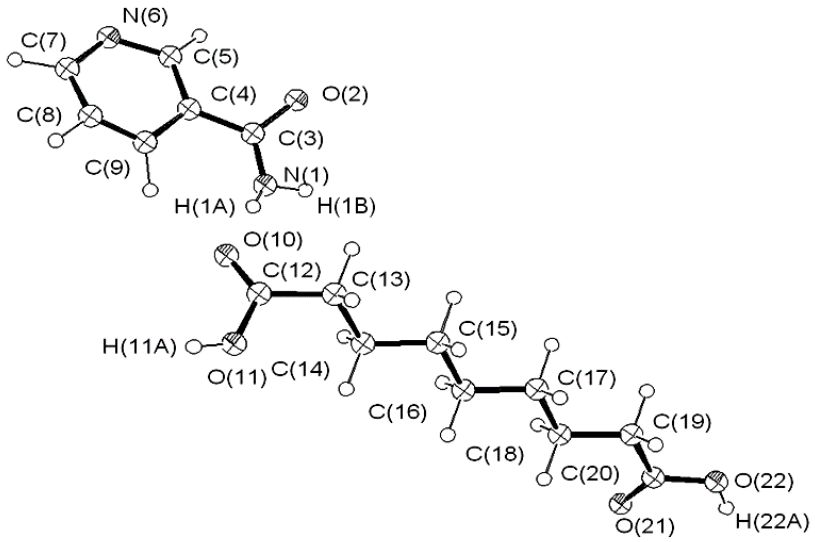

Figure 5.9.3.7: ORTEP diagram of the azelaic acid : nicotinamide (1:1) adduct showing labelling of atoms and the interaction between the two former molecules. Thermal ellipsoids are drawn at the 50% probability level.

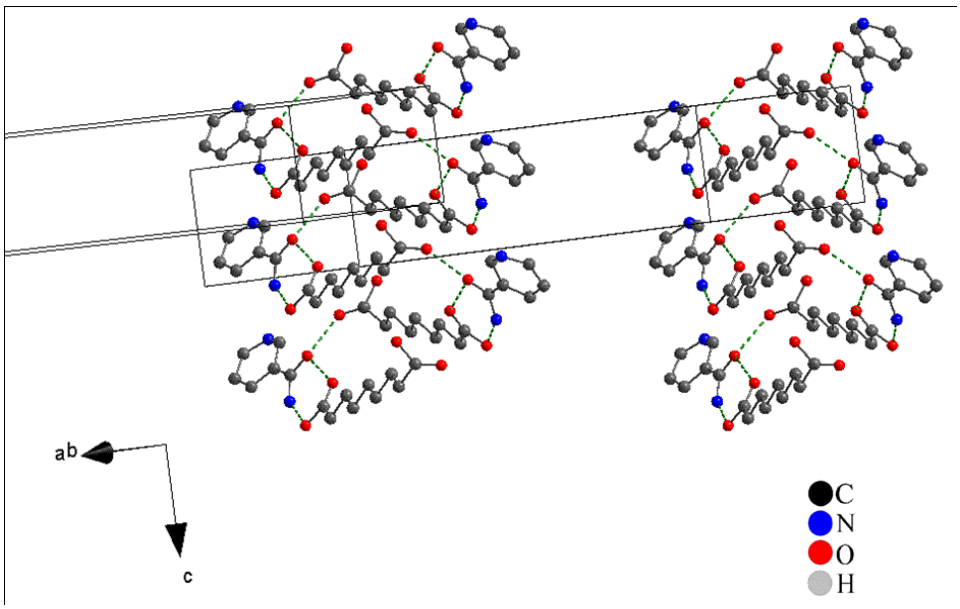

Figure 5.9.3.8: Stereoview of azelaic acid : nicotinamide (1:1) adduct, showing $R_4^4(8)$ and C(14) spiral molecular ladder along (1/2, 1, Z).

Table 5.9.3.1

Summary of crystal data for azelaic acid and nicotinamide co-crystal obtained from PXRD.

Empirical formula	$(C_6H_6N_2O_6):(C_9H_{14}O)$
Formula weight	306.32
Cell setting, space group	Monoclinic
Z	4
Radiation type	Cu $K\alpha_1$
Temperature [K]	273 (2)
λ[Å]	1.54056
Indexing	
Initial *a*[Å]	8.8816
Initial *b*[Å]	36.7807
Initial *c*[Å]	5.2585
Initial α[°]	90
Initial β[°]	90
Initial γ[°]	90
Structural solution	
Le bail R_{wp}	0.0916
Le bail χ^2	0.6759
Elements	9
K	0.99
Best F	0.3
Best R_{wp}	17.06
Refinement	
R_{wp}	11.69
χ^2	2.545
No. of reflections (Initial/final)	297/300
No. of parameters	530
No. of restraints	77

Final a (Å)	8.880 (19)
Final b (Å)	36.788 (11)
Final c (Å)	5.257 (14)
Final α (°)	90
Final β (°)	90
Final γ (°)	90
V ($Å^3$)	1717.7

Table 5.4.2

Intermolecular hydrogen bond parameters [Å, °] in the adipic acid:nicotinamide (1:2) co-crystal.

D-H···A	d(D-H)	d(H···A)	d(D···A)	<(DHA)
N(9)-H(1A)···O(10)(i)	1.01	1.933	2.598	179.92
N(9)-H(1B)---O(21)(i)	1.01	1.583	2.941	179.94
O(22)-H(22A)---O(2)(i)	1.05	1.483	2.533	171.09
O(11)-H(11A)---N(2)(ii)	1.01	1.754	2.811	-----

(i) 1-x, 1-y, -½+z (ii) (½-x, ½+y, -½+z)

5.10 Azelaic and isonicotinamide

Azelaic acid (see figure 2.2(g)) was crystallised with isonicotinamide using different solvents (methanol and ethanol) in a 1:1 starting molar ratio. Similar X-ray diffraction patterns for materials obtained from methanol and ethanol shows the formation of same new product obtained as a white crystalline solid although there may be small amount of azelaic acid also present. Solution mediated crystallisation was used for the synthesis (see figure 5.10.1).

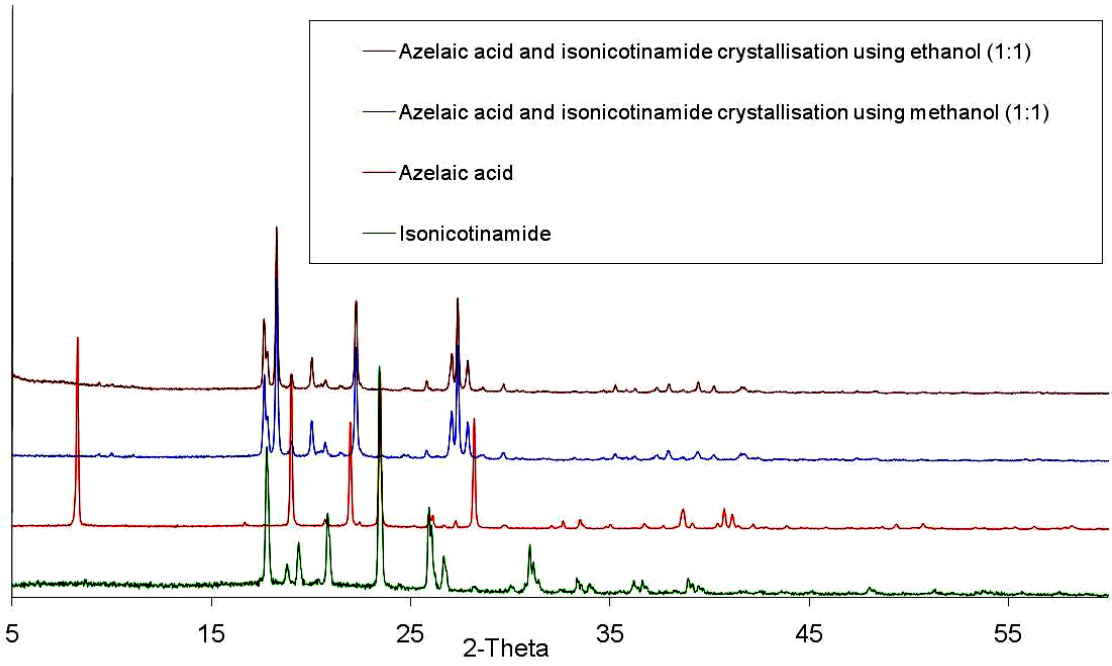

Figure 5.10.1: X-ray powder diffraction pattern for isonicotinamide and azelaic acid and product of crystallisation.

From the integral values of different peak intensities for protons in different environments on azelaic acid and isonicotinamide obtained from NMR spectra, it is evident that the new material has a 1:1 stoichiometric ratio (see figure 5.10.2).

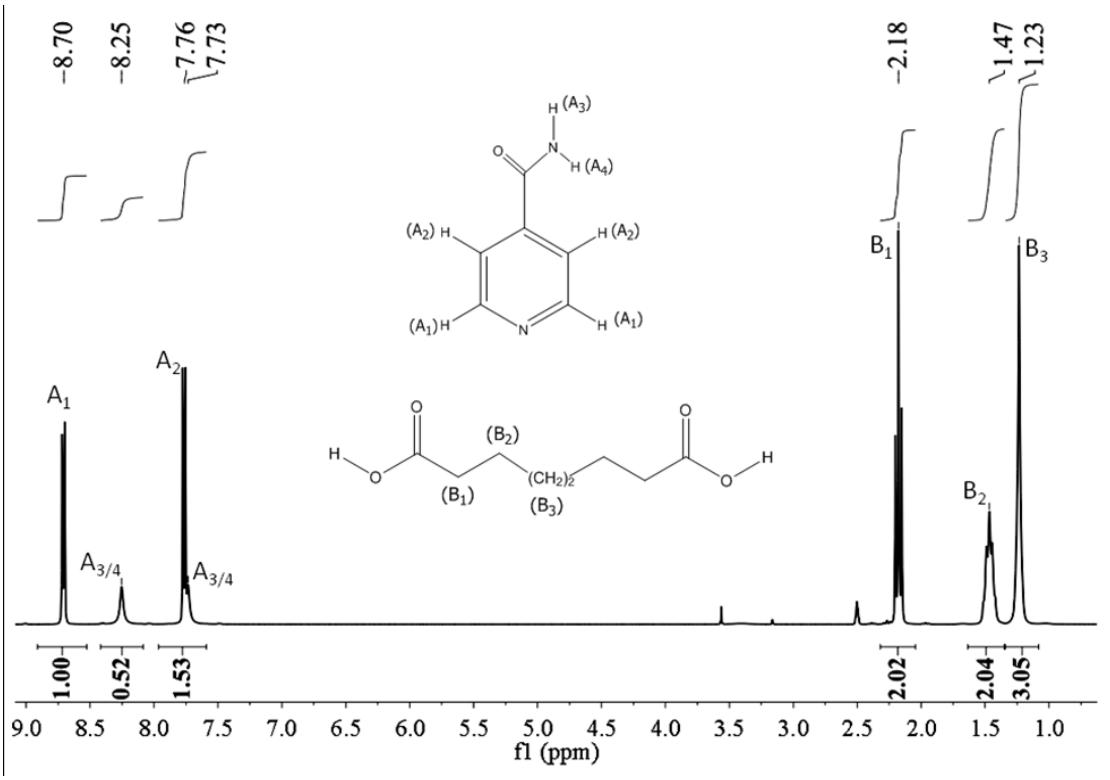

Figure 5.10.2: ^{1}H NMR of azelaic acid and isonicotinamide and product of crystallisation using DMSO as solvent. ^{1}H NMR 300MHz (DMSO-d_6): δ = 11.98(s, 2H), 8.70(dd, 2H), 8.25(s, 1H), 7.76(dd, 2H), 7.73(s, 1H) 2.18(m, 4H), 1.47(m, 4H), 1.23(m, 6H).

The IR data for the crystallisation product (1:1) is compared to that from a mixture of the starting materials (figure 5.10.3). For a discussion of characteristic IR peaks of the starting materials, please see sections 5.2 and 5.6. The absence of characteristic high tones at 3000cm^{-1} for O-H bond stretching frequency for a carboxylic acid shows the involvement of the carboxylic acid group in intermolecular bonding. There are also indications of a potential broad band at ~2449cm^{-1} and hence the discrimination between neutral co-crystal and salt form is again not clear.

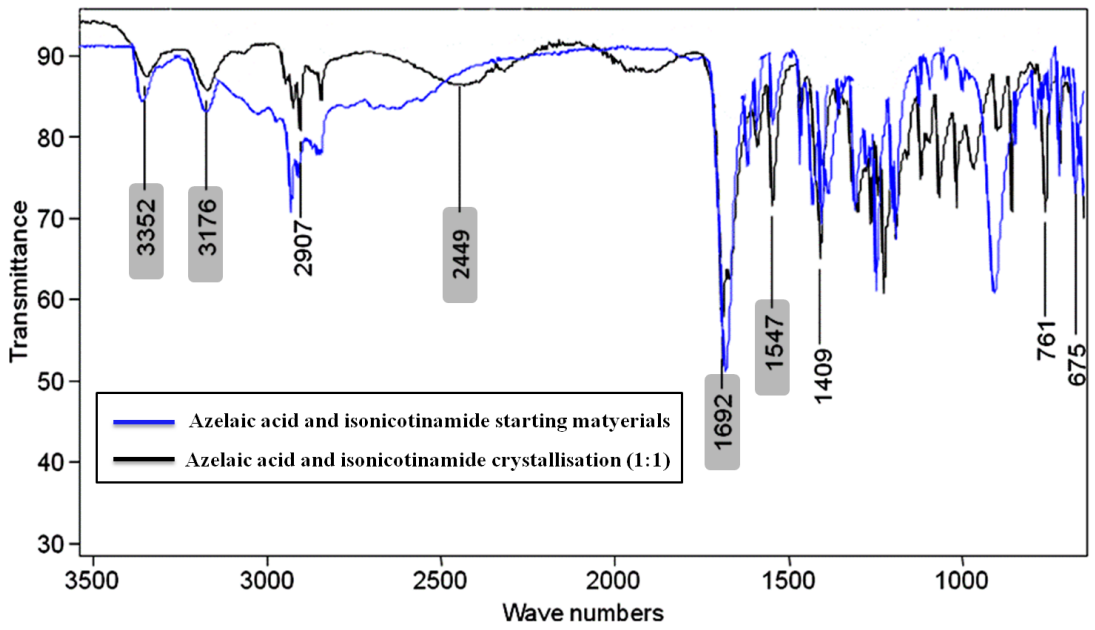

Figure 5.10.3: FTIR spectra for azelaic acid and isonicotinamide and product of crystallisation.

Possible cell parameters were obtained by indexing the twenty most intense peaks in the powder X-ray diffraction pattern using the XFIT software. *CRYSFIRE* was used to index the selected peaks (see appendix K). Possible cell parameters were chosen for Le bail pattern decomposition on the basis of the stoichiometric ratio between the molecules obtained from NMR along with cell volume calculations and figure of merit (see table 8). The accuracy of unit cell parameters would be confirmed through Le bail pattern decomposition method (see figures 5.10.4). The space group was assigned as P-1 as this gave the correct cell volume given a 1:1 stoichiometry (see table 5.10.1). The best fit between the experimental data (red) and simulated pattern (green) is quantified in terms of R-factor value (wRp) and χ^2. The lowest R-factor and χ^2 values obtained are 0.0975 and 67.62 respectively (see table 5.10.1).

Table 5.10.1

Indexed and refined cell parameters obtained for the product of azelaic acid and nicotinamide:

	Figure of Merit	*a*(Å)	*b*(Å)	*c*(Å)	α(°)	β(°)	γ(°)	Cell volume (Å^3)	Space group
PXRD indexing	13.76	9.074	18.950	5.471	95.863	102.70	89.682	912.995	P-1
PXRD Le bail fit	R_{wp} = 0.0975/ 67.62	9.074 6	18.829	5.438	96.117	102.66	89.623	902.139	P-1

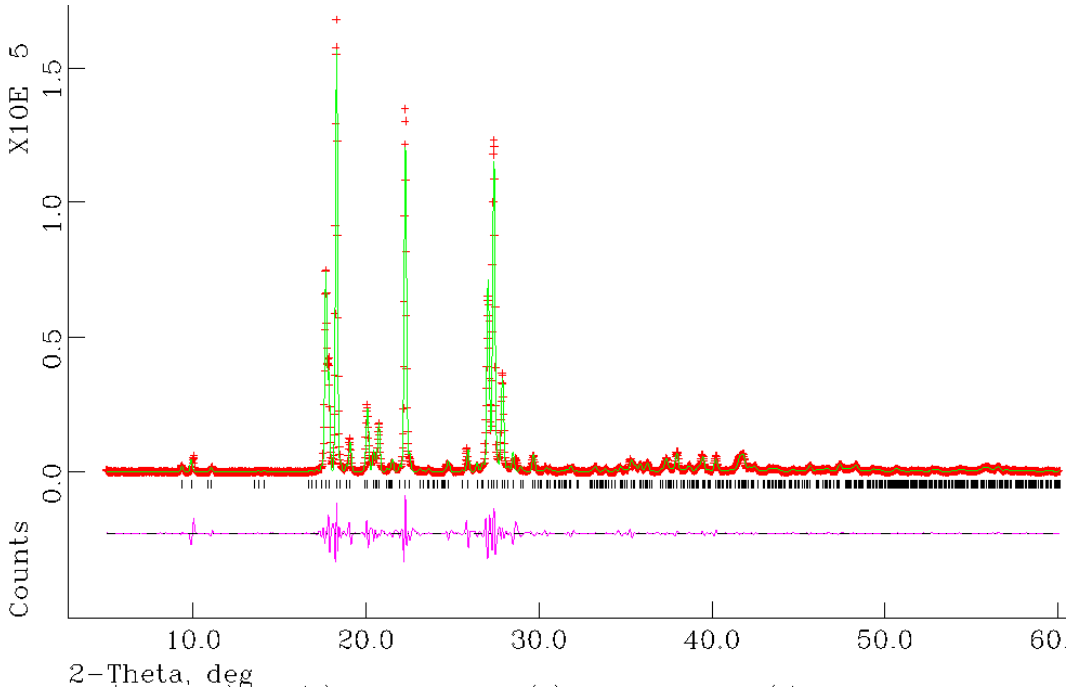

Figure 5.10.4: The Le Bail profile fitting for the product of isonicotinamide and azelaic acid crystallisation (1:1) adduct.

No further structural characterisation was carried out on this product.

5.11 Melting point alternations

The phenomenon of melting point alternations in α,ω-alkanedicarboxlic acids was first established by Caspari in 1928[70]. Since then similar research has been done by research groups building various strategies based on molecular structures, packing motifs, crystal densities and packing fraction etc due to their significance in pharmaceutical industry[5, 21, 71, 72]. These theories could be applied to the selection of suitable former molecules to modify the physical properties of an API in the form of a pharmaceutical co-crystal. The melting point alternations in the new materials obtained in this project were investigated with the intention to observe the effect of former molecules on the physical properties of the new crystalline materials formed (see chart 5.11.1). From the results obtained, it is evident that the melting points are altered through co-crystallisation. The melting points of all the new materials fell in between the values of their corresponding former materials except for the products of malonic acid : nicotinamide (1:1 and 1:2).

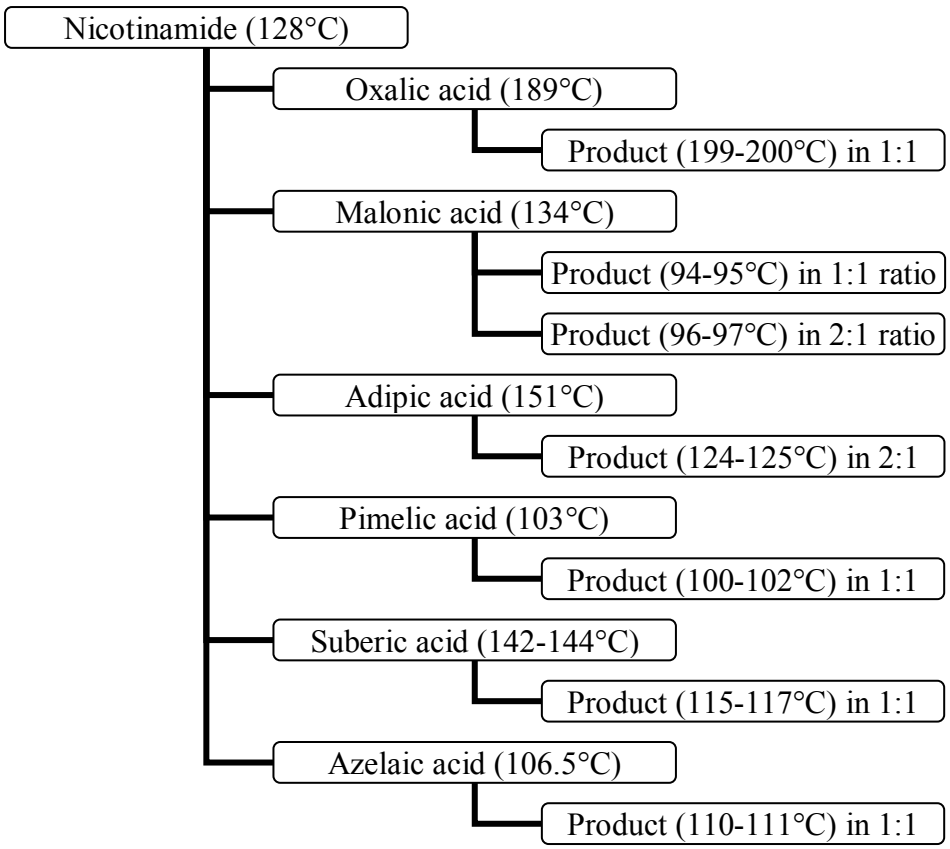

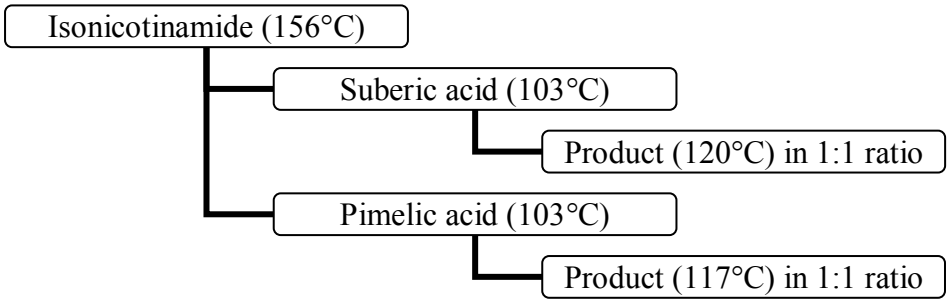

Chart 5.11.1: Chart showing melting points of starting materials corresponding products of crystallisation.

Table 5.11.1

Summary table of new materials (includes stoichiometries, status and corresponding starting materials).

Dicarboxylic acids	Former molecules	Status
Oxalic acid	Nicotinamide	Co-crystal or salt (1:1 and 1:2)- inconclusive
Malonic acid	Nicotinamide	Co-crystal rather than salt (1:1 and 1:2)- inconclusive
Succinic acid	Nicotinamide	Co-crystal or salt (1:1)- inconclusive
Adipic acid	Nicotinamide	Co-crystal (1:2)
Pimelic acid	Nicotinamide	Salt rather than co-crystal (1:1)- inconclusive
	Isonicotinamide	Salt rather than co-crystal (1:1)- inconclusive
Suberic acid	Nicotinamide	Co-crystal or salt (1:1 and 1:2)- inconclusive
	Isonicoitnamide	Co-crystal or salt (1:1)- inconclusive
Azelaic acid	Nicotinamide	Co-crystal rather than salt (1:1)- inconclusive
	Isonicotinamide	Co-crystal or salt (1:1)- inconclusive

6. CONCLUSION

The new co-crystal materials have been synthesized using both methanol and ethanol as solvents in different stoichiometric ratios using solvent drop grinding and solvent mediated crystallisation methods. In most cases, the same products were formed for different solvents showing no reliance on solvent interactions. All the starting materials were crystallized from different stoichiometric ratios (1:1, 1:2 and 2:1) but almost all products were obtained in a 1:1 stoichiometric ratio. The adipic acid : nicotinamide co-crystal was obtained only in a 1:2 stoichiometric ratio whereas a few other few materials were obtained in both 1:1 and 1:2 stoichiometries (oxalic acid, malonic acid and suberic acid : nicotinamide). Any synthesis with a 2:1 starting stoichiometric ratio resulted in either 1:1 or 1:2 products with a small quantity of excess starting materials. No products were obtained with a 2:1 stoichiometric ratio.

The crystal structure of adipic acid : nicotinamide (1:2) was solved using single-crystal X-ray diffraction and contains continuous hydrogen-bonded zigzag sheets running along the c-axis with no significant intermolecular bonds between the sheets. The crystal structure of azelaic acid : nicotinamide (1:1) was solved from X-ray powder diffraction data in which the molecules are arranged in the form of spiral chains running along the *c*-axis. These spirals are interconnected through intermolecular hydrogen bonds spreading into a three dimensional framework.

The analysis of melting point alternations in all the new materials implies that the physical properties of the formers can be modified in the form of co-crystals. The melting point values of these new products falls between the values of the corresponding starting materials with no significant pattern observed with sequential increase in the methylene groups in the dicarboxylic acids.

The former molecules of focus in this project have demonstrated that the complementary functional groups provide reliable synthons for the formation of hydrogen bonds between them. The crystal structure of adipic acid : nicotinamide contains (*pyridine*)N─acid and amide─amide motifs whereas crystal structure of azelaic acid:nicotinamide was found to contain (*pyridine)*N─acid and acid─amide motifs. In both cases, the formation of (*pyridine*)N─acid as a stronger intermolecular

bond is maintained. Comparatively, the acid─amide is stronger than the amide─amide intermolecular bond. But, the high quantity of nicotinamide in starting stoichiometries of adipic acid : nicotinamide (2:1) increases the availability of amide functional groups for intermolecular interactions leading to the formation amide-amide moieties rather than acid–amide moieties. Similarly, the equal starting stoichiometries of azelaic acid : nicotinamide (1:1) formed acid-amide moieties in the resulted crystal structure.

Although this project has generated a significant number of adduct materials further work could be done to analyse the co-crystal properties such as dissolution, solubility and the behaviour of former materials towards co-crystallisation. The crystallisation of nicotinamide with succinic acid, pimelic acid, suberic acid and isonicotinamide with pimelic acid, suberic acid and azelaic acid needs to be investigated using different stoichiometries, different solvents and synthesis methods (see section 3.1 and 3.2) to ensure whether the synthesis of materials showing polymorphic behaviour or alternative stoichiometry could be possible.

The crystal structures of the new materials oxalic acid : nicotinamide (1:2), malonic acid : nicotinamide (1:1), suberic acid : isonicotinamide (1:2) and azelaic acid : isonicotinamide (1:1) need to be determined using PXRD or SXRD techniques. Although the crystal structures of adipic acid : nicotinamide (1:2) and azelaic : nicotinamide (1:1) were obtained from PXRD, there are difficulties in distinguishing groups (or atoms) with similar electron densities, such as the position of the heterocyclic N in the ring or the conformation of this amide group (see section 5.9.3). To overcome this limitation, synchrotron data could be used to ensure the correct crystal structures. Use of laboratory PXRD to determine the position of the proton in a salt (or a co-crystal) is impossible. But it may be possible that high quantity synchrotron PXRD can determine whether the product is a salt or a co-crystal.

These results are also employed in a new project dealing with multi phase structural problems. The crystal structures throughout the project were solved from single phase powder diffraction data. The materials obtained throughout this project were crystallised from these different starting stoichiometries (1:1, 1:2 and 2:1) and the products obtained from these different stoichiometric ratios could be either pure or

mixture of the new product with a quantity of one of the starting materials in excess. This multiphase powder diffraction data is being used to investigate the determination of crystal structures from such data. The crystal structures suberic acid : isonicotinamide (1:1) and pimelic acid : isonicotinamide (1:1) have now also been solved single crystal methods, but these results are not included in this thesis due to constraints of project time and report length.

The materials (oxalic acid (1:1), malonic acid (1:2), succinic acid (1:1), adipic acid (1:2), pimelic acid (1:1), suberic acid (1:1) and azelaic acid : nicotinamide (1:1)) synthesized in the current project were assumed to be unpublished relying on the rigorous search done using the Cambridge Structural Database (CSD). Unfortunately, the content had already been published on 4th November 2008[73] and the CSD had not been updated.

8. APPENDICES

APPENDIX A

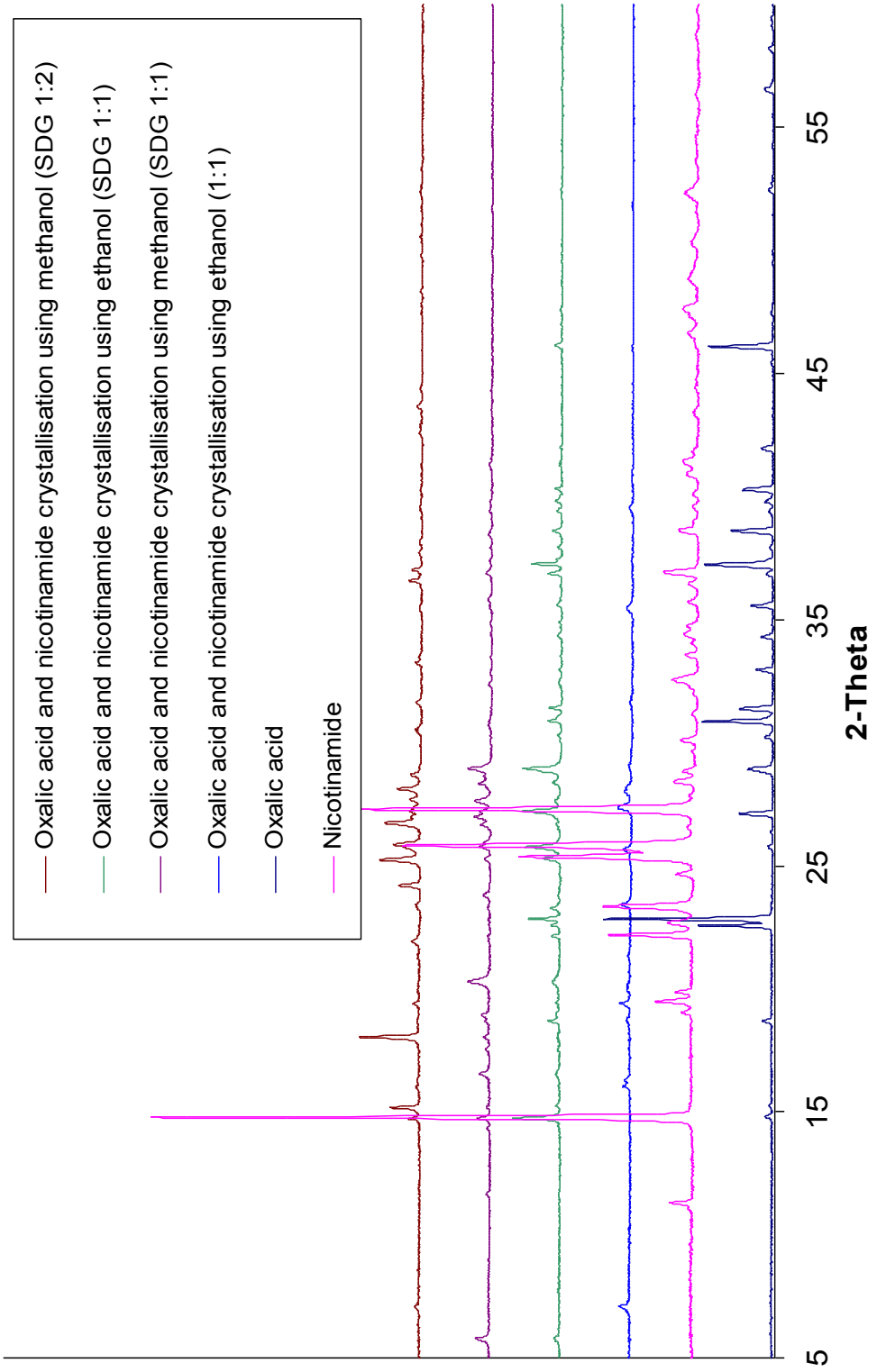

X-ray diffraction patterns of nicotinamide and oxalic acid and products of crystallisation.

APPENDIX B

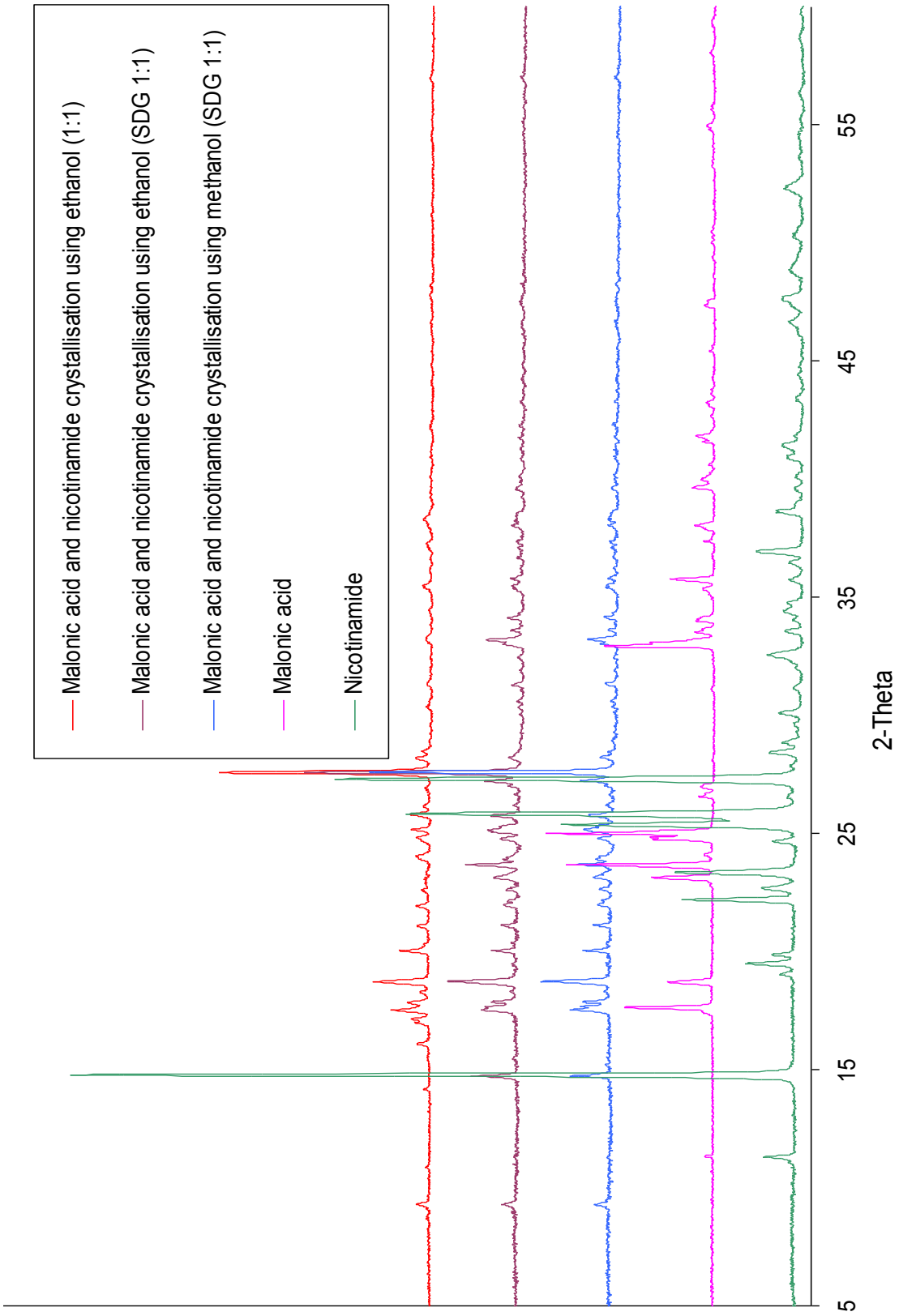

X-ray diffraction patterns of nicotinamide and malonic acid and products of crystallisation.

APPENDIX C

Cell parameters obtained from indexing the X-ray diffraction data of the product of nicotinamide and malonic acid using CRYSFIRE

I20	Merit	Volume	V/V1	a	b	c	alpha	beta	gamma
20	23.61	492.533	1	10.444	10.277	5.121	96.095	103.878	67.383
20	23.6	985.066	2	11.496	16.931	5.121	95.166	97.065	88.888
20	13.29	493.9	1	10.277	10.463	5.122	103.726	84.193	112.604
20	13.15	494.166	1	10.237	10.548	5.127	104.369	96.629	67.170
20	10.18	537.039	1.09	10.231	10.242	5.569	93.668	96.070	67.787
20	7.6	491.557	1	10.228	10.357	5.098	101.086	91.482	111.150
20	7.05	535.364	1.09	11.139	10.184	5.552	93.585	113.385	108.467
20	7.04	983.696	2	20.960	12.036	10.202	57.613	150.805	128.402
20	6.1	1987.266	4.03	13.151	15.899	10.697	90.000	117.304	90.000
20	6.1	1987.266	4.03	13.151	15.899	10.697	90.000	117.304	90.000
20	6.1	1839.829	3.74	11.990	18.950	9.831	90.000	124.543	90.000
20	6.1	1839.829	3.74	11.990	18.950	9.831	90.000	124.543	90.000
20	5.8	1840.431	3.74	11.997	18.951	10.330	90.000	128.401	90.000
20	5.8	1840.431	3.74	11.997	18.951	10.330	90.000	128.401	90.000
20	5.8	1840.425	3.74	10.330	18.951	9.832	90.000	107.020	90.000
20	5.8	1840.425	3.74	10.330	18.951	9.832	90.000	107.020	90.000
20	5.69	505.23	1.03	10.320	10.702	5.240	71.749	97.794	113.160
20	5.37	572.247	1.16	11.905	11.198	5.935	65.183	120.815	120.376
20	5.3	3742.616	7.6	64.732	9.500	6.086	90.000	90.000	90.000
20	5.3	3742.616	7.6	64.732	9.500	6.086	90.000	90.000	90.000
20	5.2	1700.141	3.45	18.990	5.994	18.193	90.000	124.819	90.000
20	5.2	1700.141	3.45	18.990	5.994	18.193	90.000	124.819	90.000
20	5.1	1699.975	3.45	18.990	5.994	17.233	90.000	119.934	90.000
20	5.1	1699.975	3.45	18.990	5.994	17.233	90.000	119.934	90.000
20	5	2002.386	4.07	13.318	15.950	10.639	90.000	117.619	90.000
20	5	2002.386	4.07	13.318	15.950	10.639	90.000	117.619	90.000
20	5	1968.474	4	25.358	5.269	19.172	90.000	129.782	90.000
20	5	1968.474	4	25.358	5.269	19.172	90.000	129.782	90.000
20	4.9	4447.09	9.03	10.116	15.897	27.653	90.000	90.000	90.000
20	4.69	3269.274	6.64	5.841	20.261	27.625	90.000	90.000	90.000
20	2.85	580.837	1.18	11.696	5.293	9.982	74.467	100.636	99.478
19	15	493.146	1	5.125	12.748	11.501	68.651	97.172	52.764
19	12.78	582.583	1.18	10.198	10.309	6.045	97.400	94.752	67.675
19	12.56	506.545	1.03	10.519	10.301	5.251	96.787	104.812	67.096
19	12.56	506.545	1.03	10.519	10.301	5.251	96.787	104.812	67.096
19	12.49	493.691	1	10.214	10.518	5.122	103.588	95.770	67.396
19	12.48	506.393	1.03	10.234	10.566	5.254	104.621	96.846	67.148
19	12.41	548.487	1.11	10.271	10.244	5.690	93.652	98.289	67.802
19	11.09	643.512	1.31	10.761	12.776	5.330	103.124	100.243	64.905
19	10.59	586.354	1.19	10.176	10.284	6.082	96.075	93.183	111.368
19	10.59	586.354	1.19	10.176	10.284	6.082	96.075	93.183	111.368

19	10.39	616.297	1.25	10.670	10.387	6.396	100.333	107.729	66.159
19	10.33	535.985	1.09	10.182	10.286	5.559	96.182	93.380	67.854
19	10.04	630.418	1.28	10.351	10.693	6.553	106.979	101.746	65.928
19	9.69	803.709	1.63	10.167	10.347	8.339	98.952	88.742	111.842
19	9.31	647.134	1.31	10.179	10.423	6.711	101.240	87.139	112.050
19	9.21	615.007	1.25	10.669	10.389	6.381	100.229	107.765	66.205
19	9.19	1080.304	2.19	11.305	11.208	11.133	114.057	118.847	64.695
19	9.13	647.605	1.31	10.179	10.429	6.715	101.299	87.133	112.062
19	9.1	1398.93	2.84	11.575	13.571	10.788	86.940	117.674	109.991
19	9.02	925.806	1.88	11.117	12.488	7.653	86.430	107.406	113.760
19	8	1251.724	2.54	20.256	10.779	5.744	90.000	93.587	90.000
19	8	1251.724	2.54	20.256	10.779	5.744	90.000	93.587	90.000
19	7.4	1249.88	2.54	10.247	12.954	10.322	99.774	111.045	93.239
19	5.7	1124.06	2.28	11.174	11.723	11.011	113.150	118.183	65.918
19	5.4	1248.87	2.54	10.241	12.955	10.316	99.777	110.997	93.248
19	4.8	1991.96	4.04	12.540	16.011	10.680	90.000	111.729	90.000
18	19.45	491.727	1	10.187	10.499	5.102	103.195	86.168	112.201
18	19.44	491.727	1	10.187	10.499	5.102	103.195	86.167	112.201
18	12.97	491.603	1	10.428	10.249	5.100	86.057	102.982	112.210
18	12.63	764.92	1.55	11.009	10.300	7.936	82.869	112.559	112.945
18	12	492.823	1	5.123	12.672	11.493	59.167	82.922	53.026
18	11.36	528.564	1.07	10.265	10.251	5.483	94.100	98.062	67.753
18	9.29	1173.009	2.38	11.786	11.892	10.225	107.650	109.479	61.875
18	8.57	1128.898	2.29	11.200	11.717	11.030	113.001	118.164	65.885
18	8	1032.816	2.1	11.585	17.191	5.266	90.000	99.991	90.000
18	8	1032.816	2.1	11.585	17.191	5.266	90.000	99.991	90.000
18	8	1032.815	2.1	11.865	17.191	5.266	90.000	105.927	90.000
18	8	1032.815	2.1	11.865	17.191	5.266	90.000	105.927	90.000
18	7	1065.715	2.16	19.119	5.262	10.654	90.000	96.129	90.000
18	7	1032.664	2.1	11.582	17.193	5.266	90.000	100.006	90.000
18	7	1032.664	2.1	11.860	17.193	5.266	90.000	105.923	90.000
18	6.5	2535.96	5.15	11.229	23.827	10.375	90.000	113.989	90.000
17	20.07	713.501	1.45	10.173	10.223	7.401	91.020	91.797	111.883
17	15.74	576.578	1.17	10.317	10.383	5.982	100.079	99.868	109.392
17	11.72	634.563	1.29	10.414	10.790	6.582	108.729	102.349	65.496
17	11.27	835.067	1.7	7.608	19.070	6.069	94.822	107.846	87.450
17	10	1064.321	2.16	12.861	9.184	10.143	90.000	117.319	90.000
17	10	1064.321	2.16	12.188	9.184	10.143	90.000	110.360	90.000
17	9.99	539.656	1.1	10.201	10.342	5.599	98.565	95.218	67.618
17	9.57	640.563	1.3	10.428	10.413	6.625	100.473	102.199	108.856
17	9.49	646.161	1.31	10.150	10.401	6.707	100.387	89.684	111.591
17	9.15	666.022	1.35	10.187	10.587	6.910	105.023	94.305	109.840
17	9	1064.451	2.16	12.191	9.183	10.142	90.000	110.361	90.000
17	8	1096.092	2.23	22.340	10.110	5.706	90.000	121.725	90.000
17	7	1103.23	2.24	9.712	19.009	5.979	90.000	92.029	90.000

APPENDIX D

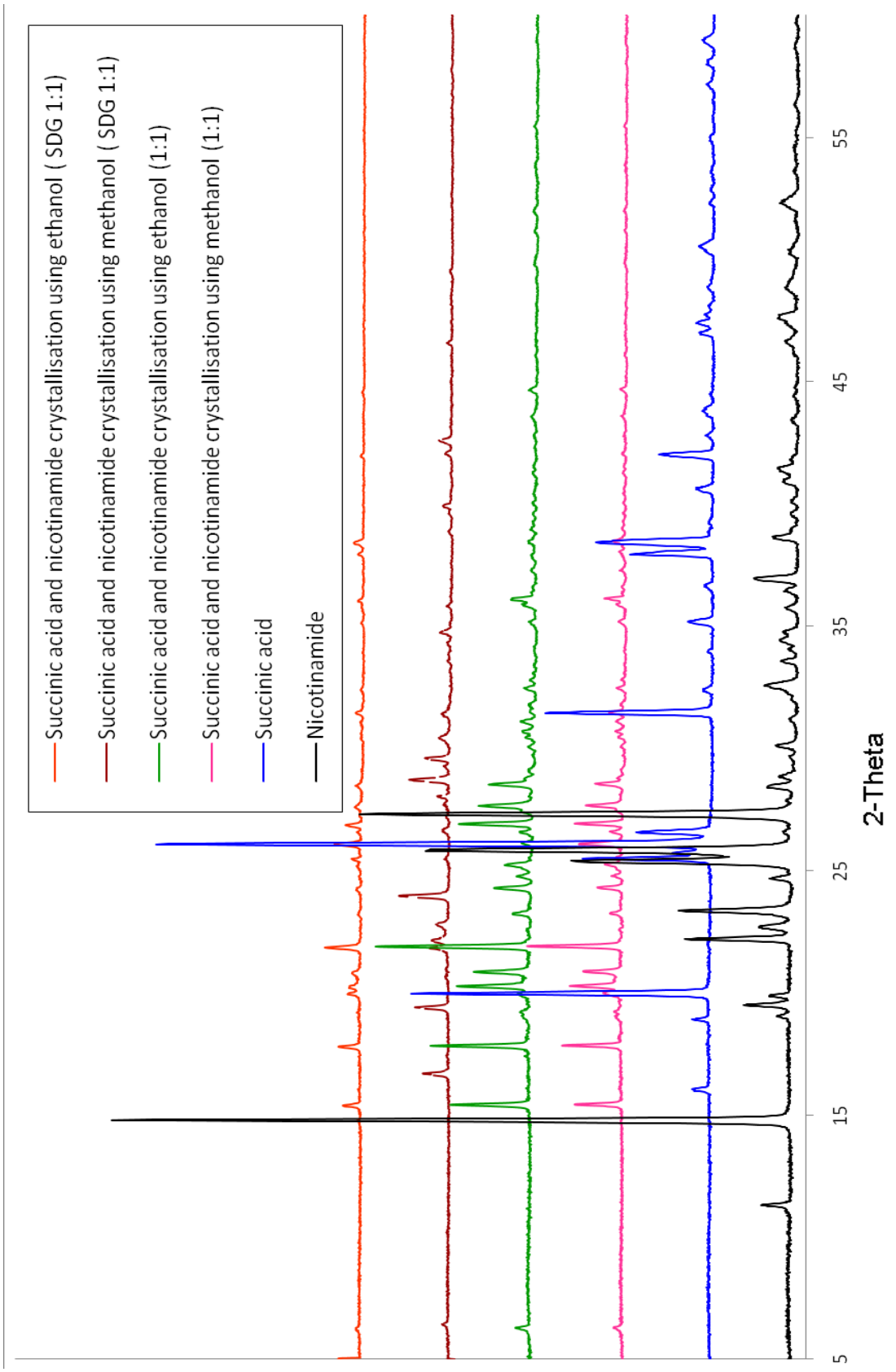

X-ray diffraction patterns of nicotinamide and succinic acid and products of crystallisation.

APPENDIX E

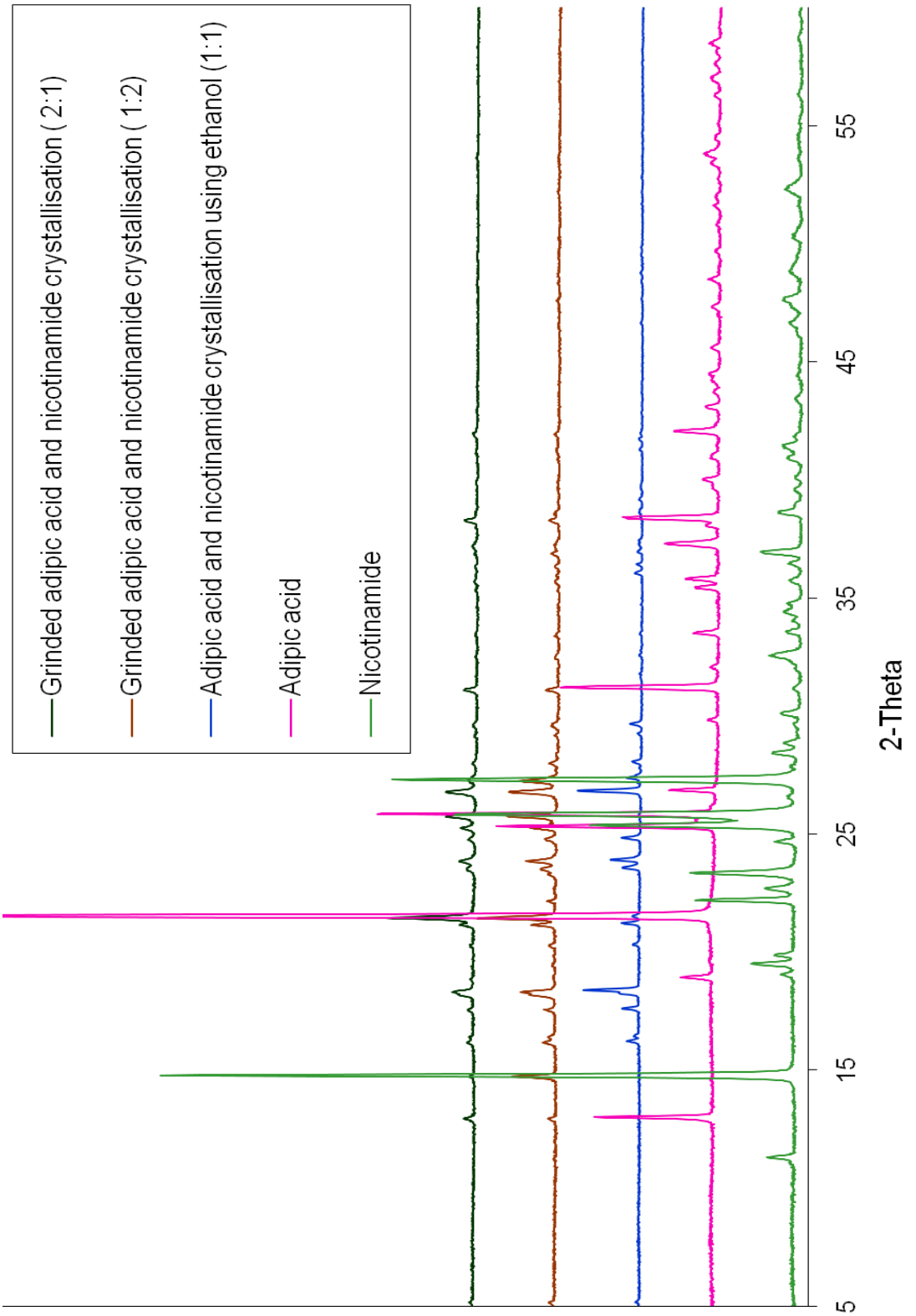

X-ray diffraction patterns of nicotinamide and adipic acid and products of crystallisation.

APPENDIX F

```
data_2009src0657

_audit_creation_method            SHELXL-97
_chemical_name_systematic
;
 ?
;
_chemical_name_common             ?
_chemical_melting_point           ?
_chemical_formula_moiety          '2(C6 H6 N2 O), C6 H10 O4'
_chemical_formula_sum
 'C18 H22 N4 O6'
_chemical_formula_weight          390.40

loop_
 _atom_type_symbol
 _atom_type_description
 _atom_type_scat_dispersion_real
 _atom_type_scat_dispersion_imag
 _atom_type_scat_source
 'C'  'C'   0.0033   0.0016
 'International Tables Vol C Tables 4.2.6.8 and 6.1.1.4'
 'H'  'H'   0.0000   0.0000
 'International Tables Vol C Tables 4.2.6.8 and 6.1.1.4'
 'N'  'N'   0.0061   0.0033
 'International Tables Vol C Tables 4.2.6.8 and 6.1.1.4'
 'O'  'O'   0.0106   0.0060
 'International Tables Vol C Tables 4.2.6.8 and 6.1.1.4'

_symmetry_cell_setting            Triclinic
_symmetry_space_group_name_H-M    'P -1'

loop_
 _symmetry_equiv_pos_as_xyz
 'x, y, z'
 '-x, -y, -z'

_cell_length_a                    5.0261(2)
_cell_length_b                    5.4280(3)
_cell_length_c                    16.8981(10)
_cell_angle_alpha                 98.147(2)
_cell_angle_beta                  91.072(3)
_cell_angle_gamma                 90.588(3)
_cell_volume                      456.24(4)
_cell_formula_units_Z             1
_cell_measurement_temperature     120(2)
_cell_measurement_reflns_used     11377
_cell_measurement_theta_min       2.91
_cell_measurement_theta_max       27.48

_exptl_crystal_description        'Cut Slab'
_exptl_crystal_colour             Colourless
_exptl_crystal_size_max           0.18
_exptl_crystal_size_mid           0.16
_exptl_crystal_size_min           0.08
_exptl_crystal_density_meas       ?
```

```
_exptl_crystal_density_diffrn     1.421
_exptl_crystal_density_method     'not measured'
_exptl_crystal_F_000              206
_exptl_absorpt_coefficient_mu     0.108
_exptl_absorpt_correction_type    Multi-scan
_exptl_absorpt_correction_T_min   0.9808
_exptl_absorpt_correction_T_max   0.9914
_exptl_absorpt_process_details   'SADABS 2007/2 (Sheldrick, G.M.,
2007)'

_exptl_special_details
;
 ?
;

_diffrn_ambient_temperature        120(2)
_diffrn_radiation_wavelength       0.71073
_diffrn_radiation_type             MoK\a
_diffrn_radiation_source          'Bruker-Nonius FR591 rotating
anode'
_diffrn_radiation_monochromator   '10cm confocal mirrors'
_diffrn_measurement_device_type
'Bruker-Nonius APEX II CCD camera on \k-goniostat'
_diffrn_measurement_method        '\f & \w scans'
_diffrn_detector_area_resol_mean  '4096x4096pixels / 62x62mm'
_diffrn_standards_number          ?
_diffrn_standards_interval_count  ?
_diffrn_standards_interval_time   ?
_diffrn_standards_decay_%         ?
_diffrn_reflns_number             7324
_diffrn_reflns_av_R_equivalents   0.0331
_diffrn_reflns_av_sigmaI/netI     0.0301
_diffrn_reflns_limit_h_min        -6
_diffrn_reflns_limit_h_max        6
_diffrn_reflns_limit_k_min        -7
_diffrn_reflns_limit_k_max        7
_diffrn_reflns_limit_l_min        -21
_diffrn_reflns_limit_l_max        21
_diffrn_reflns_theta_min          3.65
_diffrn_reflns_theta_max          27.48
_reflns_number_total              2058
_reflns_number_gt                 1880
_reflns_threshold_expression      >2\s(I)

_computing_data_collection
'COLLECT (Hooft, R.W.W., 1998)'
_computing_cell_refinement
'DENZO (Otwinowski & Minor, 1997) & COLLECT (Hooft, R.W.W.,
1998)'
#Although determined using DirAx, the cell is refined in the HKL
#package during data reduction
_computing_data_reduction
'DENZO (Otwinowski & Minor, 1997) & COLLECT (Hooft, R.W.W.,
1998)'
_computing_structure_solution     'SHELXS-97 (Sheldrick, 2008)'
_computing_structure_refinement   'SHELXL-97 (Sheldrick, 2008)'
_computing_molecular_graphics     'Ortep-3 for Windows (Farrugia,
1997)'
```

```
_computing_publication_material   'WinGX (Farrugia, 1999)'


_refine_special_details
;
 Refinement of F^2^ against ALL reflections.  The weighted R-
factor wR and
 goodness of fit S are based on F^2^, conventional R-factors R
are based
 on F, with F set to zero for negative F^2^. The threshold
expression of
 F^2^ > 2\s(F^2^) is used only for calculating R-factors(gt) etc.
and is
 not relevant to the choice of reflections for refinement.  R-
factors based
 on F^2^ are statistically about twice as large as those based on
F, and R-
 factors based on ALL data will be even larger.
;

_refine_ls_structure_factor_coef  Fsqd
_refine_ls_matrix_type            full
_refine_ls_weighting_scheme       calc
_refine_ls_weighting_details
 'calc w=1/[\s^2^(Fo^2^)+(0.0611P)^2^+0.2714P] where
P=(Fo^2^+2Fc^2^)/3'
_atom_sites_solution_primary      direct
_atom_sites_solution_secondary    difmap
_atom_sites_solution_hydrogens    geom
_refine_ls_hydrogen_treatment     constr
_refine_ls_extinction_method      none
_refine_ls_extinction_coef        ?
_refine_ls_number_reflns          2058
_refine_ls_number_parameters      128
_refine_ls_number_restraints      0
_refine_ls_R_factor_all           0.0509
_refine_ls_R_factor_gt            0.0468
_refine_ls_wR_factor_ref          0.1327
_refine_ls_wR_factor_gt           0.1294
_refine_ls_goodness_of_fit_ref    1.115
_refine_ls_restrained_S_all       1.115
_refine_ls_shift/su_max           0.000
_refine_ls_shift/su_mean          0.000

loop_
 _atom_site_label
 _atom_site_type_symbol
 _atom_site_fract_x
 _atom_site_fract_y
 _atom_site_fract_z
 _atom_site_U_iso_or_equiv
 _atom_site_adp_type
 _atom_site_occupancy
 _atom_site_symmetry_multiplicity
 _atom_site_calc_flag
 _atom_site_refinement_flags
 _atom_site_disorder_assembly
 _atom_site_disorder_group
```

```
C1 C 1.0734(3) 0.5734(3) 0.14120(9) 0.0176(3) Uani 1 1 d . . .
C2 C 1.2755(3) 0.3983(3) 0.13776(9) 0.0199(3) Uani 1 1 d . . .
H2 H 1.3984 0.3828 0.0954 0.024 Uiso 1 1 calc R . .
C3 C 1.2941(3) 0.2470(3) 0.19721(9) 0.0212(3) Uani 1 1 d . . .
H3 H 1.4295 0.1258 0.1961 0.025 Uiso 1 1 calc R . .
C4 C 1.1118(3) 0.2758(3) 0.25831(9) 0.0216(3) Uani 1 1 d . . .
H4 H 1.1241 0.1708 0.2987 0.026 Uiso 1 1 calc R . .
C5 C 1.0321(3) 0.7411(3) 0.07924(9) 0.0179(3) Uani 1 1 d . . .
C6 C 0.9011(3) 0.5912(3) 0.20542(9) 0.0190(3) Uani 1 1 d . . .
H6 H 0.7650 0.7121 0.2085 0.023 Uiso 1 1 calc R . .
N1 N 0.9189(3) 0.4457(3) 0.26276(8) 0.0212(3) Uani 1 1 d . . .
N2 N 1.2423(3) 0.7897(2) 0.03675(8) 0.0199(3) Uani 1 1 d . . .
H2A H 1.2256 0.8862 -0.0007 0.024 Uiso 1 1 calc R . .
H2B H 1.3977 0.7252 0.0461 0.024 Uiso 1 1 calc R . .
O1 O 0.8084(2) 0.8278(2) 0.06822(7) 0.0225(3) Uani 1 1 d . . .
C7 C 0.4229(3) 0.7131(3) 0.38225(9) 0.0195(3) Uani 1 1 d . . .
C8 C 0.0787(3) 0.9849(3) 0.46138(9) 0.0203(3) Uani 1 1 d . . .
H8A H -0.0455 0.9829 0.4151 0.024 Uiso 1 1 calc R . .
H8B H 0.2020 1.1287 0.4620 0.024 Uiso 1 1 calc R . .
C9 C 0.2371(3) 0.7453(3) 0.45183(9) 0.0214(3) Uani 1 1 d . . .
H9A H 0.3427 0.7396 0.5016 0.026 Uiso 1 1 calc R . .
H9B H 0.1105 0.6026 0.4456 0.026 Uiso 1 1 calc R . .
O3 O 0.4299(2) 0.8441(2) 0.32982(7) 0.0266(3) Uani 1 1 d . . .
O4 O 0.5799(2) 0.5186(2) 0.38467(7) 0.0242(3) Uani 1 1 d . . .
H4A H 0.6809 0.5042 0.3453 0.036 Uiso 1 1 calc R . .

loop_
 _atom_site_aniso_label
 _atom_site_aniso_U_11
 _atom_site_aniso_U_22
 _atom_site_aniso_U_33
 _atom_site_aniso_U_23
 _atom_site_aniso_U_13
 _atom_site_aniso_U_12
C1 0.0162(7) 0.0196(7) 0.0171(7) 0.0039(5) -0.0017(5) -0.0001(5)
C2 0.0188(7) 0.0223(7) 0.0184(7) 0.0023(6) 0.0013(5) 0.0026(6)
C3 0.0219(7) 0.0201(7) 0.0216(7) 0.0030(6) -0.0026(6) 0.0050(6)
C4 0.0252(8) 0.0209(7) 0.0198(7) 0.0072(6) -0.0022(6) 0.0018(6)
C5 0.0174(7) 0.0191(7) 0.0171(7) 0.0030(5) -0.0025(5) -0.0005(5)
C6 0.0184(7) 0.0197(7) 0.0196(7) 0.0052(6) -0.0009(5) 0.0022(5)
N1 0.0216(7) 0.0238(7) 0.0195(6) 0.0071(5) 0.0012(5) 0.0034(5)
N2 0.0174(6) 0.0246(7) 0.0196(6) 0.0093(5) 0.0006(5) 0.0031(5)
O1 0.0160(5) 0.0283(6) 0.0257(6) 0.0127(5) -0.0006(4) 0.0021(4)
C7 0.0195(7) 0.0209(7) 0.0185(7) 0.0044(6) -0.0008(5) 0.0018(6)
C8 0.0212(7) 0.0216(8) 0.0193(7) 0.0064(6) 0.0012(6) 0.0031(6)
C9 0.0230(8) 0.0225(8) 0.0199(7) 0.0070(6) 0.0026(6) 0.0044(6)
O3 0.0298(6) 0.0283(6) 0.0242(6) 0.0118(5) 0.0072(5) 0.0086(5)
O4 0.0261(6) 0.0282(6) 0.0205(6) 0.0096(5) 0.0061(4) 0.0103(5)

_geom_special_details
;
 All s.u.'s (except the s.u. in the dihedral angle between two
l.s. planes)
 are estimated using the full covariance matrix.  The cell s.u.'s
are taken
 into account individually in the estimation of s.u.'s in
distances, angles
```

```
 and torsion angles; correlations between s.u.'s in cell
parameters are only
 used when they are defined by crystal symmetry.  An approximate
(isotropic)
 treatment of cell s.u.'s is used for estimating s.u.'s involving
l.s. planes.
;

loop_
 _geom_bond_atom_site_label_1
 _geom_bond_atom_site_label_2
 _geom_bond_distance
 _geom_bond_site_symmetry_2
 _geom_bond_publ_flag
C1 C6 1.394(2) . ?
C1 C2 1.395(2) . ?
C1 C5 1.494(2) . ?
C2 C3 1.387(2) . ?
C2 H2 0.9500 . ?
C3 C4 1.386(2) . ?
C3 H3 0.9500 . ?
C4 N1 1.341(2) . ?
C4 H4 0.9500 . ?
C5 O1 1.2438(18) . ?
C5 N2 1.3333(19) . ?
C6 N1 1.3360(19) . ?
C6 H6 0.9500 . ?
N2 H2A 0.8800 . ?
N2 H2B 0.8800 . ?
C7 O3 1.2130(19) . ?
C7 O4 1.3291(18) . ?
C7 C9 1.507(2) . ?
C8 C9 1.522(2) . ?
C8 C8 1.529(3) 2_576 ?
C8 H8A 0.9900 . ?
C8 H8B 0.9900 . ?
C9 H9A 0.9900 . ?
C9 H9B 0.9900 . ?
O4 H4A 0.8400 . ?

loop_
 _geom_angle_atom_site_label_1
 _geom_angle_atom_site_label_2
 _geom_angle_atom_site_label_3
 _geom_angle
 _geom_angle_site_symmetry_1
 _geom_angle_site_symmetry_3
 _geom_angle_publ_flag
C6 C1 C2 118.17(14) . . ?
C6 C1 C5 118.63(13) . . ?
C2 C1 C5 123.19(14) . . ?
C3 C2 C1 118.95(14) . . ?
C3 C2 H2 120.5 . . ?
C1 C2 H2 120.5 . . ?
C4 C3 C2 118.89(14) . . ?
C4 C3 H3 120.6 . . ?
C2 C3 H3 120.6 . . ?
N1 C4 C3 122.65(14) . . ?
```

```
N1 C4 H4 118.7 . . ?
C3 C4 H4 118.7 . . ?
O1 C5 N2 122.38(14) . . ?
O1 C5 C1 120.36(13) . . ?
N2 C5 C1 117.25(13) . . ?
N1 C6 C1 122.94(14) . . ?
N1 C6 H6 118.5 . . ?
C1 C6 H6 118.5 . . ?
C6 N1 C4 118.38(13) . . ?
C5 N2 H2A 120.0 . . ?
C5 N2 H2B 120.0 . . ?
H2A N2 H2B 120.0 . . ?
O3 C7 O4 123.44(14) . . ?
O3 C7 C9 125.28(14) . . ?
O4 C7 C9 111.27(13) . . ?
C9 C8 C8 111.24(16) . 2_576 ?
C9 C8 H8A 109.4 . . ?
C8 C8 H8A 109.4 2_576 . ?
C9 C8 H8B 109.4 . . ?
C8 C8 H8B 109.4 2_576 . ?
H8A C8 H8B 108.0 . . ?
C7 C9 C8 115.12(13) . . ?
C7 C9 H9A 108.5 . . ?
C8 C9 H9A 108.5 . . ?
C7 C9 H9B 108.5 . . ?
C8 C9 H9B 108.5 . . ?
H9A C9 H9B 107.5 . . ?
C7 O4 H4A 109.5 . . ?

loop_
 _geom_torsion_atom_site_label_1
 _geom_torsion_atom_site_label_2
 _geom_torsion_atom_site_label_3
 _geom_torsion_atom_site_label_4
 _geom_torsion
 _geom_torsion_site_symmetry_1
 _geom_torsion_site_symmetry_2
 _geom_torsion_site_symmetry_3
 _geom_torsion_site_symmetry_4
 _geom_torsion_publ_flag
C6 C1 C2 C3 1.0(2) . . . . ?
C5 C1 C2 C3 -178.53(14) . . . . ?
C1 C2 C3 C4 -0.3(2) . . . . ?
C2 C3 C4 N1 -0.6(2) . . . . ?
C6 C1 C5 O1 -24.8(2) . . . . ?
C2 C1 C5 O1 154.72(16) . . . . ?
C6 C1 C5 N2 155.83(14) . . . . ?
C2 C1 C5 N2 -24.6(2) . . . . ?
C2 C1 C6 N1 -1.0(2) . . . . ?
C5 C1 C6 N1 178.55(13) . . . . ?
C1 C6 N1 C4 0.2(2) . . . . ?
C3 C4 N1 C6 0.6(2) . . . . ?
O3 C7 C9 C8 -9.5(2) . . . . ?
O4 C7 C9 C8 171.17(13) . . . . ?
C8 C8 C9 C7 -173.39(16) 2_576 . . . ?

loop_
 _geom_hbond_atom_site_label_D
```

```
 _geom_hbond_atom_site_label_H
 _geom_hbond_atom_site_label_A
 _geom_hbond_distance_DH
 _geom_hbond_distance_HA
 _geom_hbond_distance_DA
 _geom_hbond_angle_DHA
 _geom_hbond_site_symmetry_A
N2 H2A O1  0.88 2.06 2.9260(16) 167.9 2_775
N2 H2B O1  0.88 2.14 2.8851(17) 141.4 1_655
O4 H4A N1  0.84 1.85 2.6865(17) 174.2 .

_diffrn_measured_fraction_theta_max    0.985
_diffrn_reflns_theta_full              27.48
_diffrn_measured_fraction_theta_full   0.985
_refine_diff_density_max    0.340
_refine_diff_density_min   -0.284
_refine_diff_density_rms    0.059
```

APPENDIX G

Atomic coordinates and equivalent isotropic displacement parameters ($Å^2 x\ 10^3$) for adipic acid and nicotinamide co-crystal. U(eq) is defined as one third of the trace of the orthogonalized U^{ij} tensor.

	x	y	z	U(eq)
C(1)	10734(3)	5734(3)	1412(1)	18(1)
C(2)	12755(3)	3983(3)	1378(1)	20(1)
C(3)	12941(3)	2470(3)	1972(1)	21(1)
C(4)	11118(3)	2758(3)	2583(1)	22(1)
C(5)	10321(3)	7411(3)	792(1)	18(1)
C(6)	9011(3)	5912(3)	2054(1)	19(1)
N(1)	9189(3)	4457(3)	2628(1)	21(1)
N(2)	12423(3)	7897(2)	368(1)	20(1)
O(1)	8084(2)	8278(2)	682(1)	23(1)
C(7)	4229(3)	7131(3)	3823(1)	20(1)
C(8)	787(3)	9849(3)	4614(1)	20(1)
C(9)	2371(3)	7453(3)	4518(1)	21(1)
O(3)	4299(2)	8441(2)	3298(1)	27(1)
O(4)	5799(2)	5186(2)	3847(1)	24(1)

APPENDIX H

Standard bond lengths [Å] and bond angles [˚] for the intra-molecular bonds in adipic acid : nicotinamide (1:2) co-crystal.

	d		*d*
C(1)-C(2)	1.380	C(7)-O(4)	1.308
C(2)-C(3)	1.379	C(7)-O(3)	1.214
C(3)-C(4)	1.379	C(7)-C(9)	1.502
C(4)-N(1)	1.337	C(9)-C(8)	1.538
C(6)-C(1)	1.380	C(8)-C(8)_i	1.542
N(1)-C(6)	1.337	C(8)-H	1.092
C(1)-C(5)	1.504	C(9)-H	1.092
C(5)-O(1)	1.226		
C(5)-N(2)	1.325		
N(2)-H(2A)	0.88		
N(2)-H(2B)	0.88		
C(ar)-H	1.083		
C6 C1 C2	118.17	C5 N2 H2A	120.0
C6 C1 C5	118.63	C5 N2 H2B	120.0
C2 C1 C5	123.19	H2A N2 H2B	120.0
C3 C2 C1	118.95	O3 C7 O4	123.44
C3 C2 H2	120.5	O3 C7 C9	125.28
C1 C2 H2	120.5	O4 C7 C9	111.27
C4 C3 C2	118.89	C9 C8 C8	111.24
C4 C3 H3	120.6	C9 C8 H8A	109.4
C2 C3 H3	120.6	C8 C8 H8A	109.4
N1 C4 C3	122.65	C9 C8 H8B	109.4
N1 C4 H4	118.7	C8 C8 H8B	109.4
C3 C4 H4	118.7	H8A C8 H8B	108.0
O1 C5 N2	122.38	C7 C9 C8	115.12
O1 C5 C1	120.36	C7 C9 H9A	108.5
N2 C5 C1	117.25	C8 C9 H9A	108.5
N1 C6 C1	122.94	C7 C9 H9B	108.5
N1 C6 H6	118.5	C8 C9 H9B	108.5
C1 C6 H6	118.5	H9A C9 H9B	107.5
C6 N1 C4	118.38	C7 O4 H4A	109.5

APPENDIX I

Cell parameters obtained from indexing the X-ray diffraction data of the product of nicotinamide and adipic acid using CRYSFIRE.

I20	Merit	Volume	V/V1	a	b	c	α	β	γ
20	22.4	832.42	1	8.91	17.35	5.56	95.08	99.03	99.56
20	20.4	832.61	1	8.91	17.35	5.56	95.08	99.03	99.56
20	18.48	836.11	1	8.92	17.38	5.57	95.09	99.03	99.57
20	8.43	1663.73	2	17.77	18.22	5.55	99.17	98.35	70.10
20	7	484.14	0.58	5.14	5.84	18.82	70.20	83.40	109.69
20	6.5	1728.14	2.08	17.13	9.22	11.00	90	96.72	90
20	6.5	1728.14	2.08	17.13	9.22	11.00	90	96.72	90
20	6.5	1728.14	2.08	19.25	9.22	11.00	90	117.87	90
20	6.5	1728.14	2.08	19.25	9.22	11.00	90	117.87	90
20	5.7	3960.87	4.76	19.32	35.78	5.73	90	91.87	90
20	5.7	3502.25	4.21	30.76	20.39	5.58	90	92.09	90
20	5.1	1939.82	2.33	19.64	5.77	18.86	90	114.94	90
20	5.1	1939.82	2.33	19.64	5.77	18.86	90	114.94	90
20	5.1	1930.80	2.32	27.50	4.09	17.49	90	101.75	90
20	5.1	1930.80	2.32	27.50	4.09	17.49	90	101.75	90
20	5.1	1929.98	2.32	29.43	4.09	17.49	90	113.83	90
20	5.1	1929.98	2.32	29.43	4.09	17.49	90	113.83	90
19	57.61	471.88	0.57	5.50	17.12	5.039	90.16	90.67	96.75
19	9.63	822.23	0.99	8.83	17.31	5.57	95.34	99.69	99.27
19	8	769.19	0.92	5.54	8.16	22.56	121.17	70.85	82.83
19	8	769.19	0.92	5.54	8.16	22.56	121.17	70.85	82.83
19	8	769.19	0.92	5.54	8.16	19.62	100.31	64.59	82.83
19	6	2098.44	2.52	22.10	7.09	17.23	90	129.13	90
19	6	2098.44	2.52	22.10	7.09	17.23	90	129.13	90
18	9.1	1059.54	1.27	8.81	17.20	7.08	91.19	90.39	99.46
18	9	991.61	1.19	17.11	5.29	11.00	90	96.72	90
18	8	1529.03	1.84	17.49	5.46	16.28	90	101.24	90
18	6	1510.18	1.81	22.67	5.29	17.26	90	133.26	90
18	6	1158.03	1.39	17.18	10.17	6.64	90	94.84	90
18	6	1158.03	1.39	17.18	10.17	6.64	90	94.84	90
18	6	1158.03	1.39	17.18	10.17	6.64	90	94.84	90
18	6	1158.03	1.39	17.89	10.17	6.64	90	106.87	90
18	6	1064.83	1.28	17.40	7.07	8.76	90	99.66	90
18	6	748.35	0.9	5.58	7.93	18.18	108.41	86.57	80.57
18	6	748.35	0.9	5.58	7.93	17.51	94.17	79.47	80.57
17	13.25	649.47	0.78	6.96	17.12	5.75	94.63	107.01	95.24
17	11.15	651.17	0.78	7.03	17.06	5.75	93.73	107.52	96.57
17	11	1235.94	1.48	17.30	6.53	11.00	90	96.46	90
17	11	1235.94	1.48	19.43	6.53	11.00	90	117.76	90
17	11	1235.94	1.48	19.43	6.53	11.00	90	117.76	90
17	11	624.42	0.75	6.65	8.80	21.39	94.11	115.47	38.65
17	10.47	773.57	0.93	7.89	17.16	6.10	93.61	108.78	81.43
17	9	484.42	0.58	5.13	6.33	18.82	66.39	83.54	60.31
17	9	484.42	0.58	5.13	6.33	20.71	56.36	69.37	60.31

17	9	484.42	0.58	5.13	5.85	20.71	73.09	69.37	109.90
17	7	1158.66	1.39	20.85	10.17	6.64	90	124.73	90
17	6	1502.64	1.81	17.26	7.97	11.00	90	96.88	90
17	6	1502.64	1.81	17.26	7.97	11.00	90	96.88	90
17	6	1323.31	1.59	22.67	10.84	5.46	90	99.92	90
17	6	1323.31	1.59	22.38	10.84	5.46	90	93.98	90
16	12.04	831.04	1	8.91	17.28	5.56	94.84	99.13	99.18
16	9.45	1029.64	1.24	10.97	17.52	5.51	95.85	93.92	101.41

APPENDIX J

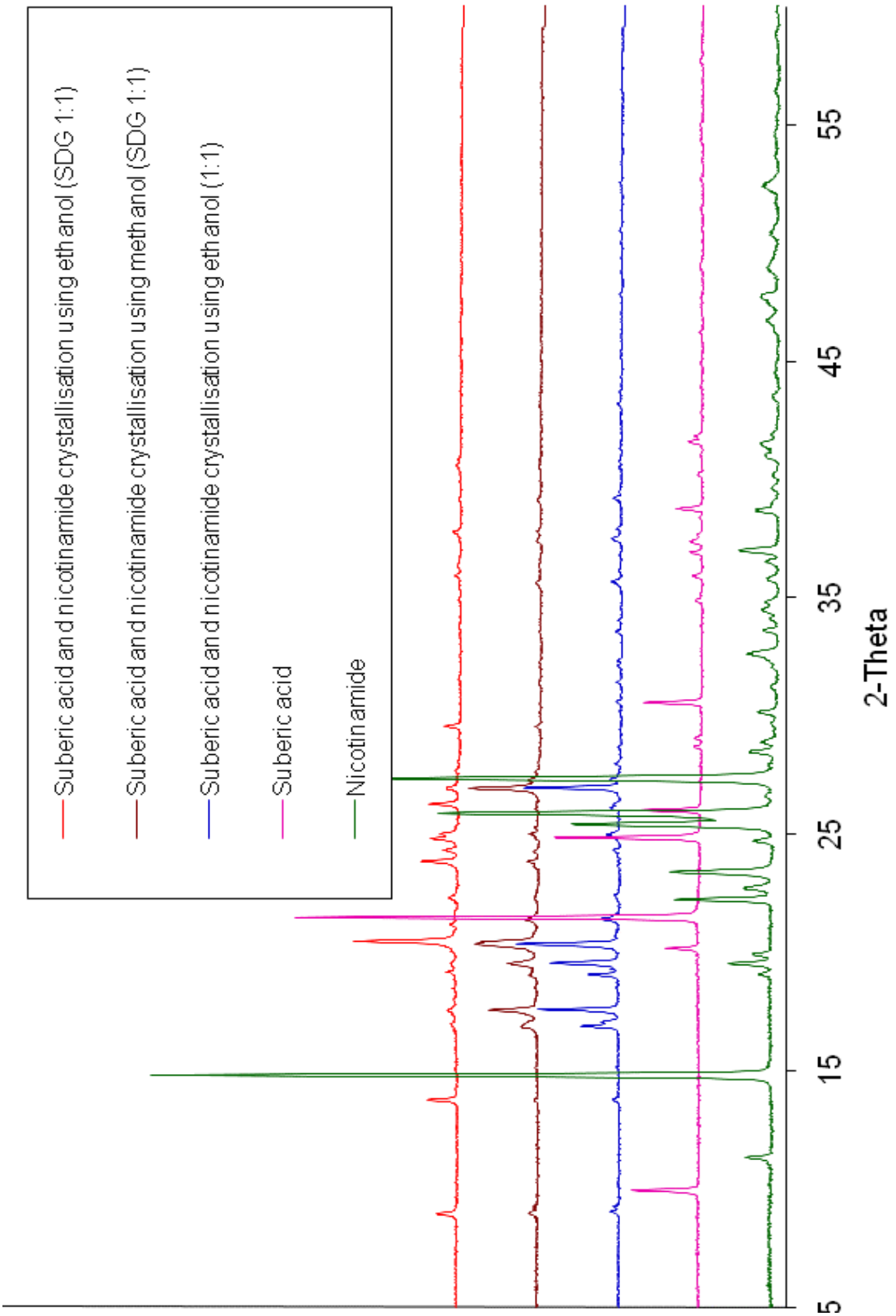

X-ray diffraction patterns of nicotinamide and suberic acid and products of crystallisation.

APPENDIX K

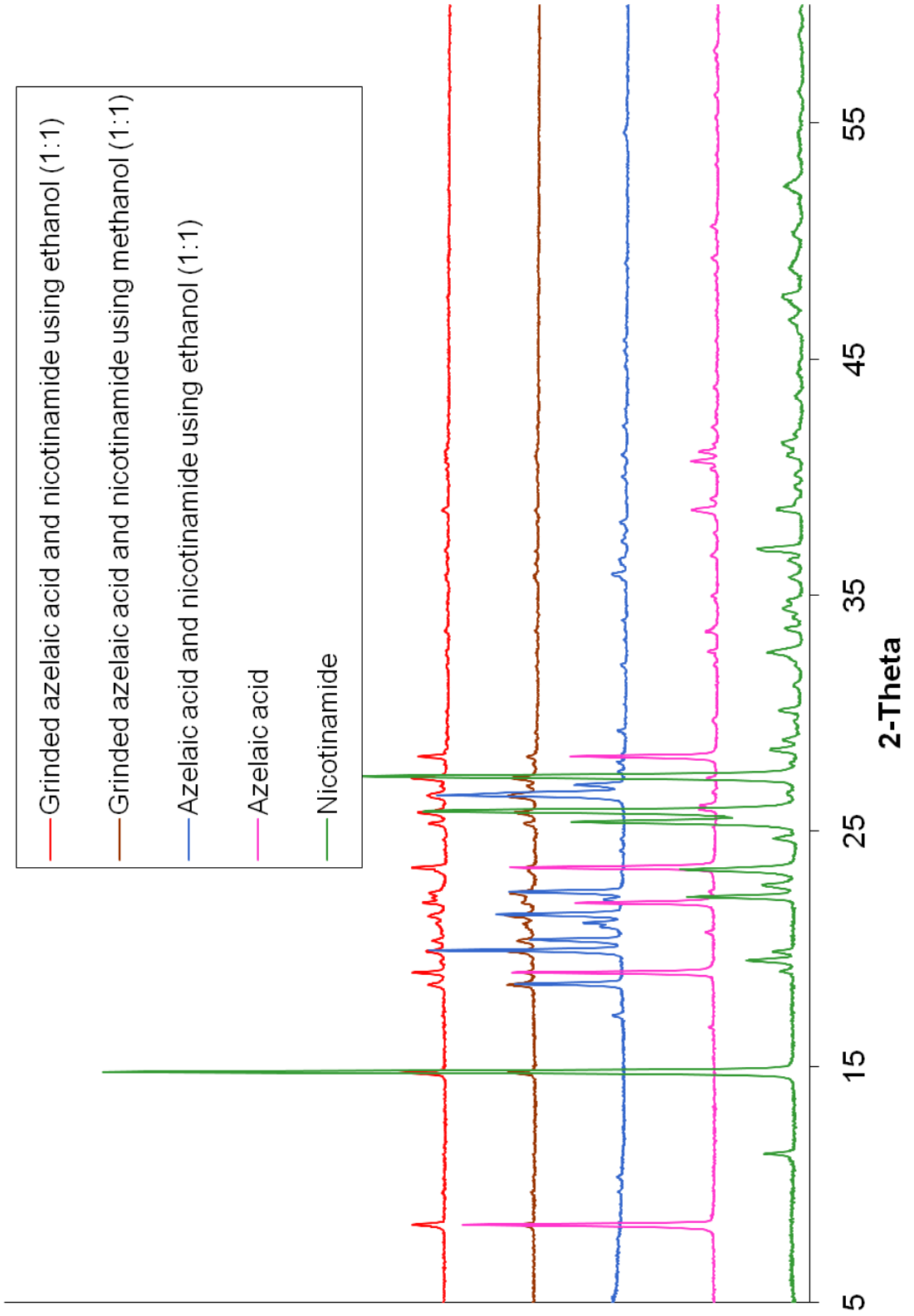

X-ray diffraction patterns of nicotinamide and azelaic acid and products of crystallisation.

APPENDIX L

Cell parameters obtained from indexing of powder X-ray diffraction data the product of nicotinamide and azelaic acid crystallisation using CRYFIRE.

I20	Merit	Volume	a	b	c	α	B	γ
20	20	1665.95	8.796	36.3453	5.2111	90	90	90
20	19.94	1672.95	8.8082	36.4064	5.217	90	90	90
20	18.5	1674.22	37.5154	5.2155	8.8013	90	103.53	90
20	18.3	1673.07	10.2441	36.3893	5.2178	90	120.66	90
20	16.8	1675.46	10.2411	36.4655	5.2164	90	120.67	90
20	16.4	1675.45	8.8082	36.4662	5.2162	90	89.95	90
20	16.3	1673.89	8.8103	36.4272	5.2157	90	90.041	90
20	16.3	1673.72	36.4317	8.8089	5.2154	90	90	90
20	14.4	1676.63	36.8675	8.8054	5.2187	90	98.25	90
20	14.4	1676.62	37.9298	8.8054	5.2187	90	105.86	90
20	13.2	1675.38	37.5177	5.2149	8.8085	90	103.55	90
20	13.2	1675.38	37.5177	5.2149	8.8085	90	103.55	90
20	12.7	1674.03	42.005	8.8103	5.2118	90	119.78	90
20	12.3	1671.47	37.4615	5.2144	8.7978	90	103.44	90
20	12.3	1671.47	37.4615	5.2144	8.7978	90	103.44	90
20	12.2	1676.21	37.5089	5.2156	8.8117	90	103.5	90
20	12.2	1675.81	37.5118	5.2157	8.8101	90	103.53	90
20	12.2	1675.56	36.4697	5.2157	8.8088	90	89.97	90
20	12.1	1676.28	36.4749	5.2153	8.812	90	89.90	90
20	12.1	1676.15	39.6826	8.8086	5.2142	90	113.12	90
20	12	1676.13	36.8571	8.8085	5.2141	90	98.043	90
20	11.9	1677.49	37.9729	8.8078	5.2202	90	106.09	90
20	11.9	1671.01	8.8062	36.3877	5.2148	90	90	90
20	11.7	1678.51	36.5093	8.806	5.2209	90	89.84	90
20	11.2	1676.19	42.013	8.8086	5.2122	90	119.65	90
20	10.7	1678.49	44.9438	8.8081	5.2203	90	125.68	90
20	10.3	1678.51	36.8579	8.8082	5.2205	90	97.96	90
20	10	1678.39	42.1087	8.8083	5.2208	90	119.91	90
20	10	1676.49	37.9467	8.8088	5.2144	90	105.87	90
20	9.9	1678.39	37.9294	8.8083	5.2208	90	105.79	90
20	9	1679.94	39.7925	8.8082	5.2244	90	113.44	90
20	7.6	1678.57	44.9136	8.8086	5.2196	90	125.62	90
20	5.3	1672.91	36.5505	8.7906	5.2067	90	90.11	90
20	5.1	1684.42	5.2162	36.4255	8.8665	90.94	90.19	89.99
19	11.07	1707.09	9.7276	18.3036	9.6306	93.57	94.06	89.74
19	11	415.47	5.2132	8.7515	9.3868	101.41	81.80	91.04
19	10.47	415.20	8.7497	9.3792	5.2144	98.19	88.95	101.37
19	9.95	1951.64	11.1164	18.4378	10.5496	96.06	114.38	83.18
19	8	1305.46	16.7012	9.1203	9.6736	90	117.62	90

APPENDIX M

Atomic coordinates and equivalent isotropic displacement parameters ($Å^2 x\ 10^3$) for azelaic acid and nicotinamide co-crystal.

		x	y	z
N1	C	0.5593	0.1153	0.5964
O2	O	0.545(4)	0.8012(8)	1.028(5)
C3	C	0.6482(34)	0.7561(6)	0.736(6)
C4	C	0.590(4)	0.7269(7)	0.867(7)
C5	C	0.724(4)	0.6876(7)	0.584(7)
N6	N	0.623(5)	0.6922(6)	0.783(6)
C7	C	0.7935(28)	0.7166(9)	0.487(7)
C8	C	0.7348(29)	0.7497(7)	0.523(5)
C9	H	0.5355	0.1691	0.6618
O10	O	0.4794	0.1145	0.4099
O11	O	0.5812	0.1452	0.7423
C12	C	0.6499	0.0836	0.7005
C13	C	0.6519	0.0505	0.5222
C14	C	0.7444	0.0188	0.6324
C15	C	0.7481	-0.014	0.451
C16	C	0.8383	-0.046	0.5606
C17	C	0.8401	-0.0787	0.3784
C18	C	0.9267	-0.1437	0.3119
C20	C	0.9294	-0.1109	0.4874
C21	C	0.603(6)	0.7942(6)	0.805(5)
O22	O	1.0118	-0.1372	0.1031
O23	O	0.8602	-0.1718	0.3523
H11A	H	0.5951	0.8421	0.7451
H1A	H	0.7219	0.8229	0.5398
H1B	N	0.634(4)	0.8195(7)	0.659(5)

APPENDIX N

Cell parameters obtained from indexing powder X-ray diffraction data of the product of isonicotinamide and azelaic acid crystallisation using CRYSFIRE.

I20	Merit	Volume	a	b	c	A	β	γ
20	9.95	929.60	9.0847	19.016	5.5755	97.222	103.341	89.319
20	9.93	929.60	9.0847	19.016	5.5755	97.222	103.341	89.319
20	9.32	913.02	8.9081	19.0293	5.4737	97.789	96.631	88.133
20	9.29	1010.99	10.0272	11.2532	10.2212	111.582	103.387	97.953
20	9.07	906.50	9.0409	18.9782	5.4318	96.127	101.925	89.757
20	5.7	1745.79	18.9525	5.227	17.6234	90	90.494	90
20	5.7	1745.79	18.9525	5.227	17.6234	90	90.494	90
20	5.6	1313.11	10.5788	14.1659	9.9861	101.837	116.296	84.786
20	5.1	4983.45	56.2239	17.5906	5.0388	90	90	90
20	5.1	4983.45	56.2239	17.5906	5.0388	90	90	90
19	16.93	835.90	8.8471	18.8571	5.0115	90.283	90.588	89.005
19	16.65	835.85	8.8476	18.8548	5.0116	90.269	90.592	89.012
19	13.76	912.99	9.0748	18.9507	5.4715	95.863	102.7	89.682
19	13.52	1123.69	10.3198	11.5533	10.3563	109.295	103.535	92.309
19	11.54	839.71	9.8002	10.7654	10.0066	117.562	114.924	71.822
19	10.45	895.79	8.868	18.9382	5.3699	95.437	93.689	90.609
19	10.03	883.10	9.0786	18.8628	5.2975	91.514	103.109	88.708
19	9.44	1582.12	9.4867	18.8602	9.0786	90.441	102.866	92.243
19	9.18	1249.99	9.147	18.9621	7.493	95.654	104.839	87.592
19	7	1005.08	11.1774	11.5446	13.8349	52.092	132.544	124.066
19	7	857.19	4.9708	10.6779	18.3095	82.468	87.589	62.86
19	7	857.19	4.9708	9.5027	18.7694	82.819	77.068	89.397
19	7	857.19	4.9708	9.5027	18.3095	82.803	87.589	90.603

7. BIBLIOGRAPHY:

1. C. B. Aakeröy, A. M. Beatty, M. Tremayne, D. M. Rowe and C. C. Seaton, *Crystal Growth & Design*, 2001, **1**, 377.

2. A. V. Trask, J. van de Streek, W. D. S. Motherwell and W. Jones, *Crystal Growth & Design*, 2005, **5**, 2233.

3. R. Pepinsky, *Physical Review*, 1955, **100**, 971.

4. P. Vishweshwar, J. A. McMahon, J. A. Bis and M. J. Zaworotko, *Journal of Pharmaceutical Sciences*, 2006, **95**, 499.

5. M. K. Stanton and A. Bak, *Crystal Growth & Design*, 2008, **8**, 3856.

6. C. B. Aakeröy, A. M. Beatty and B. A. Helfrich, *Journal of the American Chemical Society*, 2002, **124**, 14425.

7. W. Jones, S. Motherwell and A. V. Trask, *MRS Bulletin*, 2006, **31**, 875.

8. C. B. Aakeröy and D. J. Salmon, *CrystEngComm*, 2005, **7**, 439.

9. C. B. Aakeröy, M. E. Fasulo and J. Desper, *Molecular Pharmaceutics*, 2007, **4**, 317.

10. R. D. B. Walsh, M. W. Bradner, S. Fleischman, L. A. Morales, B. Moulton, N. Rodriguez-Hornedo and M. J. Zaworotko, *Chemical Communications*, 2003, 186.

11. M. C. Etter, *Accounts of Chemical Research*, 1990, **23**, 120.

12. M. L. Cheney, M. J. Zaworotko, S. Beaton and R. D. Singer, *Journal of Chemical Education*, 2008, **85**, 1649.

13. M. Tremayne, *Philosophical Transactions of the Royal Society of London Series A-Mathematical Physical and Engineering Sciences*, 2004, **362**, 2691.

14. D. P. McNamara, S. L. Childs, J. Giordano, A. Iarriccio, J. Cassidy, M. S. Shet, R. Mannion, E. O'Donnell and A. Park, *Pharmaceutical Research*, 2006, **23**, 1888.

15. B. Rodriguez-Spong, C. P. Price, A. Jayasankar, A. J. Matzger and N. Rodriguez-Hornedo, *Advanced Drug Delivery Reviews*, 2004, **56**, 241.

16. P. Vishweshwar, J. A. McMahon, M. L. Peterson, M. B. Hickey, T. R. Shattock and M. J. Zaworotko, *Chemical Communications*, 2005, 4601.

17. C. B. Aakeröy, J. Desper and M. E. Fasulo, *CrystEngComm*, 2006, **8**, 586.

18. M. Tremayne, *Engineering of Crystalline Materials Properties*, 2008, 477.

19. K. D. M. Harris, M. Tremayne and B. M. Kariuki, *Angewandte Chemie International Edition*, 2001, **40**, 1626.

20. J. Kennedy and M. Thorley, *Crystal Structure Determination*, William Clegg, Oxford University Press, 1999, 339.

21. P. Vishweshwar, A. Nangia and V. M. Lynch, *Crystal Growth & Design*, 2003, **3**, 783.

22. S. K. Callear, M. B. Hursthouse and T. L. Threlfall, *CrystEngComm*, 2009, **11**, 1609.

23. K. Biradha and L. Rajput, *Organic Crystal Engineering: Fronteirs in Crystal Engineernig*, John Wiley & Sons, 2010, 215.

24. A. Nangia, *Organic Crystal Engineering: Fronteirs in Crystal Engineernig*, John Wiley & Sons, 2010, 151.

25. O. Almarsson and M. J. Zaworotko, *Chemical Communications*, 2004, **17**, 1889.

26. M. Schmidtmann, M. J. Gutmann, D. S. Middlemiss and C. C. Wilson, *CrystEngComm*, 2007, **9**, 743.

27. L. Orola and M. V. Veidis, *CrystEngComm*, 2009, **11**, 415.

28. M. R. Caira, G. Bettinetti and M. Sorrenti, *Journal of Pharmaceutical Sciences*, 2002, **91**, 467.

29. T. Friščić, A. V. Trask, W. Jones and W. D. S. Motherwell, *Angewandte Chemie International Edition*, 2006, **45**, 7546.

30. J. H. Ter Horst and P. W. Cains, *Crystal Growth & Design*, 2008, **8**, 2537.

31. D. J. Good and N. r. Rodríguez-Hornedo, *Crystal Growth & Design*, 2009, **9**, 2252.

32. A. V. Trask, W. D. Motherwell and W. Jones, *Chemical Communications*, 2004, 890.

33. A. V. Trask and W. Jones, *Topics in Current Chemistry*, 2005, **254**, 41.

34. F. H. Allen, W. D. S. Motherwell, P. R. Raithby, G. P. Shields and R. Taylor, *New Journal of Chemistry*, 1999, **1**, 25.

35. H. G. Brittain, *Journal of Pharmaceutical Sciences*, 2008, **97**, 3611.

36. C. H. Gorbitz and H. P. Hersleth, *Acta Crystallographica*, 2000, **56**, 526.

37. S. Karki, T. Friscic, W. Jones and W. D. S. Motherwell, *Molecular Pharmaceutics*, 2007, **4**, 347.

38. P. J. Ellis and H. C. Freeman, *Journal of Synchrotron Radiation*, 1995, **2**, 190.

39. R. Shirley. (2002), *The Lattice Press, 41 Guildford Park Avenue, Guildford*, 2002.

40. S. Y. Chong and M. Tremayne, *Chemical Communications*, 2006, 4078.

41. Developed at laboratorie des Materiaux et du Genie Physique Ecole Nationale Superieure de Physique de Grenoble (INPG). Deomaine Universitaire BP 46, Sanit Martin d'Heres, France.

42. A. L. Bail, H. Duroy and J. L. Fourquet, *Material Research Bulletin*, 1988, **23**, 447.

43. A. C. Larson and R. B. V. Dreele, *Los Alamos National Laboratory Report LAUR*, 1994, 86.

44. M. Tremayne and C. Glidewell, *Chemical Communications*, 2000, 2425.

45. C. C. Seaton and M. Tremayne, *Chemical Communications*, 2002, 880.

46. E. Y. Cheung, E. E. McCabe, K. K. M. Harris, R. L. Johnston, K. M. P. Raja and P. Balaram, *Angewandte Chemie International Edition*, 2002, **41**, 494.

47. R. L. Johnston, *Application of evolutionary computation in chemistry*, Springer-Verlag, 2004, 95.

48. W. I. F. David, D. Shankland, L. B. McCusker and C. Baerlocher, *Structure Determination from Powder Diffraction Data*, Oxford University Press, 2002, 170.

49. K. D. M. Harris and M. Tremayne, *Chemistry of Materials*, 1996, **8**, 2554.

50. R. Storn and K. V. Price, *Journal f Global Optimisation*, 1997, **11**, 341.

51. K. Chisholm, *McGraw-Hill*, 1999, 147.

52. M. Wormington, C. Panaccione, K. M. Matney and D. K. Bowen, *Philosophical Transactions of the Royal Society A-Mathematical Physical and Engineering Sciences*, 1999, **357**, 2827.

53. M. Bjorck and G. Andersson, *Journal of Applied Crystallography*, 2007, **40**, 1174.

54. D. E. McRee, *Acta Crystallographica*, 2004, **60**, 2276.

55. R. Thomsen and M. K. Christensen, *Journal of Medicinal Chemistry*, 2006, **49**, 3315.

56. C. C. Seaton and N. Blagden, *American Crystallographic Association Transactions*, 2004, **39**, 90.

57. N. Chakrabaorti, P. Mishra and S. Erkoc, *Journal of Phase Equilibria and Diffusion*, 2004, **25**, 16.

58. C. C. Seaton and M. Tremayne, *POSSUM. Program for Direct-space structrue solution from Powder Diffraction Data*, School of Chemistry, University of Birmingham, UK, 2001.

59. M. Tremayne, S. Chong and D. Bell, *Frontiers of Computer Science in China*, 2009, **3**, 101.

60. M. Tremayne, C. C. Seaton and C. Glidewell, *Acta Crystallographica*, 2002, **58**, 823.

61. B. H. Toby, *Journal of Applied Crystallography*, 2001, **34**, 210.

62. R. W. W. Hooft, *COLLECT*, *Nonius B. V, Delft.*, 1998.

63. Z. Otwinowski and W. Minor, *Methods in Enzymology*, Academic Press, 1997, 307.

64. G. M. Sheldrick, *Madison, Wisconsin, USA*, 2007.

65. G. M. Sheldrick, *Acta Crystallographica*, 2008, **64**, 112.

66. L. J. Farrugia, *Journal of Applied Crystallography*, 1997, ***30***, 565.

67. C. F. Macrae, P. R. Edgington, P. McCabe, E. Pidcock, G. P. Shields, R. Taylor, M. Towler and J. van de Streek, *Journal of Applied Crystallography*, 2006, ***39***, 453.

68. A. L. Spek, *Acta Crystallographica*, 1990, **46**, 34.

69. R. F. Evans and W. Kynaston, *Journal of the Chemical Society*, 1962, 1005.

70. W. A. Caspari, *Journal of Chemical Society*, 1928, 3235.

71. T. Friscic and W. Jones, *Faraday Discussions*, 2007, **136**, 167.

72. V. R. Thalladi, M. Nusse and R. Boese, *Journal of the American Chemical Society*, 2000, **122**, 9227.

73. S. Karki, T. Friscic and W. Jones, *CrystEngComm*, 2009, **11**, 470.